

# HEALTH MANAGEMENT OF BRAKING SYSTEM OF AN AUTOMOTIVE VEHICLE

*by*

**BHASKAR CHOUHAN**

(11105016)



DEPARTMENT OF MECHANICAL ENGINEERING  
INDIAN INSTITUTE OF TECHNOLOGY, KANPUR  
KANPUR, U.P., INDIA

MAY, 2013

# **HEALTH MANAGEMENT OF BRAKING SYSTEMS OF AN AUTOMOTIVE VEHICLE**

A Thesis Submitted  
In Partial Fulfilment of the Requirements  
for the Degree Of  
**MASTER OF TECHNOLOGY**

by  
**BHASKAR CHOUHAN**

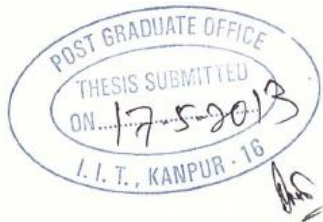


*to the*

**DEPARTMENT OF MECHANICAL ENGINEERING  
INDIAN INSTITUTE OF TECHNOLOGY, KANPUR  
KANPUR, U.P, INDIA**

**MAY, 2013**

# CERTIFICATE



It is to certify that work contained in the thesis entitled "**Health Management of Braking System of an Automotive Vehicle**" by **Bhaskar Chouhan** has been carried out under my supervision and that this work has not been submitted elsewhere for a degree.

*Nalinaksh Vyas*  
Dr. Nalinaksh S Vyas

(Professor)

Mechanical Engineering Department

Indian Institute of Technology, Kanpur

May, 2013

# **STATEMENT OF THESIS PREPARATION**

Thesis title: “**Health Management of Braking System of an Automotive Vehicle**”

1. Degree for which submitted : **Master of Technology**
2. The thesis guide was referred to for thesis preparation : **YES**
3. Specifications regarding thesis format have been closely followed : **YES**
4. The contents of the thesis were organized according to the guidelines : **YES**

Name : Bhaskar Chouhan  
Roll No. : Y11105016  
Department : Mechanical Engineering.

## **ABSTRACT**

---

The present work deals with health monitoring of an automotive brake system. A variety of possible faults in the sub-system are considered. Attempt has been made to devise an integrated instrumentation, data acquisition, signal processing and diagnosis package, which can be of utility to automotive engineers. Experiments have been conducted over a custom designed brake test rig, which represents a quarter car model of standard automobile vehicle. Faults have been deliberately introduced in the system and vibration and temperature signatures have been captured for constant speed running of the vehicle and under braking conditions. These steady state and transient signals are processed using Fast Fourier Transforms and Wavelets. Characteristic features from FFTs and Wavelets for a variety of Brake System faults are identified and extracted. They are subsequently fed as inputs to a diagnosis scheme employing artificial Neural Networks. Various training algorithms and architecture have been explored for the accuracy in training and validation. Targeted accuracy for fault identification and diagnosis speeds are investigated.

**Dedicated to My Parents,  
Brothers  
and Thesis Advisor**

## **ACKNOWLEDGEMENTS**

---

I would like to thank my thesis supervisor, **Prof. N. S. Vyas** for his innumerable suggestions, constant encouragement and valuable guidance. His openness and grant of adequate freedom to me for thesis enabled me to bring this work to the present form.

It was a pleasure to work at Vibration and Dynamics Laboratory of IIT Kanpur. My lab mates Saurabh, Gaurav, Rohit, Vaibhav and Prashant provided lively working environment and made my stay in the laboratory comfortable. I appreciate and extend my thanks to Mr. Mohsin for their untiring help in conducting my experiments.

I also want to thank Mr. Shantanu, Mr. R.K. Singh, Mr. Ramshankar, M.r Anil and Mr. Trivedi for helping me in experiments and other non academic issues.

I would like to extend my thanks to all of my class mates and my friends especially Abhijeet, Sagar, Husain, Sahil, Hemant, Arpan, Bitanu, Vimal, Nagaraj and SMD guys for making my stay at IITK enjoyable and memorable. I will cherish the moments forever.

Finally, I want to specially thank my parents, Brothers and Apeksha for their continuous support and encouragement. I would not have been able to complete my degree without their support.

**Bhaskar Chouhan**

**May, 2013, IIT Kanpur**

# CONTENTS

---

<b>CERTIFICATE .....</b>	<b>II</b>
<b>STATEMENT OF THESIS PREPARATION .....</b>	<b>III</b>
<b>Thesis title: "Health Management of Braking System of an Automotive Vehicle" .....</b>	<b>III</b>
<b>ABSTRACT .....</b>	<b>IV</b>
<b>ACKNOWLEDGEMENTS .....</b>	<b>VI</b>
<b>CONTENTS.....</b>	<b>VII</b>
<b>LIST OF FIGURES.....</b>	<b>IX</b>
<b>LIST OF TABLES.....</b>	<b>XI</b>
<b>NOMENCLATURE.....</b>	<b>XII</b>
<b>CHAPTER 1 .....</b>	<b>1</b>
1.1    Introduction .....	1
1.2    Current state of the Art .....	2
1.2.1 IVHM .....	2
Development of the IVHM Notion .....	3
Technology principles for IVHM systems .....	4
1.2.2 Wavelet Analysis .....	5
1.2.3 Artificial Neural Network .....	6
1.2.4 Thesis Organization .....	8
<b>CHAPTER 2 .....</b>	<b>9</b>
<i>VIBRATION FAULT DIAGNOSIS.....</i>	<i>9</i>
2.1    Common Faults in Vehicle .....	9
2.2    Vibration Analysis as a Predictive Maintenance Tool.....	13
2.3    Diagnostics Techniques .....	14
2.3.1 Time Domain or Wave Form Analysis .....	14
2.3.2 Frequency Domain .....	15
2.3.3 Quefrency Domain .....	15
2.3.4 Expert Systems .....	16
<b>CHAPTER 3 .....</b>	<b>18</b>
<i>WAVELET TRANSFORMS AND ARTIFICIAL NEURAL NETWORKS.....</i>	<i>18</i>
3.1    The Wavelet Transform.....	18
3.1.1 Introduction to Transform .....	18
3.1.2 Wavelets .....	20
3.1.3 Wavelet Transforms.....	23
3.1.4 Scalogram.....	24
3.1.5 Scale and Frequency .....	26
3.1.6 Instantaneous Frequency.....	27
3.1.7 Comparison of Various Transforms.....	28
3.2    Artificial Neural Networks .....	29
3.3    The Artificial Neuron .....	29
3.3.1 Synapses.....	29
3.3.2 Adder.....	29
3.3.3 Activation function.....	29
3.3.4 Threshold .....	30

3.4	Artificial Neural Network Characterization .....	31
3.4.1	Network Architectures .....	31
3.4.2	ANN Learning or Training .....	33
3.4.3	Activation Function .....	34
3.5	Back propagation training algorithm.....	35
3.5.1	Forward pass .....	37
3.5.2	Backward pass.....	38
3.6	Remarks.....	40
<b>CHAPTER 4</b>	.....	<b>41</b>
<i>EXPERIMENTAL SET-UP AND DATA ACQUISITION</i> .....		41
4.1	Brake Test Rig .....	41
4.2	Instrumentation .....	43
4.2.1	Sensor Locations .....	43
4.2.2	Sensors and DAQ Instrument Specifications .....	45
4.3	Data Acquisition, Storage and Display .....	46
4.4	Fault Simulation and Vibration Signature Analysis .....	47
4.4.1	Steady Case .....	47
4.4.2	Transient Case .....	66
4.5	Remarks.....	78
<b>CHAPTER 5</b>	.....	<b>79</b>
<i>NETWORK TRAINING AND FAULT IDENTIFICATION</i> .....		79
5.1	Feature Extraction .....	79
5.1.1	Selection of Features.....	80
5.2	ANN Input Vector Generation .....	92
5.3	Target Vector formation.....	92
5.4	Network Architecture Selection .....	93
5.5	ANN Training and Validation .....	93
5.6	Remarks.....	102
<b>CHAPTER 6</b>	.....	<b>103</b>
<i>CONCLUSIONS AND SCOPE FOR FUTURE WORK</i> .....		103
<i>REFERENCES</i> .....		105
<i>APPENDIX</i> .....		109

# LIST OF FIGURES

---

Figure 1.1 IVHM Scheme .....	3
Figure 1.2 IVHM System: Architecture .....	4
Figure 2.1 Alignments in Wheel: (a) Toe In/ Out, (b) Camber Positive/ Negative.....	10
Figure 2.2 Tree diagram of analysis techniques in time domain .....	14
Figure 3.1: Typical wavelet functions (a) Haar-Wavelet; M=1 (b) Mexican-Hat- .....	22
Figure 3.2: Scalogram of a sample signal. The analysis wavelet used is Haar.....	25
Figure 3.3: Relationship between Frequency and Scale (a) Periodic signal approximation for Mexican-Hat- Wavelet (b) Variation of Frequency with Scale for Mexican- Hat-Wavelet .....	26
Figure 3.4 Comparison of various transforms (a) Time Domain Signal (b) Fourier Transform (c) Short Time Fourier Transform (STFT) (d) Wavelet Transform .....	28
Figure 3.5 Model of a Nonlinear Neuron.....	30
Figure 3.6 Single layer feed forward network .....	32
Figure 3.7 Multi-layer feed forward network.....	32
Figure 3.8 Activation functions.....	35
Figure 3.9 Back-propagation Network architecture .....	36
Figure 4.1 Brake Test Rig .....	42
Figure 4.2 Brake Test Rig- Line Diagram.....	42
Figure 4.3 Sensor Location: Front Wheel .....	43
Figure 4.4 Sensor Location: Rear Wheel .....	44
Figure 4.5 Temperature sensor on Brake Pad .....	44
Figure 4.6 Instrumentation and data acquisition schema .....	46
Figure 4.7 Front Panel: Typical Vibration Signal at 60 Km/h (10 Hz).....	48
Figure 4.8 FFT plots at 90 Km/h (15 Hz) for Brake Caliper Sensor –Front Wheel.....	51
Figure 4.9 FFT plots at 80 Km/h (13 Hz) for Brake Caliper Sensor –Front Wheel.....	52
Figure 4.10 FFT plots at 70 Km/h (11 Hz) for Brake Caliper Sensor –Front Wheel.....	53
Figure 4.11 FFT plots at 60 Km/h (10 Hz) for Brake Caliper Sensor –Front Wheel.....	54
Figure 4.12 FFT plots at 50 Km/h (8 Hz) for Brake Caliper Sensor –Front Wheel.....	55
Figure 4.13 FFT plots at 90 Km/h (15 Hz) for Sensor at Brake drum- Rear Wheel .....	56
Figure 4.14 FFT plots at 80 Km/h (13 Hz) for Sensor at Brake drum- Rear Wheel .....	56
Figure 4.15 FFT plots at 70 Km/h (11 Hz) for Sensor at Brake drum- Rear Wheel .....	57
Figure 4.16 FFT plots at 60 Km/h (10 Hz) for Sensor at Brake drum- Rear Wheel .....	57
Figure 4.17 FFT plots at 50 Km/h (8 Hz) for Sensor at Brake drum- Rear Wheel .....	58
Figure 4.18 FFT plots at 90 Km/h (15 Hz) for Sensor at LB Arm Front Wheel .....	59
Figure 4.19 FFT plots at 80 Km/h (13 Hz) for Sensor at LB Arm Front Wheel .....	60
Figure 4.20 FFT plots at 70 Km/h (13 Hz) for Sensor at LB Arm Front Wheel .....	61
Figure 4.21 FFT plots at 60 Km/h (10 Hz) for Sensor at LB Arm Front Wheel .....	62
Figure 4.22 FFT plots at 50 Km/h (8 Hz) for Sensor at LB Arm Front Wheel .....	63
Figure 4.23 FFT plots at 90 Km/h (15 Hz) for Sensor at Rear Wheel Axle .....	64
Figure 4.24 FFT plots at 80 Km/h (13 Hz) for Sensor at Rear Wheel Axle .....	64
Figure 4.25 FFT plots at 70 Km/h (11 Hz) for Sensor at Rear Wheel Axle .....	65
Figure 4.26 FFT plots at 60 Km/h (10 Hz) for Sensor at Rear Wheel Axle .....	65
Figure 4.27 FFT plots at 50 Km/h (8 Hz) for Sensor at Rear Wheel Axle .....	66
Figure 4.28 Front Panel: Typical Vibration Signal at 60 Km/h (10 Hz) for transient .....	67

Figure 4.29 Time domain data at 30 Km/h for Torque Sensor, Case -1 Full braking (a) Front Wheel, (b) Rear Wheel.....	68
Figure 4.30 Time domain data at 30 Km/h, Case -1 Full braking (a) Front Wheel- LB Arm Accelerometer, (b) Rear Wheel- Axle Accelerometer.....	69
Figure 4.31 Time domain data at 30 Km/h, Case -1 Full braking (a) Front Wheel- Brake Caliper Accelerometer, (b) Rear Wheel- Brake drum Accelerometer.....	70
Figure 4.32 Time domain data at 30 Km/h for Temperature Sensor, Case -1 Full braking (a) Front Wheel, (b) Rear Wheel .....	71
Figure 4.33 dT/dt and Torque curves with braking time at 30 Km/h with Full Braking for Front wheel (a) Healthy system (b) WM- Camber (c) WM-Toe In (d) Wheel Unbalance (e) Brake Lining .....	72
Figure 4.34 dT/dt and Torque curves with braking time at 30 Km/h with Full Braking for Rear wheel (a) Healthy system (b) Wheel Unbalance (c) Brake Lining .....	73
Figure 4.35 Scalogram and Speed vs Time at 30 Km/h with full braking for front wheel (a) Healthy System (b) Wheel Misalignment- Camber (c) Wheel Misalignment – Toe In (d) Wheel Unbalance (e) Brake Lining.....	74
Figure 4.36 Scalogram and Speed vs Time 30 Km/h with full braking for Rear wheel (a) Healthy System (b) Wheel Unbalance (c) Brake Lining .....	75
Figure 4.37 Scalogram and Speed vs Time at 60 Km/h with full braking for front wheel (a) Healthy System (b) Wheel Misalignment- Camber (c) Wheel Misalignment – Toe In (d) Wheel Unbalance (e) Brake Lining.....	76
Figure 4.38 Scalogram and Speed vs Time 60 Km/h with full braking for Rear wheel (a) Healthy System (b) Wheel Unbalance (c) Brake Lining .....	77
Figure 5.1 Fault diagnosis algorithm .....	80
Figure 5.2 Feature extraction: Speed 90 Km/h (a) Brake Pad Sensor (b) LB Arm Sensor .....	82
Figure 5.3 Feature extraction: Speed 80 Km/h (a) Brake Pad Sensor (b) LB Arm Sensor.....	83
Figure 5.4 Feature extraction: Speed 70 Km/h (a) Brake Pad Sensor (b) LB Arm Sensor.....	84
Figure 5.5 Feature extraction: Speed 60 Km/h (a) Brake Pad Sensor (b) LB Arm Sensor.....	85
Figure 5.6 Feature extraction: Speed 50 Km/h (a) Brake Pad Sensor (b) LB Arm Sensor.....	86
Figure 5.7 Feature Extract at 30 Km/h with full braking: (a) LB Arm Sensor (b) Brake Pad Sensor .....	88
Figure 5.8 Feature Extract at 60 Km/h with full braking: (a) LB Arm Sensor (b) Brake Pad Sensor .....	89
Figure 5.9 Feature Extract at 30 Km/h with partial braking: (a) LB Arm Sensor (b) Brake Pad Sensor .....	90
Figure 5.10 Feature Extract at 60 Km/h with partial braking: (a) LB Arm Sensor (b) Brake Pad Sensor .....	91
Figure 5.11 Convergence patterns of various architectures at 90 Km/h .....	95
Figure 5.12 Convergence patterns of various architectures at 80 Km/h .....	96
Figure 5.13 Convergence patterns of various architectures at 70 Km/h .....	97
Figure 5.14 Convergence patterns of various architectures at 60 Km/h .....	98
Figure 5.15 Convergence patterns of various architectures at 50 Km/h .....	99
Figure 5.16 Convergence patterns of various architectures for Transient Case .....	100
Figure 5.17 Plot of minimum error achieved by various network architectures for Steady Case for different speed .....	101
Figure 5.18 Plot of minimum error achieved by various network architectures for Transient Case .....	101

# LIST OF TABLES

---

Table 2.1 Diagnostic Technique in Vibration Analysis .....	17
Table 3.1 Activation Functions for ANN .....	34
Table 4.1 Technical Specification and Mounting location for Sensor .....	45
Table 4.2 Faults simulated for Steady Case .....	47
Table 4.3 Faults simulated for Transient Case.....	67
Table 5.1 Numbering of Faults for Steady Case .....	81
Table 5.2 Numbering of Faults for Transient Case .....	87
Table 5.3 Sample Training sets extracted for one Accelerometer for steady case .....	92
Table 5.4 Sample Training sets extracted for one Accelerometer for Transient Case .....	92
Table 5.5 Sample Target vectors for both Cases .....	93
Table 5.6 Different Architectures simulated for the ANN for the two cases .....	94
Table 5.7 Comparison of various architectures for Steady case at 90 Km/h .....	95
Table 5.8 Sample output for test data for architecture 16-14-12-8.....	95
Table 5.9 Comparison of various architectures for Steady case at 80 Km/h .....	96
Table 5.10 Sample output for test data for architecture 16-14-12-8.....	96
Table 5.11 Comparison of various architectures for Steady case at 70 Km/h .....	97
Table 5.12 Sample output for test data for architecture 16-14-12-8.....	97
Table 5.13 Comparison of various architectures for Steady case at 60 Km/h .....	98
Table 5.14 Sample output for test data for architecture 16-14-12-8.....	98
Table 5.15 Comparison of various architectures for Steady case at 50 Km/h .....	99
Table 5.16 Sample output for test data for architecture 16-14-12-8.....	99
Table 5.17 Comparison of various architectures for transient case.....	100
Table 5.18 Sample output for test data for architecture 40-40-25-8.....	100

# NOMENCLATURE

$C(\tau)$	Cepstrum of a signal
$\Delta$	Sampling period
$\omega_c$	Center frequency of wavelet function
$\Psi$	Fourier transform of the wavelet function
$\psi$	Wavelet function
$f(t)$	Signal function
$Ff(\omega)$	Fourier transform of the signal
$g(t)$	Analysis function of a transform
$M$	Number of vanishing moments of wavelet
$s$	Detail size or scale
$Sf(u, s)$	Short time Fourier transform of the signal
$T(\cdot)$	Transform of a function
$u$	Localized time
$\omega(t)$	Windowing function for short time Fourier transform
$Wf(u, s)$	Wavelet transform of the signal
$Z_x(t)$	Analytic function
$P_\omega f(u, s)$	Scalogram function
$x_{k1}$	Input signal to the neuron
$u_k$	Linear combiner output
$\varphi(\cdot)$	Activation function
$\rho$	Smoothening constant
$\theta_L^h$	Threshold for node L of layer $h$
$y_k$	Output signal of the neuron
$v_k$	Output from the neuron after summation
$w_{ji}^h$	Weight of the layer $h$ from node $i$ to node $j$
$E_p$	Overall mean square error
$\Delta_p w_{kj}^h$	Weight change at layer $h$
$\delta_{pk}^h$	Individual error for input vector p at node k in layer h

$\eta$	Learning rate
$\alpha$	Momentum
$net_{pj}^h$	Net input values to hth hidden layer
$O_{pk}^h$	Output at output units
$f_{m1}$	Motor/ Wheel running frequency
HLF	Healthy System Front
HLR	Healthy System Rear
WM-Camber	Wheel Misalignment due to Camber
WMT	Wheel Misalignment due to Toe-In
WUF	Wheel Unbalance in Front
WUR	Wheel Unbalance in Rear
WWF	Worn Wheel in Front
WWR	Worn Wheel in Rear
BRLF	Brake Lining in front (Brake Pad)
BRLR	Brake Lining in Rear (Brake Shoe)

# CHAPTER 1

## INTRODUCTION

### 1.1 Introduction

An Integrated Health Management System of automotive vehicle is a concept incorporating diagnostic and prognostic tools at the component, sub-system and system levels of the vehicle in an integrated manner [1, 2]. The ambition is to put into service superior health management policy that allows constant monitoring and instantaneous evaluation of vehicle health, to predict remaining life or near breakdown conditions, and to use this information to improve operational decisions and their consistency and system life ([1] and [3] to [5]).

The objective of this project is to develop validated tools for automated detection, and diagnosis that can enable abatement of undesirable events while vehicle is running. Undesirable events may be from system, subsystem, or component faults or failures due to accident, abasement, or environmental hazards. While, the present work is focused on fault diagnosis at the sub-system-level of the automotive vehicle it addresses some relevant condition monitoring issues of the complete vehicle system (Typical Small car on Indian road), as a whole.

IVHM capabilities enable rapid detection and diagnosis of adverse events (in both the hardware and the software) [7], essential to the safe operation of the vehicle and enable estimation of the condition severity and the remaining useful life with confidence bounds for the affected system(s). Maintenance workers, crew, adaptive configuration systems and other control systems can take advantage of the estimated remaining useful life to enhance the safety profile of the vehicle.

Developing the real-time automated reasoning and decision making tools and techniques to integrate messages from the health management systems of individual test

rig/vehicle(s) and combining them with results from analysis of wide vehicle health assessments is a critical challenge.

Integrated vehicle health management (IVHM) concept embraces an integration of sensors, communication technologies, and artificial intelligence to provide vehicle-wide abilities to diagnose problems and recommend solutions.

Vibration Analysis of the collected data has proven to be a powerful tool in assessing the health of a system. Vibration analysis with appropriate instrumentation can provide reliable knowledge of machine condition. It allows relatively inexpensive repair on a pre-scheduled controlled basis in comparison to catastrophic failure whose repair may cost much more in terms of money and time.

There is requirement of reliable data analysis and decision making while carrying out fault diagnosis based on vibration measurements.

The present work focuses on the Braking System of a typical small Indian Family Car. A test-rig developed for this exercise has been employed for fault simulation and data generation, Vibration, speed and temperature signatures obtained from the test-rig are processed to develop a Neural Network based diagnosis scheme. Signal processing is done through Fast Fourier Transforms for Steady state signals, while Wavelet technique is deployed for Transient conditions.

## 1.2 Current state of the Art

### 1.2.1 IVHM

An IVHM system includes logistics management, Hess et al [4, 8]. It requires accessibility of continuously updated and thorough vehicle health information to start the logistic actions. Such IVHM systems are known to exist for aerospace vehicles, typically in the US Joint Strike Fighter (JSF) aircraft. Automotive manufacturers have been increasingly, interested in developing similar IVHM strategies for road vehicles.

Baroth et al [10] and Vachtesvanos et al [11] have proposed that new vehicles should be equipped with latest technology-based intelligence system that should provide more informed decisions on handling, maintenance, design and support.

Schmalzel et al [13] have discussed various hurdles faced by IVHM technologies in implementation at vehicular level. However, an intensive and harmonized research program could deal with many of these barriers.

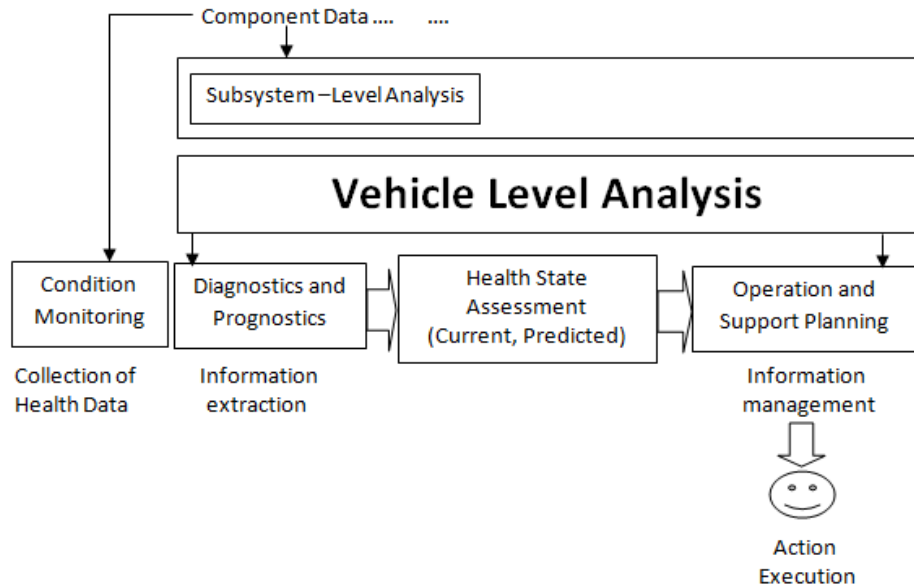


**Figure 1.1 IVHM Scheme**

Figure 1.1 shows the strategy of an IVHM system. Healthy data are acquired from vehicle system, subsystem and used to formulate diagnoses and prognoses of the vehicle for present and future health. Extracted information is then further processed to devise suitable action and is offered to the individuals who should make a decision and carry out the actions.

## Development of the IVHM Notion

IVHM was initially used in the aerospace sectors. Bird et al [9], Baroth et al [10], Ofsthun et al [14], and Scandura et al [19] recommended that similar IVHM technology can be implemented in other types of vehicle such as automobile, military vehicle, land vehicles and marine vehicles.

IVHM was initially gestated by NASA. The first written report was found in 1992, entitled ‘Research and Technology Goals and Objectives for IVHM’ [15]. It was stated that IVHM is uppermost priority technology for upcoming NASA space transportation systems.

The notion of IVHM is said to have its beginning in 1970s [6, 15], even though there is no confirmation of this in the literature of those years. The article on this technology has been primarily appeared in 1990s. IVHM grew gradually during 1997–98, reached its peak during 2001-02 and then has been experiencing steady activities, thereafter.

## Technology principles for IVHM systems

Architecture of an IVHM system has shown in Figure 1.2 First move is the use of sensors to measure state awareness variables that are indicative of potential failure modes. Apart from the conventional sensors (e.g. torque, tachometer, and temperature) sensor devices that are exclusively adapted to health management applications (e.g. accelerometers, acoustic emission sensors, strain gauges, and proximity devices) can be used for monitoring and control [20]. Similarly, the accessibility of an explicit protocol is nurturing an exhaustive use of wireless sensor networks, which make sure speedy and precise information transfer with enormous space savings [11, 21].

A few examples of this application are available in the literature. Some initiative has been recently undertaken in various manufacturing sectors too; so far these systems are in evolution stage. Baroth et al. [10] give outline of this most important application in the automotive, military, commercial aviation and space sectors.

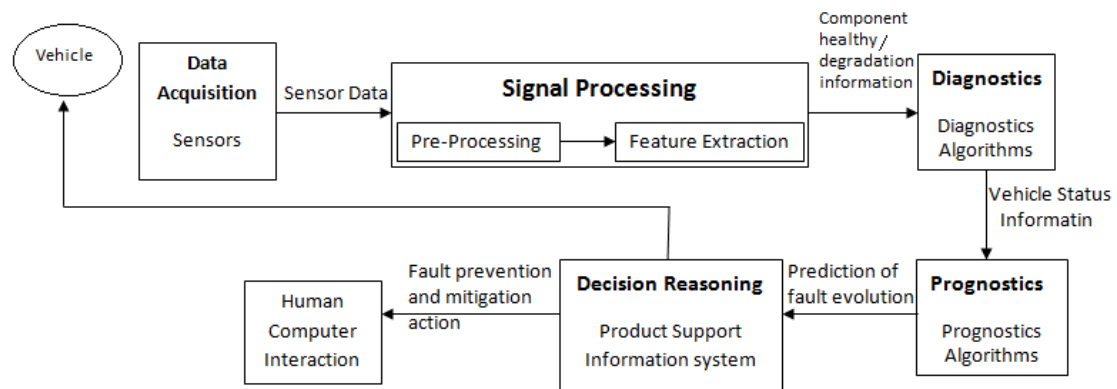


**Figure 1.2 IVHM System: Architecture**

### 1.2.2 Wavelet Analysis

FFT is one of the popularly used and well-established methods of Signal Processing. However, methods based on FFT are not appropriate for transient signal analysis and they are not capable of revealing all inherent information from the transient signals. Generally, these transient components contain enormous information about machine faults. Time–frequency analysis is extensively used method for the analysis of transient signals, like Wigner–Ville distribution (WVD) [23] and the short time Fourier transform [24] (STFT). These time–frequency analysis methods experience various problems. WVD gives good concentration in the time–frequency plane, but interference terms can be seen in time–frequency plane though, support areas of the signal do not overlap with each other. Without exemption, however, abolition of one shortcoming will always lead to the loss of other merits. For example, the reduction of interference terms will bring the loss of time–frequency concentration [25]. The difficulty with STFT is that it gives constant resolution for all frequencies as it uses the similar window for the analysis of the whole signal, which means if someone wishes for a good frequency resolution using wide windows, as is required for the analysis of low-frequency components, he/she would not be able to obtain good time resolution (narrow window), which is required for the analysis of high-frequency components. Therefore, the STFT is appropriate for the quasi-stationary signal analysis.

Coifman, Wickerhauser and Meyer, developed the wavelet package in 1992, which was a normal expansion of the MRA. Different from the STFT, the wavelet transform can be used for multi-scale analysis of a signal by dilation and translation; as a result it can extract time–frequency features of a signal successfully. Hence, the wavelet transform is appropriate for the analysis of transient signals [25]. Wavelets have obtained immense success in machine fault diagnostics for its numerous unique advantages, not only for its capability in the analysis of non-stationary signals.

In early 1990, Leducq [26] had used wavelet to analyze the hydraulic noise of the centrifugal pump. In 1993, Wang and McFadden [27] applied wavelet to analyze the gear vibration signals, and found that it is capable of identifying the incipient mechanical failure. Newland, in 1994, published a number of papers [28–31], in which the wavelet

transform was introduced systematically and the basic theory, the methods and application examples on the use of the wavelet for vibration signal analysis were specified. Furthermore, he proposed a new wavelet—harmonic wavelet and discussed its properties and applications. In 1999, he used the harmonic wavelet to identify the ridge and phase of the transient signals effectively [32]. Newland's work made the wavelet popular in engineering applications, especially for vibration analysis; and later on, the wavelets prevailed in the machine fault diagnostics. Boulahbal et al. [33] used the scalogram on the residual vibration signal of gears. Some unique features of the cracked tooth were obtained and the accurate position of a crack was detected. Adewusi et al [34] observed the start-up and steady-state vibration signals of the rotor with a propagating transverse crack by scalograms and space-scale energy distribution graphs. Peng et al. [35] analysed three kinds of typical faults: rub-impact, oil whirl and coupling misalignment, which frequently take place in rotating machinery, by scalograms. More research on the rub-impact in the rotor system was passed out with scalograms and wavelet phase spectrums [36].

### **1.2.3 Artificial Neural Network**

ANN has been attracting the interest of scientists and technologies for long. McCulloh and Pitts formulated the formal definition of a synthetic neuron model based on biological model in 1943. Psychologist Frank Rosenblatt invented the first artificial neural network in 1958. Afterwards, it was realized that pattern recognition and learning capabilities of artificial neural networks approved them to deal with several problems that were very difficult to solve by standard computational and statistical methods. Standard algorithms fail to deal with noise and incomplete data available in real life. But ANN can handle such problem because of its capability to learn to on its own. Though, neural networks require great amount of computation because of its extremely parallel distributed processor. Non-availability of fast and affordable computing power had limited the growth of ANN applications till the last decade of twentieth century. But in recent years ANN is being widely used in gear and bearing fault diagnosis because of advancement in computing technologies. Vyas *et al* [37] made use of shore's [38] knowledge base to train back-propagation and probabilistic Neural Networks to identify

rotor faults, whereas McCormick et al [39] have done real-time fault classification of rotating machinery using artificial neural networks. Abu-Mahfouz [40] has done comparative study of three artificial neural networks for the detection and classification of gear faults. Singh [41] has used frequency domain based features of vibration signature to train the neural network for prediction of geared rotor faults.

The work on development of integrated health management of automotive vehicle on condition-based vibration monitoring for the brake test rig can be divided into following phases.

- a) Phase one: includes collection of relevant vibration data and other operating parameters using on board sensors and conditioning them online.
- b) Phase two: consists of feature identification from measured signals.
- c) Phase three: Use of knowledge-based systems to identify the reasons for departures from normal behaviour.

Artificial Neural Networks (ANN) is instrumental in the phase three of monitoring strategy. Artificial Neural Networks offer an efficient platform for condition monitoring strategies in machinery and plants where the number of components and processes are too many and complex to be mathematically modeled appropriately. Vibration parameters like amplitude, frequency and direction, etc. are widely accepted indicators of the health of a rotating machine. Once trained, the neural network has a small computational cost, which allows real time condition monitoring at reasonably low costs.

The emphasis in the present study has been towards simulating faults for the quarter car model of a standard vehicle on the brake test rig for steady and transient condition. Patterns of the signals obtained for faults are very similar to each other so a foolproof algorithm is required to extract the exact features of these faults so that the details are not missed. Total of eight faults were simulated and classification was carried out using the above procedure.

An effort has been made to integrate techniques of Artificial Neural Networks with Virtual Instrumentation hardware and software to carry out experimental investigation on Brake test Rig for fault identification. The rig is used to simulate a variety of vehicle

faults in a phased manner. Vibration signals are picked up from various sensors located on the test rig. In the present case accelerometer sensors have been used. LabVIEW 10.0 software has been employed for online data acquisition and displaying time domain data. Fast Fourier Transformations and frequency domain display is carried out by developing a Virtual Instrument in LabVIEW 10.0 for steady case. Wavelet transform (Scalogram) of the transient signal has been carried out in MATLAB R2011a. Feature extraction from the frequency domain data (for Steady case) and Scalogram (Wavelet transform of transient signals) has been carried out in MATLAB R2011a respectively. Artificial Neural Network (ANN) training was carried using toolbox available in MATLAB R2011a.

#### **1.2.4 Thesis Organization**

Chapter 2 gives a brief insight into commonly occurring faults in automotive vehicle and available techniques of fault diagnosis.

Chapter 3 covers the Wavelet transform and the important features of Artificial Neural Networks.

Chapter 4 discussed the experimental set-up, data acquisition and results obtained for steady and transient case.

Chapter 5 covers the aspects of feature extraction, network training and validation.

Chapter 6 covers conclusions and scope for future work.

# CHAPTER 2

## VIBRATION FAULT DIAGNOSIS

Components of braking system and wheels of an automobile continuously encounter severe vibrations due to application of brake and waviness present on the road. Subjected to rigorous working conditions, they are prone to damage. Most commonly problems like wheel unbalance, wheel misalignments, brake-pad wear etc occur in the brake system of a vehicle. Vibration signatures obtained from the faulty system of the quarter car model in the test rig reflects clear variation from normal behaviour due to introduction of any fault.

### 2.1 Common Faults in Vehicle

Commonly occurring faults in automotive wheel and brake systems are Wheel Unbalance, Wheel Misalignment due to Camber and Toe, Wheel Wobble, Wheel Bearing faults, Brake Fade, Braking Pressure in the hoses etc. These are discussed in the succeeding sections along with the causes and possible symptoms.

#### Wheel Unbalance

Unbalance in wheels arises due to eccentricity of wheel and tire; that may cause the entire vehicle to vibrate excessively. If on checking, eccentricity is not found, the defect may be due to incorrect tire pressure, statically unbalanced wheels or statically unbalanced brake drum. This in turn may cause excessive wear in bearings, bushings, and substantially reduce their service life. Vibration due to unbalance prominently occurs at a frequency equal to the wheel speed. Unbalance can be identified by driver/ passenger(s) through vibration inside the vehicle, even on good road surface conditions. It can also be identified by vibrations felt over steering wheel i.e. wheel shimmy. Unbalance arises mainly due to manufacturing defects in wheels/ tires, or passing of the vehicle over bumps (or ditches) frequently or due to running of the vehicle continuously on badly conditioned road surfaces. Vehicle suspensions get excited by unbalance forces when the rotating speed of the wheel equals the suspension's resonant frequency.

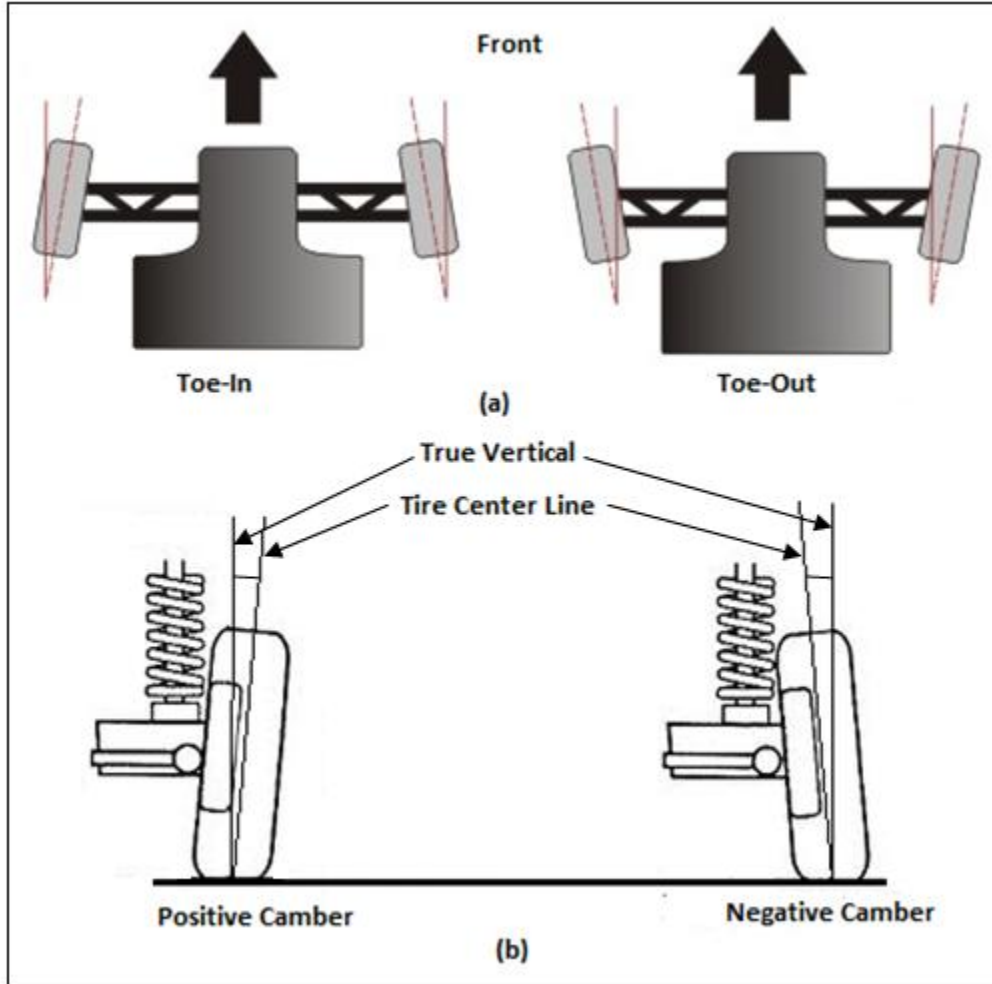


**Figure 2.1 Alignments in Wheel: (a) Toe In/ Out, (b) Camber Positive/ Negative**

## Wheel Alignment

### Toe-in/ Toe-out

Misalignments of wheels in the vehicles are one of the most common problems that occur frequently. Misalignment is present in almost every vehicle because as a limited misalignment is also desirable and given intentionally in the wheel. However, beyond specified limits misalignments are not permissible for longer durations. Limited wheel misalignment is required for stability and control of the vehicle while in motion. In the event wheels are pointing inward misalignment is termed as Toe-In, whereas if they are pointing outward they are said to have Toe-Out as shown in Figure 2.1(a). Both these situations are undesirable because in either case while rolling forward, each wheel will be simultaneously slipping laterally, due to which a continuous cross-tread scrubbing would

take place. Thus the result of the net toe-in or toe-out of the wheels during running is excessive tread wear, heavy steering, greater fuel consumption, driver lost control over the vehicle i.e. at normal speed/ high speed when driver leave steering wheel, vehicle automatically tends to go left or right, even when driver do not leave wheel.

### **Camber**

Camber is the tilt of the car wheels from the vertical as shown in Figure 2.1(b). Camber is positive if the tilt is outward at the top, whereas it is negative if the tilt is inward. It is desirable that tire should roll on the ground vertically so that the wear is uniform. If while running, the tires are inclined from the vertical either inward or outward, they will wear more on one side than the other. In case of positive camber, as the vehicle turns, the outside suspension tends to rise on the wheel. When the wheel returns to straight ahead position, the weight of the vehicle press down on the steering axis and this helps straighten the wheel. Thus positive camber increase straight-ahead stability. A positive camber causes the wheel to toe-out. Therefore if the camber on the two front wheels is not equal, the vehicle will try to pull towards the side where the camber is higher.

Misalignment can be due to Camber or Toe or due to combined presence. Alignment angle changes over the time, due to wear and tear of normal every day driving. This needs to be checked periodically and corrected when necessary.

### **Wheel Wobble**

Oscillation of the front wheel at low speeds is called wheel wobble (Low speed shimmy). This is generally due to dynamic unbalance of the wheel assembly, which may have developed due to unevenly worn tires, incorrect balance weights fitted to the wheel, worn out ball joints, or may be due to incorrect/ uneven camber. The oscillation of the front wheels at high speed is called high speed shimmy. Apart from dynamic unbalance it may cause due to buckled wheel rim, worn out or loose front wheel bearings, incorrect toe-in and may be due to uneven tire pressure.

## Bump-Steer

Bump Steer occurs when the length of the tie rod is not correct or it is installed at an incorrect angle. The outer tie rod end moves up and down whenever the suspension compresses and extends. If either the length or angle of tie rod is incorrect, it would pull or push the steering arm, which would turn the wheel in a new direction. This is felt prominently when the steering load jerks to a side as the vehicle goes over a bump or ditch and is called bump-steer or toe-change.

## Brake Faults

The main defects that are caused in the braking system of automobile vehicle are:

### **Brake Fade**

With prolonged application of brakes, their effectiveness decreases. This is called fading of brakes. This happens on account of reversible changes in the friction properties of the brake linings on account of high temperatures produced due to prolonged application. It may be due to use of deteriorated brake fluid, poor contact between brake lining and drum.

### **Loss of Braking Efficiency**

This may cause due to leakage of brake fluid from wheel cylinder into the brake drum and soaked by the brake lining, presence of air in the brake hoses, smooth worn brake lining, and distorted brake shoe or due to defective master cylinder.

### **Brakes overheating**

The overheating of the brakes is most likely due to the same reasons as for brakes fade. Apart from these, this may occur due to prolonged use of brakes while descending a hill. In case of disc brakes apart from the above, overheating may be due to seized piston of the caliper.

### **Grabbing Brakes**

If the brakes are too sensitive to actuation on application of slightest pedal pressure, they are called Grabbing Brakes. This may be due to greasy brake lining or the brake fluid that

may have leaked on them, improper shoe adjustment, scoured brake drum, charred brake lining, or may be due to presence of dirt/ dust in brake shoe assembly.

## 2.2 Vibration Analysis as a Predictive Maintenance Tool

Different maintenance regimes are followed in various industries as per the requirement to keep the downtime of the machines as low as possible. These maintenance techniques can be broadly classified in the following manner

- a) Corrective Maintenance involves replacement of defective parts of a machine once it has been observed to function irregularly. This technique is also commonly referred to as Breakdown Maintenance and can only be used for non-critical machinery.
- b) Preventative Maintenance with plant downtime becoming more expensive, a failure could be quite expensive in lost production time, and thus preventative maintenance evolved. This involves regular inspections and overhauls at predetermined intervals. An efficiently planned preventive maintenance program can be quite effective in discovering the faults in a machine before they reach a terminal state. The main drawback of this method is machines are overhauled while they are still in good condition, and it turns out to be an expensive method. This is also sometimes referred to as PPM (Planned Preventive Maintenance).
- c) Predictive Maintenance with the development of condition monitoring techniques, methods were available to determine the actual condition of the machine, and even calculate the time to failure. This enables planners to overhaul a machine when it needed it, and to concentrate on the problem areas. This is known as predictive maintenance.

Predictive Maintenance has gained special emphasis in past decade or so. Some of the benefits from a predictive maintenance program are: (i) early warning of problems allows correction without overtime, with minimal impact to production, and without high expediting costs to procure replacement parts; (ii) elimination of unexpected failures which create extensive, costly repairs and expensive loss of production, whereas early correction would have been inexpensive; (iii) effective scheduling of the maintenance workforce during outages to concentrate on the equipment most in need of repair; (iv)

extended maintenance intervals for those machines with healthy vibration signatures; (v) isolating the cause of problems without resorting to shot gunning of the solution; (vi) no capital expenditure or staff involvement is necessary - we do everything required; (vii) no modification to machines or disruption to production.

## 2.3 Diagnostics Techniques

The clear advantages offered by the applications of the Condition Monitoring approach has in recent times led to development of vast number of techniques. These can be broadly classified as described below.

### 2.3.1 Time Domain or Wave Form Analysis

Time domain signal is an unprocessed record of the vibration as picked up from a transducer. If understood properly, it can yield enormous amount of information. A serious limitation is that it can be too complex for analysis if excessive noise, signal modification or several frequencies are present. Further analysis is generally carried out so that some characteristics not observed visually are highlighted.

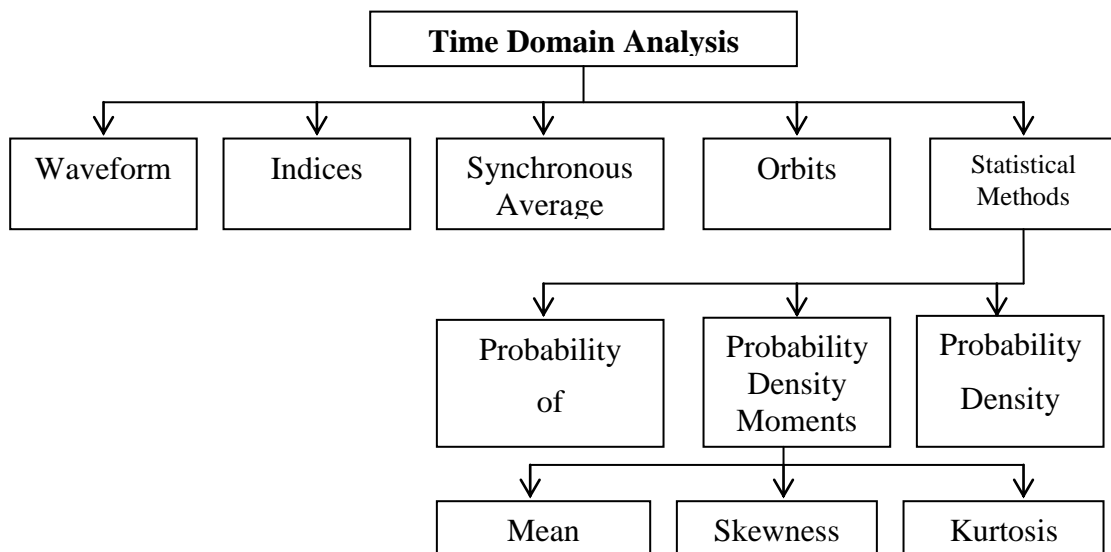


**Figure 2.2 Tree diagram of analysis techniques in time domain**

Several techniques have been proposed or have been used in Condition Monitoring as shown in Figure 2.2. Wave form analysis are useful in identifying beats and vibrations that are non synchronous with shaft speeds. Indices have been used to quantify the time

signal. They are (i) the peak level (ii) root mean square (rms) level and (iii) the crest factor. In addition, various other statistical parameters can be extracted from the time histories of the noise and vibration signals. However, the time domain data is normally too difficult to analyze as signals are not always periodic and are mostly polluted by noise. Noise can be reduced by signal conditioners but cannot be eliminated altogether. Time between events represents the frequency component specific to the machine.

### **2.3.2 Frequency Domain**

DFT (Digital Fourier Transform) or the FFT (Fast Fourier Transform) of the line waveform have become the most popular method of deriving the frequency domain signal. The information on frequency, phase and amplitude of the component sinusoids is obtained from the DFT or FFT. The FFT spectrum of a signal can be obtained by standard digital algorithms. Vibration signals of rotating machinery mainly comprise of peaks at the machine's rotating frequency (RF) and its harmonics (2xRF, 3xRF, 4xRF). The magnitudes of some of these peaks vary considerably in presence of faults. For example, the spectrum of a machine with mass unbalance will normally show a clear peak at the rotating frequency, while in a misaligned machine the second harmonic of the rotating frequency is usually particularly excited. Other types of peaks that can be observed in the frequency domain are side bands of the bearing defect frequencies with the rotating frequency. The appearance of side bands in the power spectrum is an effect of the modulation of a signal with frequency  $f_1$  by another signal with frequency  $f_2$ . If the periodic signal  $\cos(2\pi f_1)$  is modulated by the signal  $\cos(2\pi f_2)$ , the resulting signal will be  $\cos(2\pi f_1) \cos(2\pi f_2)$ . The power spectrum of such a signal consists of two peaks at frequencies  $(f_1 + f_2)$  and  $(f_1 - f_2)$ .

### **2.3.3 Quefrency Domain**

Quefrency is the abscissa for the cepstrum which is defined as the spectrum of logarithm of power spectrum. It is thus the spectrum of a spectrum, and has certain properties that make it useful in many types of signal analysis. It is used to highlight periodicities that occur in the spectrum in same manner as spectrum is used to highlight periodic components occurring in the time domain signal. If a spectrum contains several sets of sidebands or harmonic series, they can be confusing because of overlap. But in the

cepstrum, they will be separated in a way similar to the way the spectrum separates repetitive time patterns in the waveform. The cepstrum is closely related to the auto correlation function. The word cepstrum was coined by reversing the first syllable in the word spectrum. The cepstrum exists in a domain referred to as quefrency (reversal of the first syllable in frequency) which has units of time.

The real cepstrum of a digital signal  $x(n)$  is defined as:

$$c(n) = \frac{1}{2\pi} \int_{-\pi}^{\pi} \ln |X(\omega)| e^{j\omega n} d\omega \quad (2.1)$$

and the complex cepstrum is defined as:

$$\hat{x}(n) = \frac{1}{2\pi} \int_{-\pi}^{\pi} \ln |X(\omega)| e^{j\omega n} d\omega \quad (2.2)$$

where the complex logarithm is used:

$$\hat{x}(\omega) = \ln X(\omega) = \ln |X(\omega)| + j\theta(\omega) \quad (2.3)$$

$$\theta(\omega) = \arg(X(\omega)) \quad (2.4)$$

Power cepstrum analysis is generally used as a complementary tool to spectral analysis. It helps identify items, which are not readily identified by spectral analysis. Its main limitation is that it tends to suppress information about the overall spectral content of a signal, spectral content, which might contain useful information in its own right. It is thus recommended that cepstrum analysis always be used in conjunction with spectral analysis. Another type of cepstrum, which is sometimes used in signal analysis, is the complex cepstrum. The complex cepstrum is defined as the inverse Fourier transform of the logarithm of the forward Fourier transform of a time signal.

### 2.3.4 Expert Systems

Conventional manual trend checking methods and diagnosing often require human experts to analyze the vibration signature. In Expert Systems attempt is made to develop an algorithm on the basis of human expertise, which is available. These are often considered to be one of the most popular applications of artificial intelligence (AI). Knowledge base is the most important part of any expert system. It is stored in the form of facts and rules. The facts are termed as deep knowledge and rules are simply the

heuristics. The knowledge is controlled by an inference engine, which interacts with the user and the knowledge base according to the rules contained in it. Since the knowledge or data in most cases may be incomplete or uncertain, the models employ probabilistic reasoning technique such as Bayes's rule, fuzzy logic, Dempster-Shafer calculus etc. Table 2.1 gives a summary of the common diagnostic tools for rotating machinery.

**Table 2.1 Diagnostic Technique in Vibration Analysis**

Technique	Domain	Use	Description	Instrument Type
Time-domain analysis	Time	Modulation, Pulses, Phase, Truncation, glitch	Amplitude versus time	Analog and digital oscilloscope, FFT spectrum analyzer
Orbital analysis	Time	Shaft motion, sub-synchronous whirl	Relative displacement of rotor bearing in X, Y directions	Digital vector filter, Oscilloscope
Spectrum analysis	Frequency	Direct frequencies, natural frequencies, sidebands, beats, sub-harmonics, sum and difference frequencies	Amplitude versus frequency	FFT spectrum analyzer
Cepstrum analysis	Quefrency	Sideband and harmonic frequency measurement, accurate quantification of sideband and harmonic severity.	Inverse Fourier transform of logarithmic power spectrum	FFT spectrum analyzer

The work carried out in this thesis is based on Artificial Neural Network techniques, which are described in the next chapter.

# CHAPTER 3

## WAVELET TRANSFORMS AND ARTIFICIAL NEURAL NETWORKS

### 3.1 The Wavelet Transform

A signal processing method that can detect changes in levels of vibration is an essential part of any fault diagnostic process. The most widely used conventional method is Fast Fourier transforms. Wavelet transform is relatively a new tool when it comes to signal processing for fault identification. The concept of wavelet transform is also not very old. It replaces the Fourier transform's sinusoidal waves by a family generated by translations and dilations of a window called a wavelet. Haar, Morlet, Symlet and Coiflet are few examples of wavelet functions. They have advantages over traditional Fourier methods in analyzing physical situations where the signal contains discontinuities and sharp spikes. In the proceeding sections the wavelet transform is described. The chapter begins with an introduction to transforms in general followed by details of the wavelet transform.

#### 3.1.1 Introduction to Transform

A signal can be represented by a function  $f(t)$  depending on time. All the mathematical transforms try to transform  $f(t)$  into a representation, which incorporates the desired information about the signal as compactly as possible. The Fourier transform supplies information about the contribution of certain frequencies to the signal, the wavelet transform indicates whether the details of a certain size are present in the signal and quantifies their respective contributions.

All the transforms are based on a common principle: The signal is multiplied with a certain analysis function and integrated about the time domain

$$Tf(\gamma) = \int_{-\infty}^{+\infty} f(t) g^*(t) dt, \quad (3.1)$$

where  $g(t)$  is analysis function and  $*$  denotes complex conjugate. It is the analysis function that classifies the transform. For the Fourier transform

$$g(t) = e^{j\omega t} \quad (3.2)$$

Thus, the Fourier transform of any signal can be defined as

$$Ff(\omega) = \int_{-\infty}^{+\infty} f(t)e^{-j\omega t} dt \quad (3.3)$$

The power of standard Fourier transform is that it allows the decomposition of the signal into individual frequency components and establishes the relative intensity of each component. The energy spectrum does not tell us the occurrence of those frequencies in time. It is not possible to localize the appearance of frequency in time. In this context, the Short Time Fourier Transform (STFT), or Windowed Fourier Transform (WFT) is introduced for the localization of frequency in time  $u$ . The STFT looks for the appearance of frequency  $\omega$  at a certain time. The corresponding analysis function for STFT is written as

$$g_{u,\omega}(t) = e^{j\omega t}\omega(t-u) \quad (3.4)$$

Thus, STFT for any signal can be defined as

$$Sf(u, \omega) = \int_{-\infty}^{+\infty} f(t)e^{-j\omega t}\omega(t-u)dt \quad (3.5)$$

Here,  $\omega(t-u)$  is translation of  $\omega(t)$ , which is a window function, to a time  $u$ . The window function is usually centered about the origin. The transformed signal is a function of  $u$  and  $\omega$ . Thus, the transform provides not just the global information about the appearance of frequency, but in addition the time of this appearance. However, there occur many signals whose content is changing so rapidly that it is difficult to find an appropriate short time window. Also, decreasing time window so that one may locate events in time reduces frequency resolution. Hence, there is an inherent trade-off between time and frequency resolution. Zooming into very tiny signal details (high frequencies) in a small neighborhood of time is not supported by STFT.

The wavelet transform has such zooming property. It looks for detail sizes  $s$  at a certain time  $u$ . The corresponding analysis function for wavelet transform is written as

$$g_{u,s}(t) = \frac{1}{\sqrt{s}}\psi\frac{(t-u)}{s} \quad (3.6)$$

Thus, Wavelet transform for any signal is defined as

$$Wf(u, s) = \int_{-\infty}^{+\infty} f(t) \frac{1}{\sqrt{s}} \psi^* \frac{(t-u)}{s} dt \quad (3.7)$$

The analysis function here is formed by translating and scaling the wavelet function  $\psi(t)$ . This wavelet function is also known as mother wavelet or simply wavelets.

### 3.1.2 Wavelets

Wavelets are small oscillatory waves. They serve as analysis functions for the wavelet transforms. Mathematically, wavelets are defined as a class of functions used to describe any function in space and scale. A wavelet function  $\psi(t)$  is a real or complex valued continuous time function satisfying the following conditions:

**Zero Mean** The wavelet function integrates to zero, i.e.

$$\int_{-\infty}^{+\infty} \psi(t) dt = 0 \quad (3.8)$$

**Square Integrable** The wavelet function has finite energy, i.e.

$$\int_{-\infty}^{+\infty} |\psi(t)|^2 dt < \infty \quad (3.9)$$

#### Admissibility Criterion

$$C_\psi = \int_0^{+\infty} \frac{|\Psi(\omega)|^2}{|\omega|} d\omega < \infty \quad (3.10)$$

where,  $\Psi(\omega)$  is the Fourier transform of  $\psi(t)$ .

Condition 1 suggests that the function  $\psi(t)$  will oscillate around the t-axis, since the contribution of positive and negative function values to the total area, bounded by the function graph and the t-axis, must cancel each other.  $\psi(t)$  being a finite energy function, for  $t \rightarrow \pm\infty$  the function will decrease more rapidly. The function satisfying these two conditions is termed as *mother wavelet*. The admissibility condition is useful in formulating simple inverse wavelet transform.

Thus, in contrast to sinusoidal functions (used in Fourier transforms), wavelets have wavy appearance. Moreover, wavelets generally have a finite duration of support, as opposed to sinusoids which are supported for an infinite duration. For example,

Daubechies 4 wavelet (db4) is a compactly supported wavelet. It is possible for a wavelet to have infinite support duration, as in case of Morlet wavelet.

### 3.1.2.1 Construction of wavelets

Consider a function  $f(t)$  with  $M$  vanishing moments, i.e.

$$\int_{-\infty}^{+\infty} \psi(t) t^m dt = 0 \quad (m = 0, 1, \dots, M-1) \quad (3.11)$$

Let  $F(f(t))$  be the Fourier transform of  $f(t)$  given by

$$F(f(t)) = f(\omega) = \int_{-\infty}^{+\infty} f(t) e^{-j\omega t} dt \quad (3.12)$$

It can be shown that

$$F(f(t)t^m) = j^m \frac{d^m F(\omega)}{d\omega^m} \quad (3.13)$$

$$F\left(\frac{d^M f(t)}{dt^M}\right) = (j\omega)^M F(\omega) \quad (3.14)$$

Consider  $\phi(t)$  as a piecewise smooth function and  $M$  times differentiable. To construct wavelets with  $M$  vanishing moments, define the wavelet  $\psi(t)$  as

$$\psi(t) = \frac{d^M \phi(t)}{dt^M} \quad (3.15)$$

Then, from equations (3.14) and (3.15)

$$F(\psi(t)) = F\left(\frac{d^M \phi(t)}{dt^M}\right) = (j\omega)^M \Phi(\omega) = \Psi(\omega) \quad (3.16)$$

Then,

$$F(\psi(t)t^m) = j^m \frac{d^m (j\omega)^M \Phi(\omega)}{d\omega^m} \quad (m = 0, 1, \dots, M-1) \quad (3.17)$$

Any moment integral can be written as

$$\int_{-\infty}^{+\infty} \psi(t) t^m dt = \int_{-\infty}^{+\infty} \psi(t) t^m e^{-j\omega t} dt \quad (3.18)$$

It is identical to Fourier transform of  $\psi(t)t^m$ , evaluated at  $\omega = 0$ . Therefore,

$$\int_{-\infty}^{+\infty} \psi(t) t^m dt = \left| j^m \frac{d^m (j\omega)^M \Phi(\omega)}{d\omega^m} \right|_{\omega=0} \quad (m = 0, 1, \dots, M-1) \quad (3.19)$$

If  $\Phi(0)$  and derivatives  $\Phi'(0), \Phi''(0), \dots, \Phi^{M-1}(0)$  exist and are finite,

$$\left| \frac{d^m(j\omega)^M \Phi(\omega)}{d\omega^m} \right|_{\omega=0} = 0 \quad (m = 0, 1, \dots, M-1) \quad (3.20)$$

Thus, it is established from equations (3.18) and (3.20) that  $\psi(t)$  has vanishing  $M$  moments, i.e.

$$\int_{-\infty}^{+\infty} \psi(t) t^m dt = 0 \quad (m = 0, 1, \dots, M-1) \quad (3.21)$$

#### The Haar-Wavelet: M=1

Consider

$$\phi(t) = \begin{cases} t & 0 \leq t \leq \frac{1}{2} \\ 1-t & \frac{1}{2} \leq t \\ 0 & \text{else} \end{cases} \quad (3.22)$$

The wavelet with one vanishing moment is known as Haar-wavelet and is defined as

$$\psi(t) = \frac{d\phi(t)}{dt} = \begin{cases} 1 & 0 \leq t \leq \frac{1}{2} \\ -1 & \frac{1}{2} \leq t \\ 0 & \text{else} \end{cases} \quad (3.23)$$

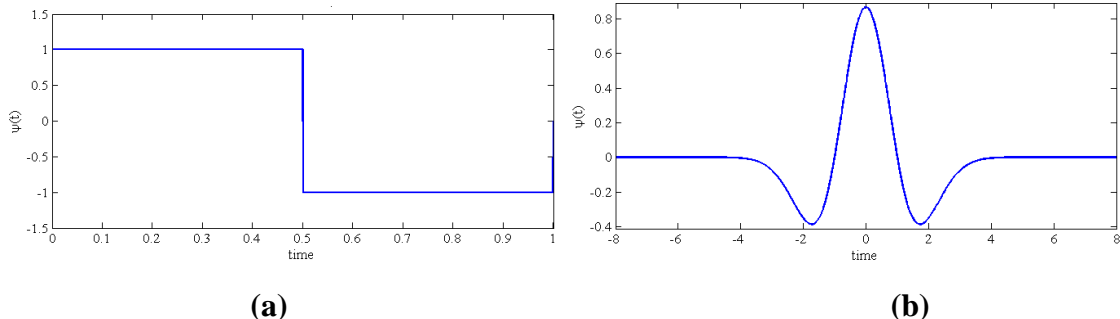


**Figure 3.1: Typical wavelet functions (a) Haar-Wavelet; M=1 (b) Mexican-Hat Wavelet; M=2**

The vanishing moment condition becomes

$$\int_{-\infty}^{+\infty} \psi(t) dt = 0 \quad (3.24)$$

A typical plot of Haar-wavelet is shown in Figure 3.1(a).

### The Mexican-Hat-Wavelet: M=2

For Mexican-Hat-wavelet

$$\phi(t) = -\frac{2}{\sqrt{3}}\pi^{-\frac{1}{4}}e^{\frac{-t^2}{2}} \quad (3.25)$$

The wavelet with two vanishing moments is known as Mexican-Hat-Wavelet and is defined as

$$\psi(t) = \frac{d^2\phi(t)}{dt^2} = -\frac{2}{\sqrt{3}}\pi^{-\frac{1}{4}}(1-t^2)e^{\frac{-t^2}{2}} \quad (3.26)$$

The vanishing moment condition becomes,

$$\int_{-\infty}^{+\infty} \psi(t) t dt = 0 \quad (3.27)$$

A typical plot of Mexican-Hat-wavelet is shown in Figure 3.1**Error! Reference source not found.**(b).

The vanishing moments condition plays an important role in selection of wavelet function for any signal while computing continuous wavelet transform. A signal can be well modeled by piecewise polynomial of certain degree  $n$ . The continuous wavelet transform for any polynomial will be zero if the number of vanishing moments (for the chosen wavelet)  $M < n$ . Thus to capture any change in signal (which means change in polynomial), the wavelet  $\psi(t)$  must have sufficient number of vanishing moments.

### 3.1.3 Wavelet Transforms

#### *Definition*

The wavelet transform of any square integrable function  $f(t)$  with respect to a wavelet  $\psi(t)$  is defined as

$$Wf(u, s) = \langle f, \psi_{u,s} \rangle = \int_{-\infty}^{+\infty} f(t) \frac{1}{\sqrt{s}} \psi^* \frac{(t-u)}{s} dt \quad (3.28)$$

where  $u$  and  $s$  are real. Thus, the wavelet transform is a function of two variables. The transform can also be written as

$$Wf(u, s) = \int_{-\infty}^{+\infty} f(t) \psi_{u,s}^* dt \quad (3.29)$$

$\psi_{u,s}(t)$  is obtained by scaling  $\psi(t)$  by  $s$  and translating it by  $u$  as

$$\psi_{u,s}(t) = \frac{1}{\sqrt{s}} \psi \left( \frac{t-u}{s} \right) \quad (3.30)$$

The normalizing factor  $\frac{1}{\sqrt{s}}$  ensures that energy remains same for all  $u$  and  $s$ .

Thus, wavelet transform can be seen as a mapping operator that takes a member of square integrable functions of one real variable and transforms it to a member of the set of functions of two real variables.

## Properties of the Wavelet Transform

Some important properties of the wavelet transforms are stated as under:

*Linearity*

$$W[\alpha f(t) + \beta g(t)] = \alpha[Wf(t)] + \beta[Wg(t)]$$

For some scalar  $\alpha$  and  $\beta$

*Translational Invariance*

$$W[f(t - \tau)] = Wf(u - \tau, s)$$

*Scaling Variance*

For any scalar  $\alpha > 0$ ,

$$W\left[\frac{1}{\alpha}f\left(\frac{t}{\alpha}\right)\right] = W\left(\frac{u}{\alpha}, \frac{s}{\alpha}\right)$$

### 3.1.4 Scalogram

The modulus of the wavelet transform shows how the energy of the signal varies with time and frequency. In engineering application, the square of the modulus of the CWT is often called as scalogram, defined as Eq. (3.31), which has been widely used for fault diagnostics.

$$P_\omega f(u, s) = |Wf(u, s)|^2 \quad (3.31)$$

It is a measure of fit between  $f(t)$  and the wavelet  $\psi(t)$ . It is usually a graph with time on the horizontal axis, scale or frequency on the vertical axis and the amplitude  $P_\omega f(u, s)$  represented by gray values. High amplitude are coded with bright, low values are coded with dark gray values. A typical scalogram for a sample signal is shown in Figure 3.2.

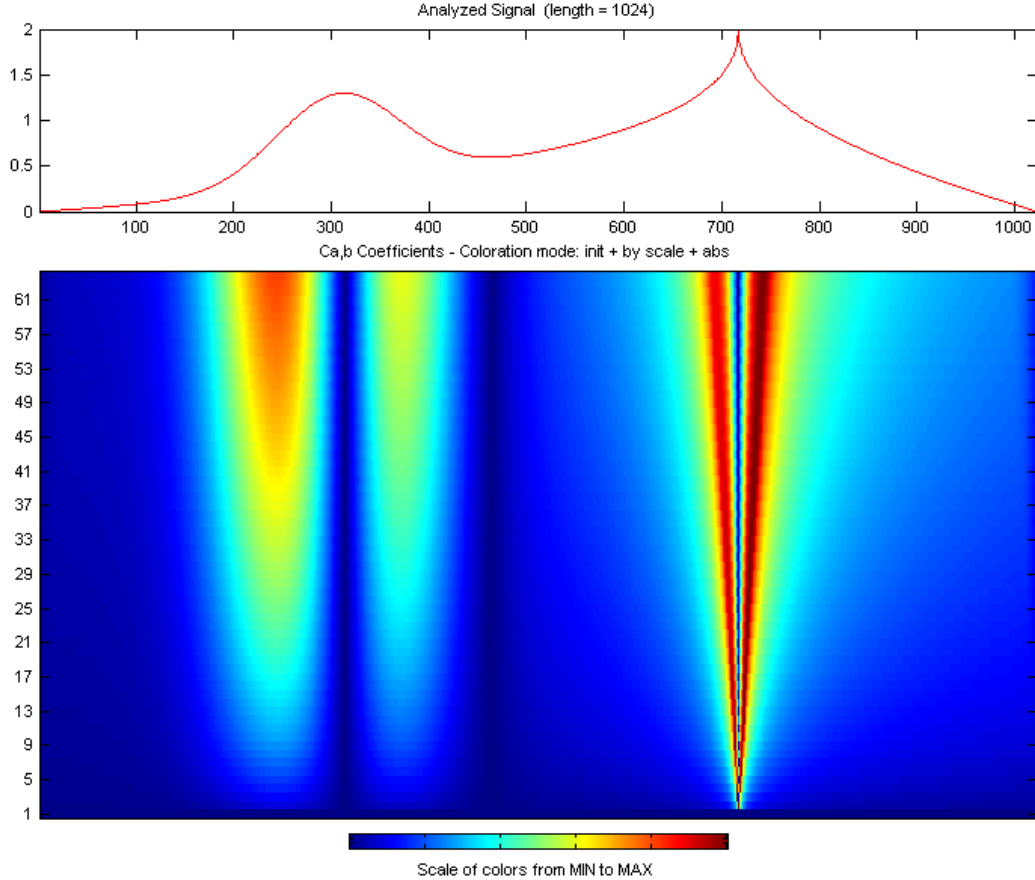


**Figure 3.2: Scalogram of a sample signal. The analysis wavelet used is Haar.**

From Cauchy-Schwarz inequality,

$$|Wf(u, s)|^2 \leq \|f(t)\|^2 \|\psi_{u,s}(t)\|^2 \quad (3.32)$$

This means that  $|Wf(u, s)|$  always exists because the signal and the wavelet have finite norms. In equation equality holds if and only if

$$\psi_{u,s}(t) = \alpha f(t) \quad (3.33)$$

for some scalar  $\alpha$ . Therefore, the scalogram achieves its maximum value for those pairs of  $(u, s)$ , for which the equality holds. A measure of fit between the signal  $f(t)$  and the wavelet  $\psi(t)$  is given by

$$\|f(t) - Wf(u, s)\|^2 = \|f(t)\|^2 + \|Wf(u, s)\|^2 - 2\text{Re}[Wf(u, s)] \quad (3.34)$$

For the closest fit, the left-hand side of the equation is to be minimized. The only variable in the right-hand side of equation (3.34) is  $\text{Re}[Wf(u, s)]$ . Thus, the maximum value of  $\text{Re}[Wf(u, s)]$ , because it corresponds to minimum value of lefthand side, yields the values of  $u$  and  $s$  that provide best possible fit between the signal and the wavelet.

### 3.1.5 Scale and Frequency

In contrast to Fourier transform or STFT, the wavelet transform does not look for frequency but rather for detail sizes or scales  $s$ . High frequencies correspond to small details and vice versa. Thus, frequencies and scales are inversely proportional, i.e.

$$\omega = \frac{\delta}{s} \quad (3.35)$$

where  $\delta$  is a constant depending on the wavelet function and sampling period of signal under consideration. To establish the relation between scale and frequency, a periodic signal frequency  $\omega_c$  is associated with the wavelet function as shown in Figure 2.3(a). It is known as center frequency of the wavelet. For a wavelet dilated by  $s$ , the center frequency becomes  $\omega_c/s$ . Now for any signal with sampling period  $\Delta$ , the frequency at scale  $s$  becomes

$$\omega = \frac{\omega_c}{s \cdot \Delta} \quad (3.36)$$

From equation (3.35) and (3.36),

$$\delta = \frac{\omega_c}{\Delta} \quad (3.37)$$

for any wavelet and sampling period of the signal. A typical variation of frequency  $\omega$  with scale  $s$  for Morlet-Wavelet and a sampling frequency of 1024 samples per second is shown in Figure 3.3 (b). It is evident from the graph that frequency decreases at a rapid rate for small values of scales.

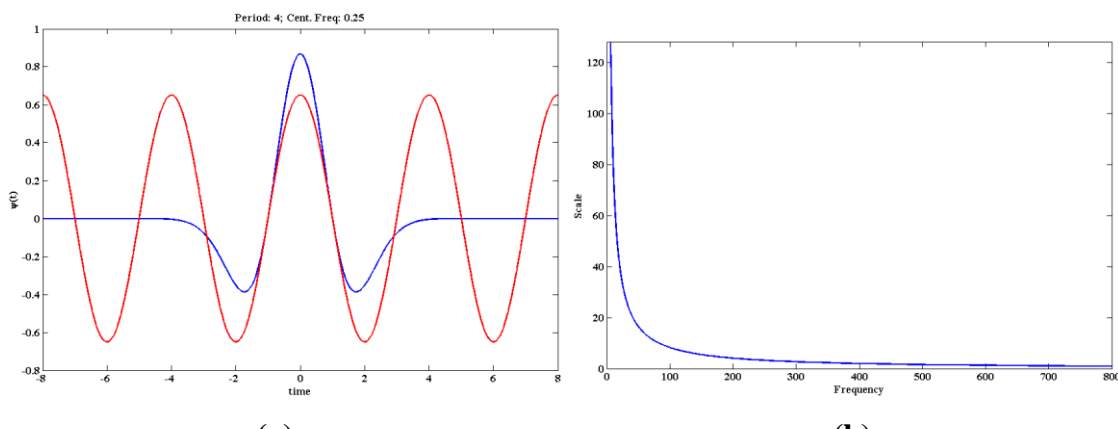


**Figure 3.3: Relationship between Frequency and Scale** (a) Periodic signal approximation for Mexican-Hat-Wavelet (b) Variation of Frequency with Scale for Mexican-Hat-Wavelet

### 3.1.6 Instantaneous Frequency

Consider a monochromatic wave, which can be represented by

$$f(t) = \cos(\omega t + \theta) = a \cos \varphi(t) \quad (3.38)$$

where  $a$  and  $\omega$  are the amplitude and frequency respectively. The frequency  $\omega$  is the derivative of the phase  $\varphi(t)$ . Any real signal can be written as amplitude modulated with a time varying phase:

$$f(t) = a(t) \cos \varphi(t); a(t) \geq 0 \quad (3.39)$$

The instantaneous frequency is defined as a positive derivative of the phase:

$$\omega t = \varphi'(t) \quad (3.40)$$

The expression in equation (3.40) is not unique. There can be many possible choices of  $a(t)$  and  $\varphi'(t)$ , which means that  $\omega t$  is not uniquely defined relative to  $f(t)$ . The solution to this problem can be obtained by forming analytic signal of  $f(t)$ . The signal in equation is said to be asymptotic if

$$\left| \frac{d\varphi(t)}{dt} \right| \gg \left| \frac{1}{a(t)} \frac{da(t)}{dt} \right| \quad (3.41)$$

It means that oscillations coming from phase terms are much faster than variation of the amplitude. If equation (3.41) is satisfied, the analytic form of the signal in equation can be represented as

$$Z_x(t) \approx A(t) e^{j\varphi(t)} \quad (3.42)$$

Now, to estimate the instantaneous frequency of the signal, consider  $\psi(t)$  to be an analytic wavelet, i.e.

$$\psi(t) = g(t) e^{j\omega_c t} \quad (3.43)$$

The wavelet transform of the signal in equation (3.42) can be obtained as the inner product of analytic signal and the analytic wavelet function.

$$Wf(u, s) = \langle f(t), \psi_{u,s}(t) \rangle \geq \frac{1}{2} \langle Z_x, e^{j\omega_c t} g_{u,s}(t) \rangle \quad (3.44)$$

Under asymptotic conditions of equation (3.41), it can be shown that

$$Wf(u, s) = \frac{\sqrt{s}}{2} A(u) \exp(j\varphi(u)) [G(s(\omega - \varphi'(u))] \quad (3.45)$$

where  $G(\omega)$  is the Fourier transform of  $g(t)$ .

### 3.1.7 Comparison of Various Transforms

The most common transform used in signal analysis, Fourier transform, has its basis as sinusoidal functions which are well localized in frequency domain but do not decay with time. So, it only gives global information about the frequency content in the signal. In other words, it only provides global support. In contrast to Fourier transform, STFT provides local support. The basis function, known as window function, is centered about origin and localized at analysis time. The degree of time-frequency resolution depends on window function, usually a Gaussian. But, STFT fails to provide high frequency as well as time resolution at the same time. The wavelet transform is well localized in frequency as well as time domain. It provides high frequency and time resolution at the same time. Thus, it is most suitable to extract time-frequency variations in a signal. When compared to STFT, the computation time of wavelet transform is small. Figure 3.4 shows representation of different transforms [42].

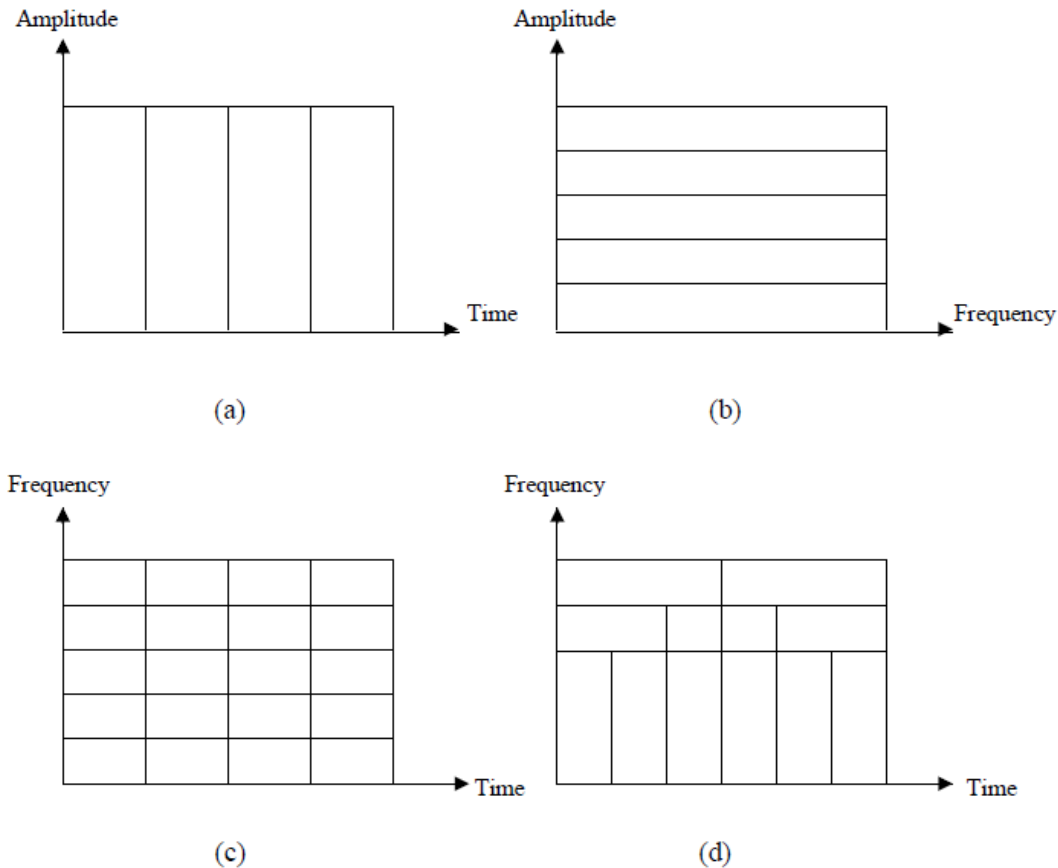


**Figure 3.4 Comparison of various transforms (a) Time Domain Signal (b) Fourier Transform (c) Short Time Fourier Transform (STFT) (d) Wavelet Transform**

## 3.2 Artificial Neural Networks

Artificial Neural Networks (ANNs) are nonlinear information processing devices, built from interconnected elementary units called neurons. It consists of simple processing elements connected in a complex layer structure which enables the model to approximate a complex non-linear function with multi-inputs and multi-outputs. A processing element comprises of nodes and weights. Similar to the human brain ANNs learn by example and generalize from previous examples to new ones. For unknown function it adjusts its weights with observations of input and output. This process is usually called as training of an ANN.

## 3.3 The Artificial Neuron

The artificial neuron was developed to imitate the first order characteristics of the biological neuron. An artificial neuron is an informing processing unit that is fundamental to the operation of a neural network. A set of inputs is applied, each representing the output of another neuron. Each input is multiplied by a corresponding weight, analogous to a synaptic strength, and all of the weighted inputs are then summed to determine the activation level of the neuron. Figure 3.5 shows a typical model of a neuron. The three basic elements of the neuron model are described below.

### 3.3.1 Synapses

Synapses are connecting links, each of which is characterized by a weight or strength of its own. It specifies the connection between a signal  $x_j$  at the input of the sample  $j$ , and a neuron  $k$ . The weighting factor is  $w_{kj}$ .

### 3.3.2 Adder

Adder sums up the input signals weighted by the respective synapses of the neuron. The operation is similar to that of a linear adder.

### 3.3.3 Activation function

An activation function defines the output of a neuron in terms of the activity level of its input. It limits the amplitude of the output of the neuron and introduces non-linearity into the network. The activation function is also referred to as squashing function since it is

used to limit the output values of a neuron in a definite small range irrespective of the inputs to it.

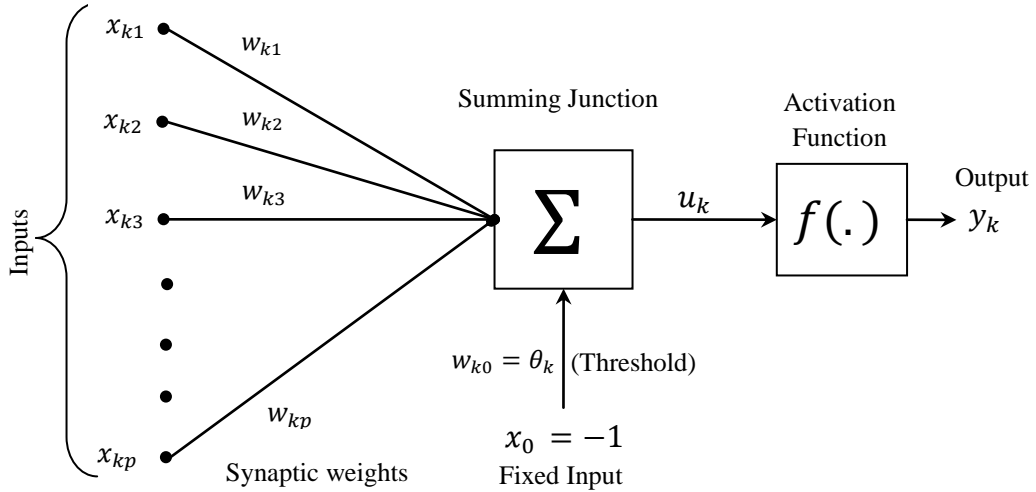


**Figure 3.5 Model of a Nonlinear Neuron**

### 3.3.4 Threshold

The neuron also includes an externally applied threshold function  $\theta_k$ , which has the effect of lowering the net input of the activation function. On another hand, employing a bias term rather than a threshold may increase the net input of the activation function. The bias is the negative of the threshold. In mathematical terms, output of neuron  $k$  has been described by

$$u_k = \sum_{j=1}^p w_{kj} x_j \quad (3.46)$$

$$y_k = f(u_k - \theta_k) = f(v_k) \quad (3.47)$$

where,  $x_1, x_2, \dots, x_p$  are the input signals and  $w_{k1}, w_{k2}, \dots, w_{kp}$  are the synaptic weights of the neuron  $k$ ,  $u_k$  is the linear combiner output,  $\theta_k$  is the threshold,  $f(\cdot)$  is the activation function and  $y_k$  is the output signal of the neuron.  $v_k$  is the output from the neuron after summation. Equation (3.2) can be equivalently written as

$$v_k = \sum_{j=0}^p w_{kj} \quad (3.48)$$

$$y_k = f(v_k) \quad (3.49)$$

In Equation (3.49) a new synapse has been added, whose input and weight, respectively are,

$$X_0 = -1; \quad w_{k0} = \theta_k \quad (3.50)$$

## 3.4 Artificial Neural Network Characterization

Artificial Neural Network is an information processing system in which neurons process the information and the signals are transmitted by means of connection links which are synapses. The synapses possess an associated weight, which is multiplied along with the incoming signals (net inputs). Adder sums the weighted inputs and the output signal is obtained by applying activation function on output of adder. These ANNs are characterised and classified on the basis of following entities

- i. Network Architecture
- ii. Training or Learning
- iii. Activation function

### 3.4.1 Network Architectures

The arrangement of neurons into layers and the pattern of connection within and in-between layers are generally called as the architecture of the network. The way in which the neurons in a network are structured is intimately linked with the learning algorithm used to train the network. Some commonly used classes of network architectures are discussed below

#### 3.4.1.1 Feed forward networks

The generic feed forward network is characterized by the lack of feedback, they allow signals to travel one way only; from input to output. As there is no feedback (loops), the output of any layer does not affect that same layer. These networks are extensively used in pattern recognition in two forms

##### i) Single layer feed forward network:

It is the simplest form of a network, consisting of an input layer of source nodes that project onto an output layer of neurons, but not vice versa. In single layer network, the

weights from one output unit do not influence the weights of other output unit. This type of network is shown in Figure 3.6.

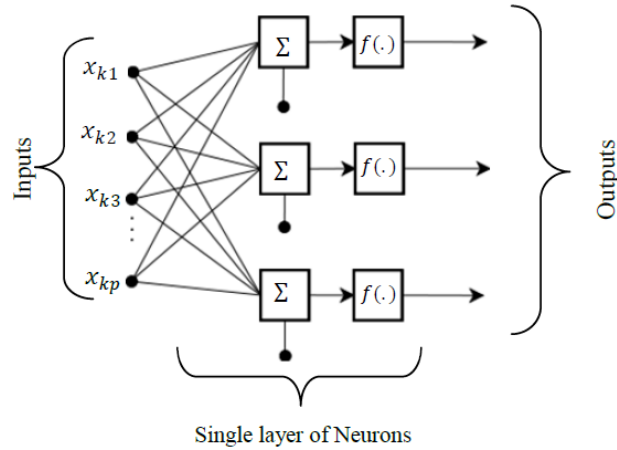


**Figure 3.6 Single layer feed forward network**

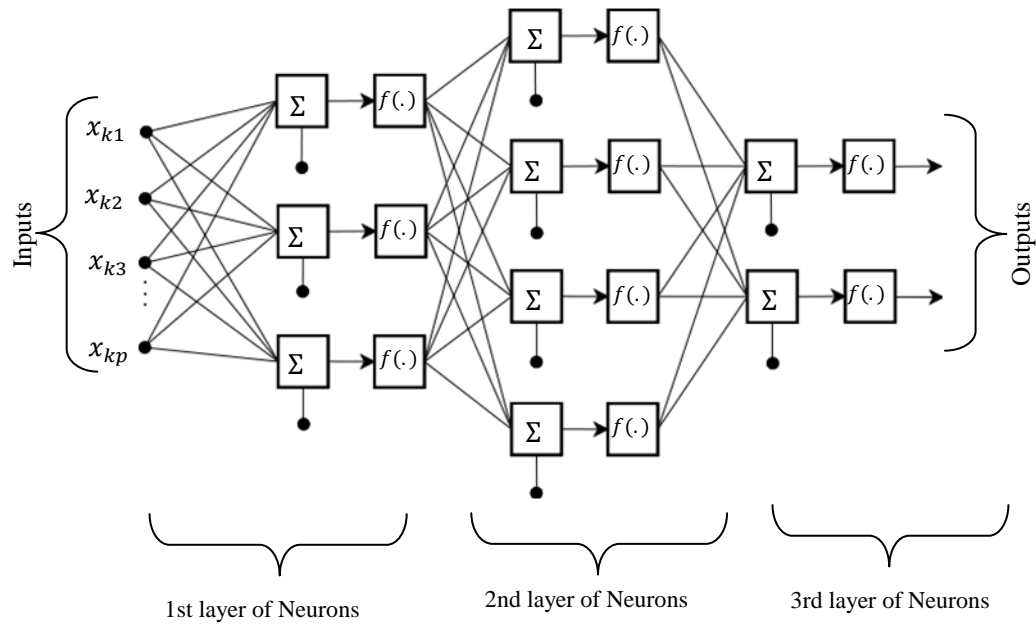


**Figure 3.7 Multi-layer feed forward network**

## ii) Multi-layer feed forward network:

Multi-layer feed forward network is similar to the single layer feed forward network, except that it has one or more hidden layers of neurons. Hidden layers of neurons are

interfaced between the input and output layers. Generally, to approximate the complex functions multi-layered network is required. It is observed that some problems converge better when these hidden layers are used. Figure 3.7 shows the three layered feed forward network. Multilayer networks are more powerful than single-layer networks. For instance, a two-layer network having a sigmoid first layer and a linear second layer can be trained to approximate most functions arbitrarily well. Single-layer networks cannot do this.

### **3.4.2 ANN Learning or Training**

The method of setting the value for the weights enables the process of learning or training. The process of modifying the weights and biases of the network with objective of achieving the expected output is called training or learning of the network. There are two types of learning; supervised and unsupervised.

#### **3.4.2.1 Supervised Learning**

Majority of the artificial neural network solutions have been trained with supervision, that is with a teacher. In supervised learning, the actual output of a neural network is compared with the desired output. Weights, which are randomly initialised to begin with, are then adjusted by the network so that the next iteration will produce a closer match between the desired and the actual output. The learning method tries to minimize the current errors of all processing elements. This global error reduction is created over time by continuously modifying the input weights until acceptable network accuracy is reached.

The training phase takes a very long time. Though supervised learning requires huge data for training a neural network, it gives more reliable results once trained. Some of the supervised learning algorithms include Hebb net, Pattern association memory net, counter propagation net and Back Propagation net. Out of these back propagation net has been used in this study.

### 3.4.2.2 Unsupervised Learning

Unsupervised learning, also known as clustering, is the great promise of the future since it forms natural groups or clusters of patterns. Presently, this learning technique is limited to networks known as self-organizing maps. Though these networks are not commonly applied, it has been proved that unsupervised learning can provide better solutions in some cases. This promising field of unsupervised learning is sometimes called self supervised learning. These networks do not use any external tempts to adjust their weights; instead, they internally monitor their performance. These networks look for regular patterns in the input signals and make adaptations according to the function of the network. Even without being told whether it's right or wrong, the network still must have some information about how to organize itself. This information is built into the network topology and learning rules. At the present state of the art, unsupervised learning is not well understood and is still the subject of research. This research is currently of interest to the government because military situations often do not have a data set available to train a network until a conflict arises.

### 3.4.3 Activation Function

The activation function denoted by  $f(\cdot)$  defines the output of a neuron in terms of the activity level at its input. Various types of transfer functions are employed in developing a neuron. Activation functions for the hidden layer are required to introduce non-linearity into the network. Without non-linearity, hidden units would not make network more precise.

**Table 3.1 Activation Functions for ANN**

S. No.	Activation Function	Mathematical Representation	Output Range
1.	Linear	$f(x) = x$	$[-\infty, +\infty]$
2.	Positive Linear	$\begin{aligned} f(x) &= x && \text{for } x \geq 0; \\ &= 0 && \text{for } x < 0 \end{aligned}$	$[0, \infty]$
3.	Hyperbolic linear tangent sigmoid	$f(x) = \frac{2}{1 + \exp(-\rho x)} - 1$	$[0, 1]$
4.	Logistic sigmoid	$f(x) = \frac{1}{1 + \exp(-\rho x)}$	$[-1, 1]$

where  $\rho$  is a constant called steepness parameter.

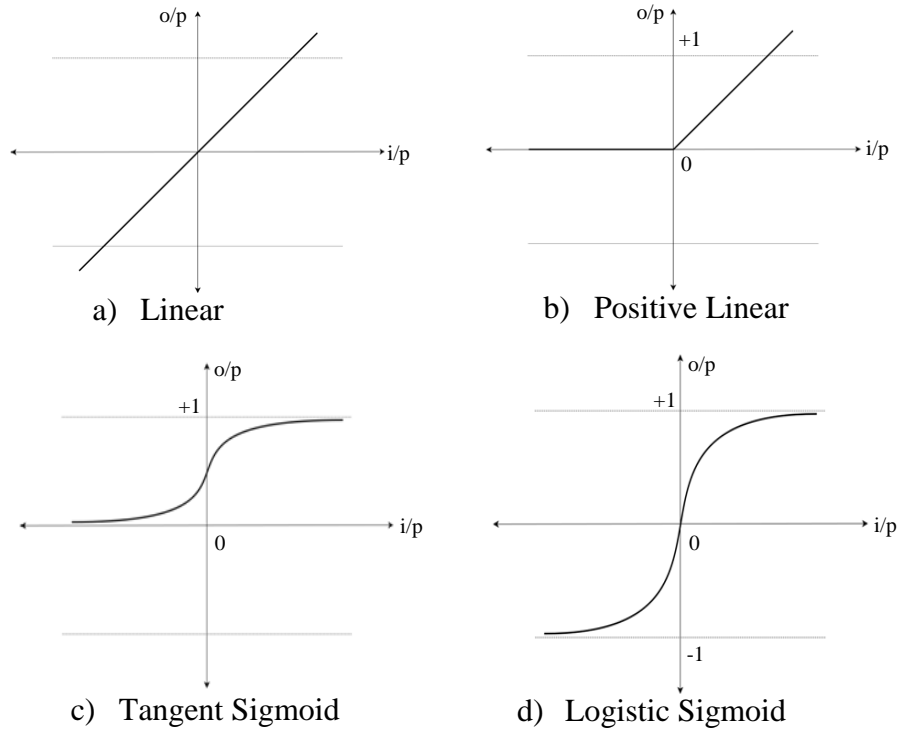


**Figure 3.8 Activation functions**

There are linear as well as nonlinear activation functions. Generally, nonlinear activation functions are preferred in multi-layered network to reflect the complexity of the systems. Almost any nonlinear function does the job, although for back propagation learning, it must be differentiable and it helps if the function is bounded. The sigmoid functions such as logistic and tangent are most common choices. Some of the commonly used activation functions are graphically represented as shown in Figure 3.8 and tabulated in Table 3.1.

### 3.5 Back propagation training algorithm

Most popular and commonly used feed forward training algorithm is the back propagation training algorithm, well known as BP Algorithm. This algorithm's main attraction is its suitability to a large number of applications and high rates of convergence. Back propagation is a systematic method for training multi layer neural networks. As it is a supervised learning algorithm, it learns by examples and learning sets consist of input vectors with corresponding known outputs. This algorithm is intended to solve the problems of choosing weight values for layered artificial neural networks with

feed forward connections from input layer to hidden layer and then to the output layer. The algorithm performs the input to output mapping by minimizing a cost function using a gradient search technique.

The cost function, which is equal to the mean squared difference between the desired and the actual net output, is minimized by making wide connection adjustments according to the error between the computed and target output processing element values. There are two stages in the development of a back-propagation algorithm, namely Forward pass and backward pass. During the forward pass all the weights of the network are initialized randomly and the network outputs and the difference between the actual and target output i.e. the error, are calculated for the initialized weights. During the backward step, the initialized weights are adjusted to minimize the error by propagating the error backwards. The network outputs and error are calculated again with the updated weights and the process repeats till the error is acceptably small. All these steps are described below and the whole algorithm can be represented schematically as shown in Figure 3.9.

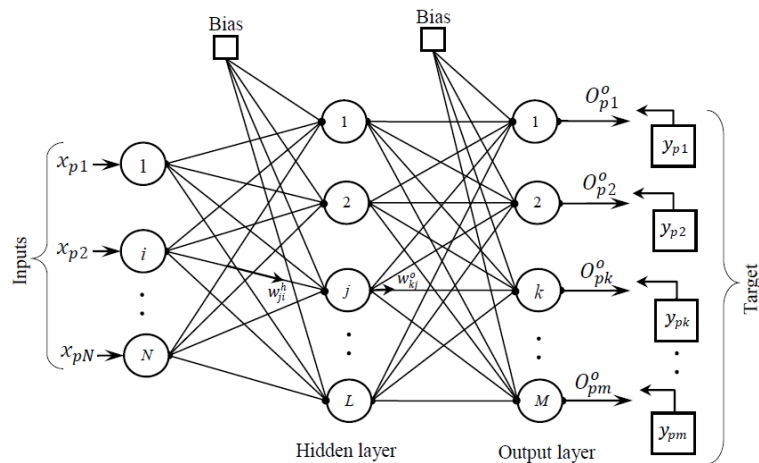


**Figure 3.9 Back-propagation Network architecture**

The training algorithm of back propagation involves four stages

1. Initialization of weights
2. Forward pass
3. Backward pass
4. Updating of the weights and biases

During first stage, which is the initialization of weights, some small random values are assigned. During feed forward stage each input unit receives an input signal and transmits this signal to each of the hidden units. Each hidden layer units then calculates the activation function and sends its signal to each output unit. The output unit calculates the activation function to form the response of the net for the given input pattern. During back propagation of errors, each output unit compares its computed activation with its target value to determine the associated error for that pattern with that unit. Based on the calculated error, the error at output unit is distributed back to all units in the previous layer. Similarly, for each hidden unit, same procedure is followed. During final stage, the weight and biases are updated using calculated factors and the activations.

Figure 3.9 shows the three layered feed forward network architecture for back propagation training, which contains  $N$  input layer neurons,  $L$  hidden layer neurons and  $M$  output layer neurons respectively. With reference to above architecture back propagation algorithm formulation has been derived bellow.

### 3.5.1 Forward pass

The  $p^{th}$  input vector to the network can be described as

$$x_p = (x_{p1} \dots x_{pN}) \quad (3.51)$$

Where  $x_{pi}$  represent the input attribute  $i$  for the vector  $p$ . The net input to the hidden layer then becomes

$$net_{pj}^h = \sum_{i=1}^N w_{ji}^h x_{pi} + \theta_j^h \quad (3.52)$$

Where,  $w_{ji}^h$  represents the weight of the layer  $h$  from node  $i$  to node  $j$  and  $\theta_j^h$  represents the threshold for the node  $L$  of the layer  $h$ .

The outputs from the hidden layer (which is the input to the output layer) are

$$O_{pj}^h = i_{pj} = f_j^h(net_{pj}^h) \quad (3.53)$$

Where  $O_{pj}^h$  is from the node  $j$  of the hidden layer  $h$ ,  $f_j^h$  is the activation function at node  $j$  of the hidden layer  $h$ .

The net-input values at output layer unit are

$$net_{pk}^o = \sum_{j=1}^L w_{kj}^o i_{pj} + \theta_k^o \quad (3.54)$$

While the outputs at output units are

$$O_{pk}^o = f_k^o(net_{pk}^o) \quad (3.55)$$

Individual error at each output unit is

$$\delta_{pk} = y_{pk} - O_{pk}^o \quad (3.56)$$

From which the overall mean square error can be computed as

$$E_p = \frac{1}{2} \sum_{k=1}^m \delta_{pk}^2 \quad (3.57)$$

### 3.5.2 Backward pass

Weight adjustment is carried out at the output layer through the following procedure.

Using equations (3.56) and (3.57), the mean square error,  $E_p$  can be expressed as

$$E_p = \frac{1}{2} \sum (y_{pk} - O_{pk}^o)^2 = \frac{1}{2} \sum \{y_{pk} - f_k^o(net_{pk}^o)\}^2 \quad (3.58)$$

The weight change of an output layer weight is the negative gradient of  $E_p$  with respect to output layer weights  $w_{kj}^o$  and can be written as

$$\frac{\partial E_p}{\partial w_{kj}^o} = -(y_{pk} - O_{pk}^o) \frac{\partial f_k^o}{\partial (net_{pk}^o)} \frac{\partial (net_{pk}^o)}{\partial w_{kj}^o} \quad (3.59)$$

However, from equation (3.54)

$$\frac{\partial (net_{pk}^o)}{\partial w_{kj}^o} = \frac{\partial (\sum w_{kj}^o i_{pj} + \theta_k^o)}{\partial w_{kj}^o} = i_{pj} \quad (3.60)$$

And from equation (3.55)

$$\frac{\partial f_k^o}{\partial (net_{pk}^o)} = f_k^o(net_{pk}^o) = O_{pk}^o(1 - O_{pk}^o) \quad (3.61)$$

Therefore, the weight change at the output layer weight is

$$\Delta_{pk}^o w = -\frac{\partial E_p}{\partial w_{kj}^o} = (y_{pk} - O_{pk}^o)f_k^o(net_{pk}^o) \times i_{pj} \quad (3.62)$$

Now denoting

$$\delta_{pk}^o = (y_{pk} - O_{pk}^o)f_k^o(net_{pk}^o) \quad (3.63)$$

The weight change at the output layer weights can be written as

$$\Delta_p^o w = \delta_{pk}^o i_{pj} \quad (3.64)$$

To make the learning process smooth and to ensure the weight change take place in the same direction, two network parameters-learning rate coefficient  $\eta$  and the momentum  $\alpha$  are introduced in lieu of direct application of the above mentioned weights, so that

$$w_{kj}^o(t+1) = w_{kj}^o(t) + \eta(y_{pk} - O_{pk}^o) f_k^o(\text{net}_{pk}^o) \times i_{pj} + \alpha w_{kj}^o(t-1) \quad (3.65)$$

A small value of  $\eta$  implies that the network will have to make a large number of iterations. Its value is usually reserved between 0.05 and 0.9. It is often possible to increase its value as the network error decreases, thereby increasing the speed of convergence. Another way to boost convergence speed is by adopting an extra momentum term while uploading the weights. This additional term tends to keep the weight changes in the same direction.

While updating the weights for the hidden layers, it should be noted that there is no target output and therefore the adjustment of weights is proportional to their initial contribution. From equations (3.54) and (3.55) one gets

$$E_p = \frac{1}{2} \sum_p \{y_{pk} - f_k^o(\sum w_{kj}^o i_{pj} + \theta_k^o)\}^2 \quad (3.66)$$

The weight change of hidden layer weights is the negative gradient of  $E_p$  with respect to hidden layer weights  $w_{ji}^h$  and is given by

$$\frac{\partial E_p}{\partial w_{ji}^h} = - \sum_k (y_{pk} - O_{pk}^o) \frac{\partial O_{pk}^o}{\partial (\text{net}_{pk}^o)} \frac{\partial (\text{net}_{pk}^o)}{\partial i_{pj}} \frac{\partial i_{pj}}{\partial (\text{net}_{pj}^h)} \frac{\partial (\text{net}_{pj}^h)}{\partial w_{ji}^h} \quad (3.67)$$

And the individual terms on the right hand side of the above equation can be expanded as

$$\frac{\partial O_{pk}^o}{\partial (\text{net}_{pk}^o)} = \frac{\partial (f_k^o(\text{net}_{pk}^o))}{\partial (\text{net}_{pk}^o)} = f_k^o(\text{net}_{pk}^o) = O_{pk}^o(1 - O_{pk}^o) \quad (3.68)$$

$$\frac{\partial (\text{net}_{pk}^o)}{\partial (i_{pj})} = \frac{\partial (\sum w_{kj}^o i_{pj} + \theta_k^o)}{\partial (i_{pj})} = w_{kj}^o \quad (3.69)$$

$$\frac{\partial i_{pj}}{\partial (net_{pj}^h)} = \frac{\partial (f_j^h net_{pj}^h)}{\partial (net_{pj}^h)} = f_j^h(net_{pj}^h) = O_{pj}^h(1 - O_{pj}^h) \quad (3.70)$$

$$\frac{\partial (net_{pj}^h)}{\partial w_{ji}^h} = \frac{\partial (\sum w_{kj}^o i_{pj} + \theta_k^o)}{\partial w_{ji}^h} = x_{pi} \quad (3.71)$$

Substituting equations (3.68)-(3.69) in equation (3.67) one gets

$$\Delta_p w_{ji}^h = -\frac{\partial E_p}{\partial w_{ji}^h} = x_{pi} O_{pj}^h (1 - O_{pj}^h) \sum_k (y_{pk} - O_{pk}^0) O_{pk}^o (1 - O_{pk}^o) w_{kj}^o \quad (3.72)$$

Network parameters  $\eta$  and  $\alpha$  can be introduced in a manner similar to that in the case of the output layer to express the final weight change at the hidden layer as

$$w_{ji}^h(t+1) = w_{ji}^h(t) \eta x_{pi} O_{pj}^h (1 - O_{pj}^h) \sum_k (y_{pk} - O_{pk}^0) O_{pk}^o (1 - O_{pk}^o) w_{kj}^o + \alpha w_{ji}^h(t-1) \quad (3.73)$$

### 3.6 Remarks

In this chapter basics of wavelet transform and artificial neural networks have been reviewed. Applications of wavelet transform and neural network for fault diagnosis have been explored. Different network architectures and back propagation training algorithm are discussed in detail.

# CHAPTER 4

## EXPERIMENTAL SET-UP AND DATA ACQUISITION

Experimental simulation of vehicle faults is conducted on Brake Test Rig. Faults were deliberately introduced in the test rig. Accelerometers have been used to pick up vibration signature from various stations on rig whereas torque, temperature and speed signature have been recorded by Base Inline torque sensor, temperature sensor (RTD type) and Tachometer respectively. Signals were acquired and processed by virtual instrumentation technique employing LabVIEW 2010 software. Features have been extracted from acquired data, compiled together to form training vector and then fed into the neural network for its training. MATLAB code has been developed for integration of data acquisition process, feature extraction, neural network training and fault diagnosis.

### **4.1 Brake Test Rig**

Brake test rig is a custom built test rig, designed by IIT Kanpur and fabricated by SpectraQuest Inc. USA, to simulate quarter car model of a standard vehicle for experimental and educational purposes. It is also provided with controls to regulate motor speed and the brake torque.

Brake test rig (Figure 4.1 - 4.2) is driven by 50HP AC motor (480V 3 Phase, 240 ft-lb torque). The motor control system consists of an AC Vector Drive operating in closed loop vector control. The user is able to specify speed and motor torque profiles. Using speed controller, we can perform coast up, coast down tests at desired acceleration and deceleration. A blower motor is connected with the main motor for the cooling purpose. A flywheel of 450 Kg; 24in. Diameter, to add inertia equivalent to the single front wheel's fraction of a sub-compact vehicle's kinetic energy at 100 km/hr is provided and supported on shaft by pillow block bearings. Drive shaft connects motor/flywheel to front side wheel. The test rig has provision to accommodate several types of hydraulically actuated vehicle brakes including disk and drum brakes.



**Figure 4.1 Brake Test Rig**

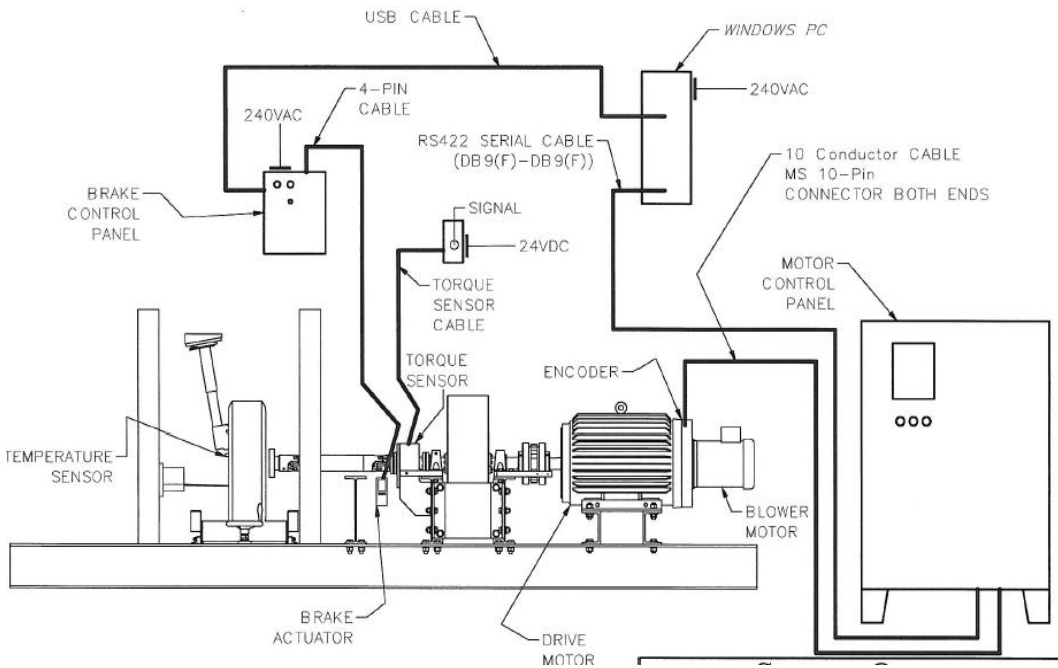


**Figure 4.2 Brake Test Rig- Line Diagram**

Brake control is controlled by pneumatically actuated cylinder to apply force to the brake master cylinder. A standard vehicle suspension system including control arms, ball joints, wheel, and tire mounted in the test rig. A custom driveshaft with universal joints on each

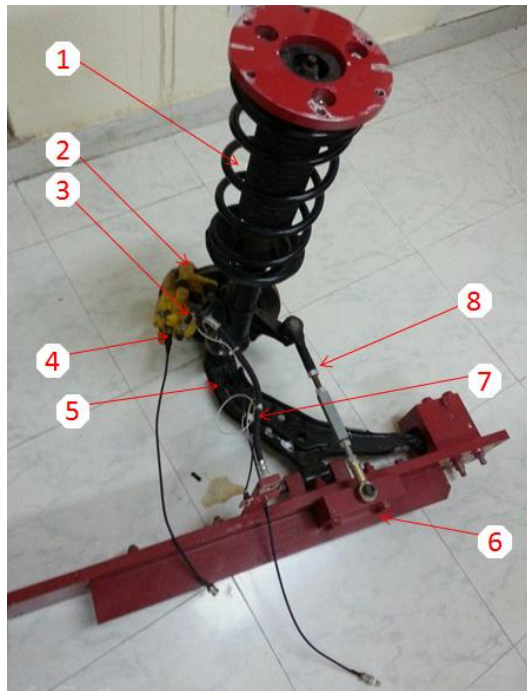
end transmits energy from the motor and flywheel to the wheel. Computer with custom software for remote operation and data acquisition is used for rig. The rig has provision for introducing various vehicle faults.

## 4.2 Instrumentation

Prior to selecting sensors and their mounting locations, a detailed study has been done. During experimentation, in total five sensors were used-two accelerometers, one tachometer, one torque sensor and one temperature sensor.

### 4.2.1 Sensor Locations

Precise data acquisition depends upon number of factors; sensor mounting location being one of them. A proper study has been made and the following suitable locations are selected for mounting the sensors.



1. Suspension System for Front wheel
2. Disc Brake Assembly
3. Temperature Sensor RTD Type
4. Accelerometer on Brake Caliper
5. Lower Wishbone Arm (LB Arm)
6. Rigid Mountings to Test Rig
7. Accelerometer on LB Arm
8. Steering Linkage

**Figure 4.3 Sensor Location: Front Wheel**

### Lower wishbone Arm (LB Arm) and Brake Caliper

Vibrations are generated mainly due to unbalance or due to misalignment in the wheel. These vibrations get transmitted from the wheel to the entire chassis of vehicle and driver/ passengers easily sense those vibrations in the vehicle. In actual vehicle chassis is connected to the wheel through LB arm/ axle and brake system; hence the LB arm and

brake caliper (axle and back plate of drum brake in case of rear wheel) are the appropriate locations for mounting vibration sensor. Accelerometer mounted over the LB arm and caliper gives acceleration of vibration signal in vertical and horizontal direction respectively. Figure 4.3 - 4.4 shows location of accelerometers in front and rear wheel system.

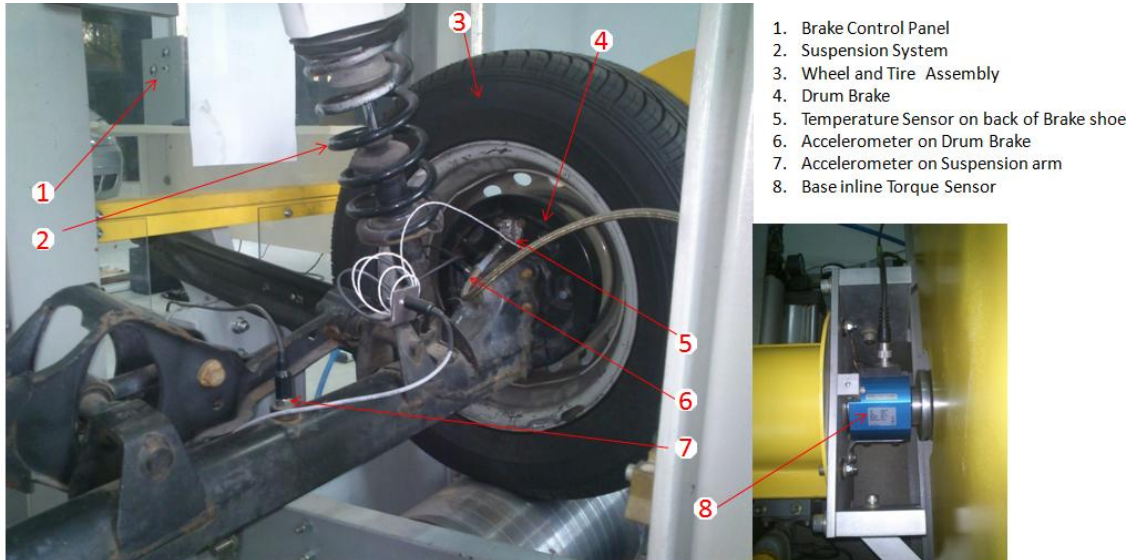


**Figure 4.4 Sensor Location: Rear Wheel**

### **Torque Sensor**

Torque sensor provided with the test rig (Base In-Line Torque sensor) is used for the torque measurement specially in braking condition. It gives signals in terms of voltage which is further processed in LabVIEW 2010. Figure 4.4 shows the location of torque sensor on the rig.



**Figure 4.5 Temperature sensor on Brake Pad**

### **Temperature Sensor**

To measure the temperature of disc/drum temperature sensor (RTD type) is used in the rig. It measures the temperature while applying brakes. Sensor mounted on the brake pad of disc brake as shown in Figure 4.5 and brake shoe of the drum brake respectively.

### **Tachometer**

Tachometer provided with test rig is used for monitoring the rotating speed of input shaft/wheel. It gives a pulse signal comprising one pulse per revolution of input shaft. This signal is further processed in LabVIEW 2010 and used for digitally indicating the operating speed of the vehicle.

Vibration data has been obtained simultaneously from above mentioned five sensors and acquired into a desktop PC through 8 channel data acquisition system with NI cDAQ Chassis (Type 9272, National Instruments).

### **4.2.2 Sensors and DAQ Instrument Specifications**

Acceleration signals were picked up using two accelerometers. Accelerometers used were of piezoelectric voltage type, which give voltage proportional to sensed acceleration. Vibration signatures have been sent to the data acquisition device through BNC cables. Table 4.1 indicates the technical specifications and mounting location for the sensors used in the experiment.

**Table 4.1 Technical Specification and Mounting location for Sensor**

S. No.	Sensor Name	Make & Model	Sensitivity	Mounting Location
1.	Accelerometer	B & K, Type 4513B	1.029mV/ms <sup>2</sup>	On LB Arm, in Vertical direction
2.	Accelerometer	B & K, Type 4513B	1.040mV/ms <sup>2</sup>	On Brake Caliper, in Horizontal direction
3.	Temperature	OMEGA, Type RTD	-	On Brake Pad/ Brake Shoe
4.	Torque	KISTLER, Type 4520A	-	On Drive Shaft
5.	Tachometer	-	-	On Motor Shaft (Inside Casing)

LabVIEW (short form of Laboratory Virtual Instrumentation Engineering Workbench) is a system design platform and development environment for a visual programming language from National Instruments. Originally released for the Apple Macintosh in 1986, LabVIEW is commonly used for data acquisition, instrument control, and industrial automation. LabVIEW programs/subroutines are called as Virtual Instrument (VIs) because of their appearance and operations that can imitate actual instruments. Each VI has three components: a front panel, a block diagram and a connector panel. Front panel contains controls and indicators which allow an operator to input data into or extract data from a running virtual instrument. Block diagram holds all graphical programming logic and processing blocks, interconnected with wires. Front takes the user interactive inputs through controls and passes it on to block diagram for processing and outputs are displayed back on front panel through different indicators.

### 4.3 Data Acquisition, Storage and Display

Figure 4.6 shows the overall instrumentation scheme, in which analog data from all sensors is converted into the digital data by cDAQ hardware. This digital data in desired form then processed, displayed and stored in computer through LabVIEW VI.

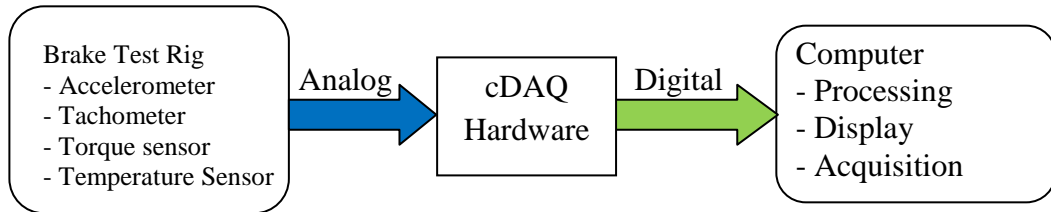


**Figure 4.6 Instrumentation and data acquisition schema**

A LabVIEW VI has been developed for acquisition, display and to store the vibration data. Some of the salient features of program are listed below:

- a) Time domain vibration data acquisition and display from five channels with following user controls:
  - i. Scan rate
  - ii. Number of data points to be read before display
  - iii. File path

- b) Conversion of time domain data to frequency domain data by Fast Fourier Transform (FFT) after applying Hanning window to acquired time domain signal.
- c) Use of Tachometer signal for calculating operating speed in Hz/RPM/Kmph.
- d) Option for writing the time domain data and frequency domain data to excel file at any desired instance.
- e) Display features
  - Five graphical indicators of time domain waveform
  - Five graphical indicators of Frequency domain data
  - Five graphical indicators of RMS value
  - Meter indicator for speed of wheel in Km/h
  - Thermometer indicator for Temperature

## 4.4 Fault Simulation and Vibration Signature Analysis

Faults have been deliberately inserted in the Test-Rig to study their influence on the vibration and thermal parameters. Tests have been conducted for Healthy and Faulty conditions for steady speed operations as well as during braking (transient conditions).

### 4.4.1 Steady Case

Faults have been deliberately introduced in the quarter car model. Faults have been simulated for speed range 8 Hz to 15 Hz (i.e. 50 Km/h to 90 Km/h). Provision is given in the rig and set of faulty pair of wheels supplied with test rig was used to produce these faulty conditions. Faults that have been simulated are listed in Table 4.2. Figure 4.7 shows typical vibration signal at 60 Km/h (10 Hz) in Front Panel of LabVIEW.

**Table 4.2 Faults simulated for Steady Case**

Front Wheel	Rear Wheel
a) Healthy System b) Wheel Misalignment due to Positive Camber c) Wheel Misalignment due to Toe-In d) Wheel Unbalance e) Worn Wheel/Tire	a) Healthy System b) Wheel Unbalance c) Worn Wheel/Tire

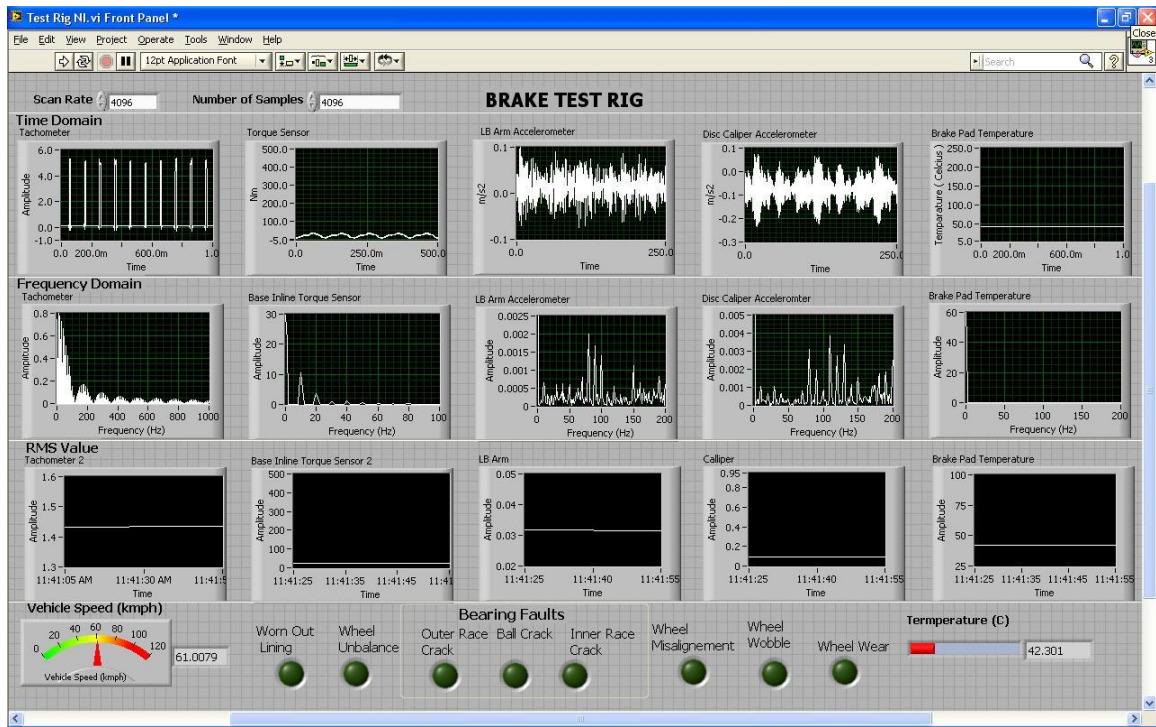


**Figure 4.7 Front Panel: Typical Vibration Signal at 60 Km/h (10 Hz)**

The vibration signatures for the various faults were acquired and stored in Desktop PC. Fourier spectrums of these acquired vibration signals from the two accelerometers for listed faults at different speed have been shown in Figure 4.8 to Figure 4.8 FFT plots at 90 Km/h (15 Hz) for Brake Caliper Sensor –Front Wheel Figure 4.27. It can be observed that each fault carries its own distinct signature in the frequency domain. The location and magnitude of particular peaks in frequency spectra can serve as indicators of faults. A total of 100 sets of vibration signals were acquired for each of the fault. Selected features were extracted from the FFT of the signals, which were further used to train and validate the neural network.

## Vibration Signature Analysis

It is difficult to distinguish faults from the raw time domain waveform. Therefore, time domain data has been converted into frequency domain by taking Fast Fourier Transform (FFT) of each signal. These FFT plots have been studied further to analyse individual faults through frequencies and corresponding amplitudes. FFTs of the averaged signals

for various faults have been discussed in following paragraphs. Experimentation has been carried out for a speed range of 50 Km/h to 90 Km/h.

## **Healthy System**

Frequency spectra for the healthy system (HLF and HLR) have been shown in Figure 4.8 - 4.27, for the two accelerometers used in the study. It can be clearly seen that running frequency and its harmonics are dominant features in all the plots. Higher harmonics (up to 200 Hz) of running frequency is also present.

**Brake Caliper** accelerometer shows second harmonics of  $f_{m1}$  as dominant frequency, whereas  $f_{m1}$  and their third harmonics are much lower in amplitude. **Brake drum** accelerometer gives second harmonics of  $f_{m1}$  as dominant frequency, whereas  $f_{m1}$  and their third, fourth harmonics are also prominent in amplitude. **LB Arm** accelerometer, located at the front wheel in the vertical direction shows  $f_{m1}$  frequency and its second harmonic of smaller peak than its higher i.e. sixth and seventh harmonic, whereas **Rear Axle** accelerometer gives  $f_{m1}$  and its fifth, sixth and seventh harmonics with prominent amplitudes.

## **Wheel Misalignment**

For Wheel Misalignment (WM- Camber and WM Toe-In), the FFT of signals have been shown in Figure 4.8 – 4.27 for the same two accelerometers. Misalignments have been recorded in front wheel only.

### **WM-Camber**

**Brake Caliper** accelerometer gives second harmonics of  $f_{m1}$  as dominant frequency, whereas  $f_{m1}$  and its fourth, sixth and eighth harmonics are equally prominent in amplitude in the entire speed range. **LB Arm** accelerometer at front wheel shows  $f_{m1}$  frequency but no peak at its second harmonic (except at 90 Km/h), whereas fifth, sixth and eighth harmonics of  $f_{m1}$  are more prominent in amplitude in high speed range.

### **WM-Toe In**

**Brake Caliper** accelerometer gives second harmonics of  $f_{m1}$  as less dominant in amplitude, whereas fourth, sixth and higher even harmonics are more prominent in

amplitude in higher speed range. **LB Arm** accelerometer shows that second harmonic of  $f_{m1}$  is not significant in amplitude, whereas fourth and sixth harmonics are more prominent than second harmonic in high speed range.

## Wheel Unbalance

For Wheel Unbalance (WUF and WUR), the FFT of signals have been shown in Figure 4.8 - 4.27 for the two accelerometers used for each of the front and rear wheel. From the **Brake Caliper** accelerometer it is seen clearly that  $f_{m1}$  as dominant frequency, whereas second, third, fourth and fifth harmonics of  $f_{m1}$  are also prominent in amplitude. **Brake drum** accelerometer shows second harmonic of  $f_{m1}$  as dominant frequency, whereas  $f_{m1}$  and its third harmonics is relatively little less prominent in amplitude. **LB Arm** accelerometer shows no peaks at  $f_{m1}$  frequency and its second, sixth and seventh harmonics are small though more prominent than other harmonics (a clear peak can be seen in the range 80 Hz-90 Hz at all speed ranges). **Rear Axle** accelerometer shows  $f_{m1}$  and second harmonic of  $f_{m1}$  are equally dominant in all speed ranges, whereas higher harmonics (seventh, eighth and ninth) harmonics are prominent in all speed ranges.

## Worn Wheel

For Worn Wheel (WWF and WWR), the FFT of signals have been shown in Figure 4.8 to Figure 4.27 for the two accelerometer used for each front and rear wheels. From the **Brake Caliper** accelerometer, second harmonics of  $f_{m1}$  is seen clearly as dominant frequency, whereas  $f_{m1}$ , third and fourth harmonics are present but with relatively low amplitude in comparison to the second harmonic. **Brake drum** accelerometer shows  $f_{m1}$  as dominant frequency, whereas other harmonics of  $f_{m1}$  are relatively little less prominent in amplitude. **LB Arm** accelerometer shows no clear peaks at  $f_{m1}$  frequency, whereas fourth, sixth and eighth harmonics are less prominent. **Rear Axle** accelerometer shows higher harmonics of  $f_{m1}$  are more prominent than  $f_{m1}$  and second harmonic for all speed range.

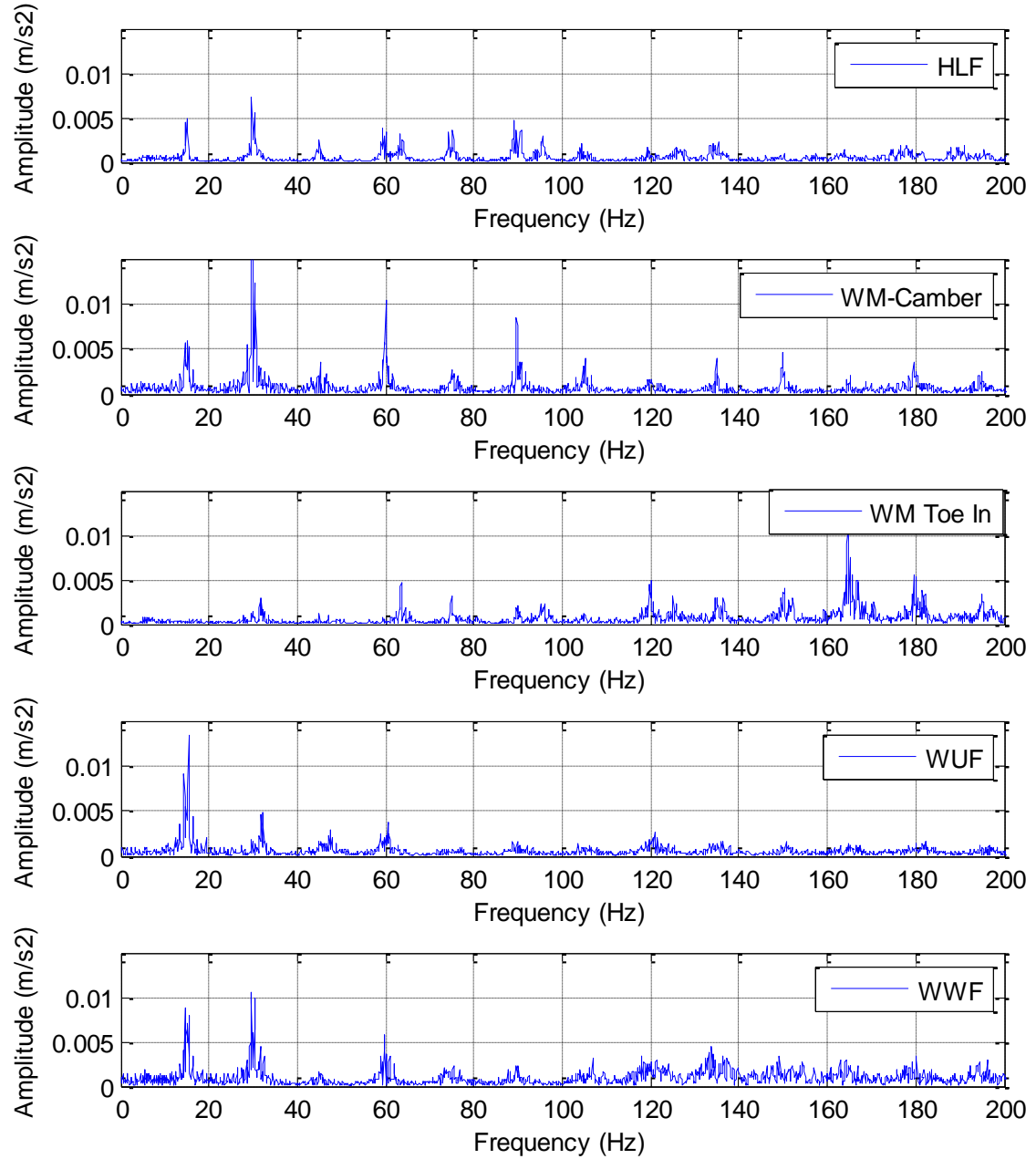


**Figure 4.8 FFT plots at 90 Km/h (15 Hz) for Brake Caliper Sensor –Front Wheel**

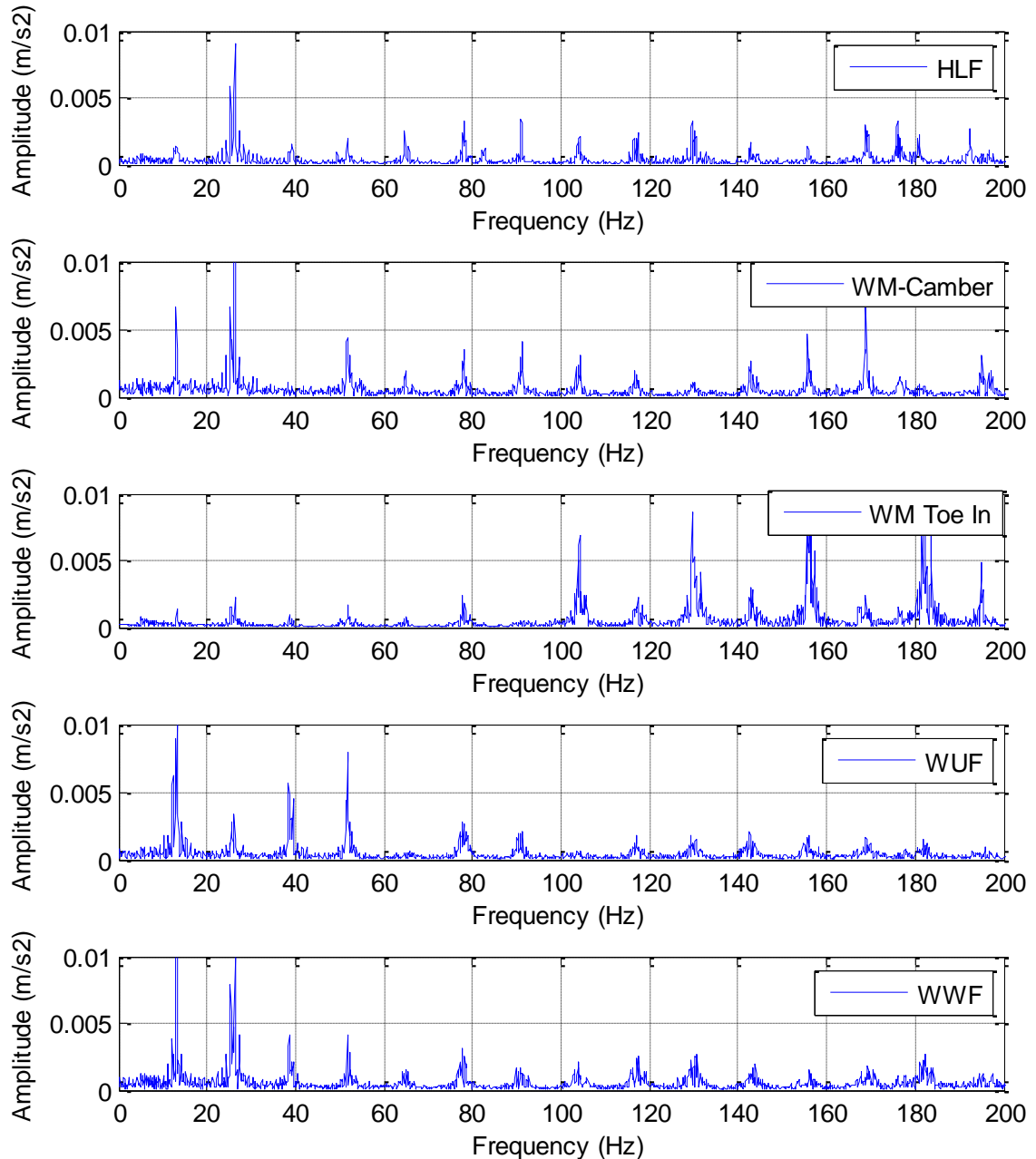


**Figure 4.9 FFT plots at 80 Km/h (13 Hz) for Brake Caliper Sensor –Front Wheel**

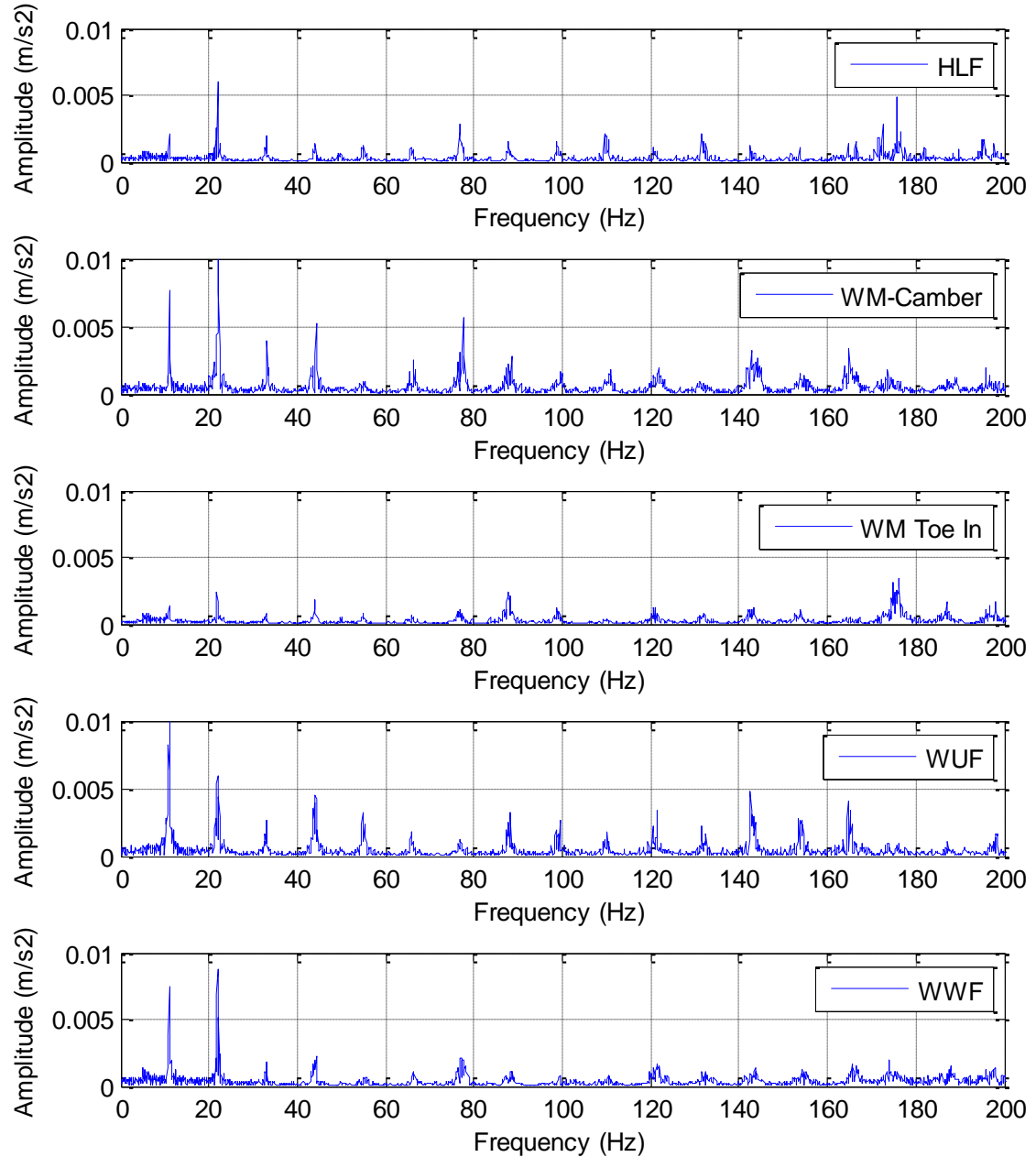


**Figure 4.10 FFT plots at 70 Km/h (11 Hz) for Brake Caliper Sensor –Front Wheel**

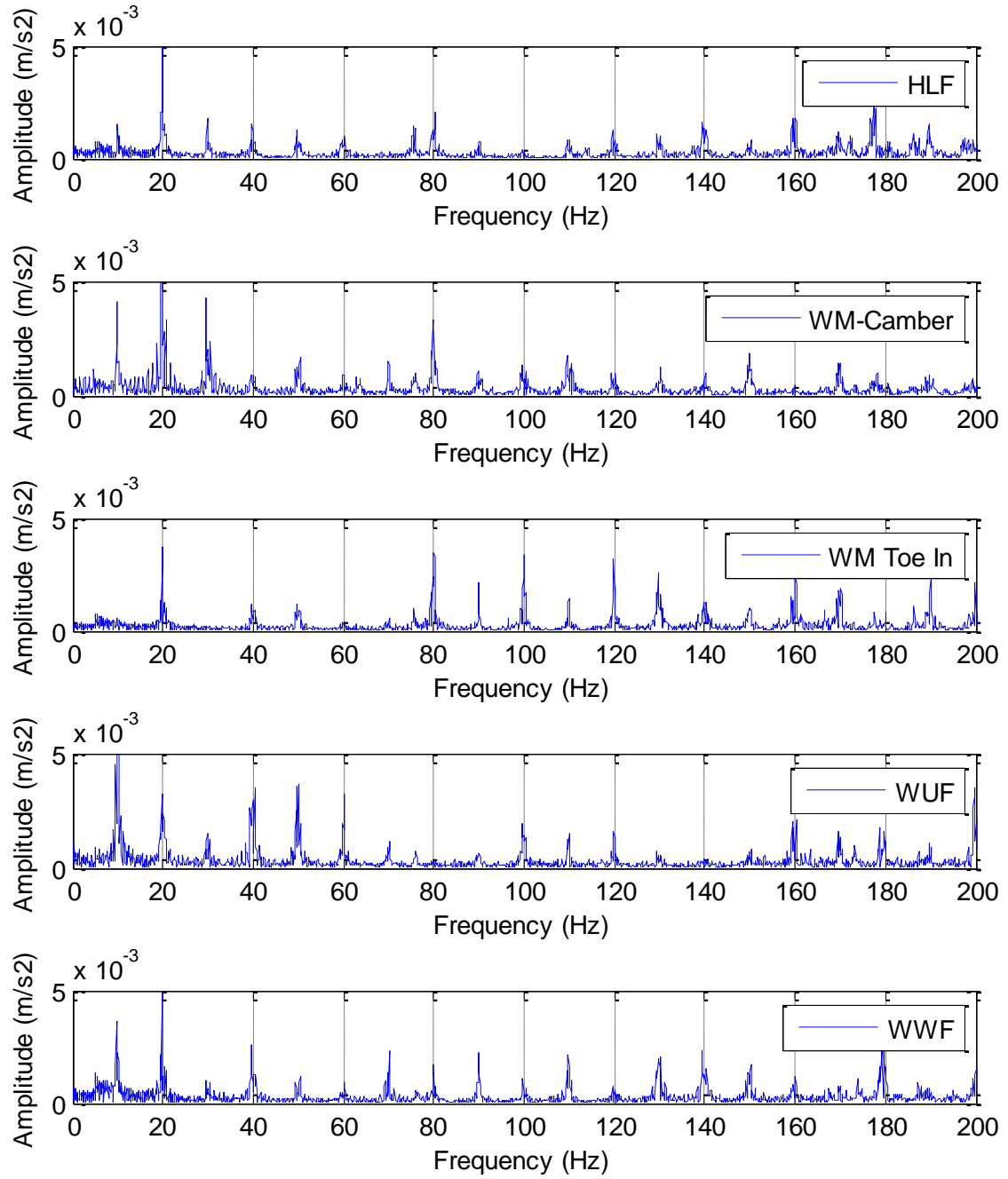


**Figure 4.11 FFT plots at 60 Km/h (10 Hz) for Brake Caliper Sensor –Front Wheel**

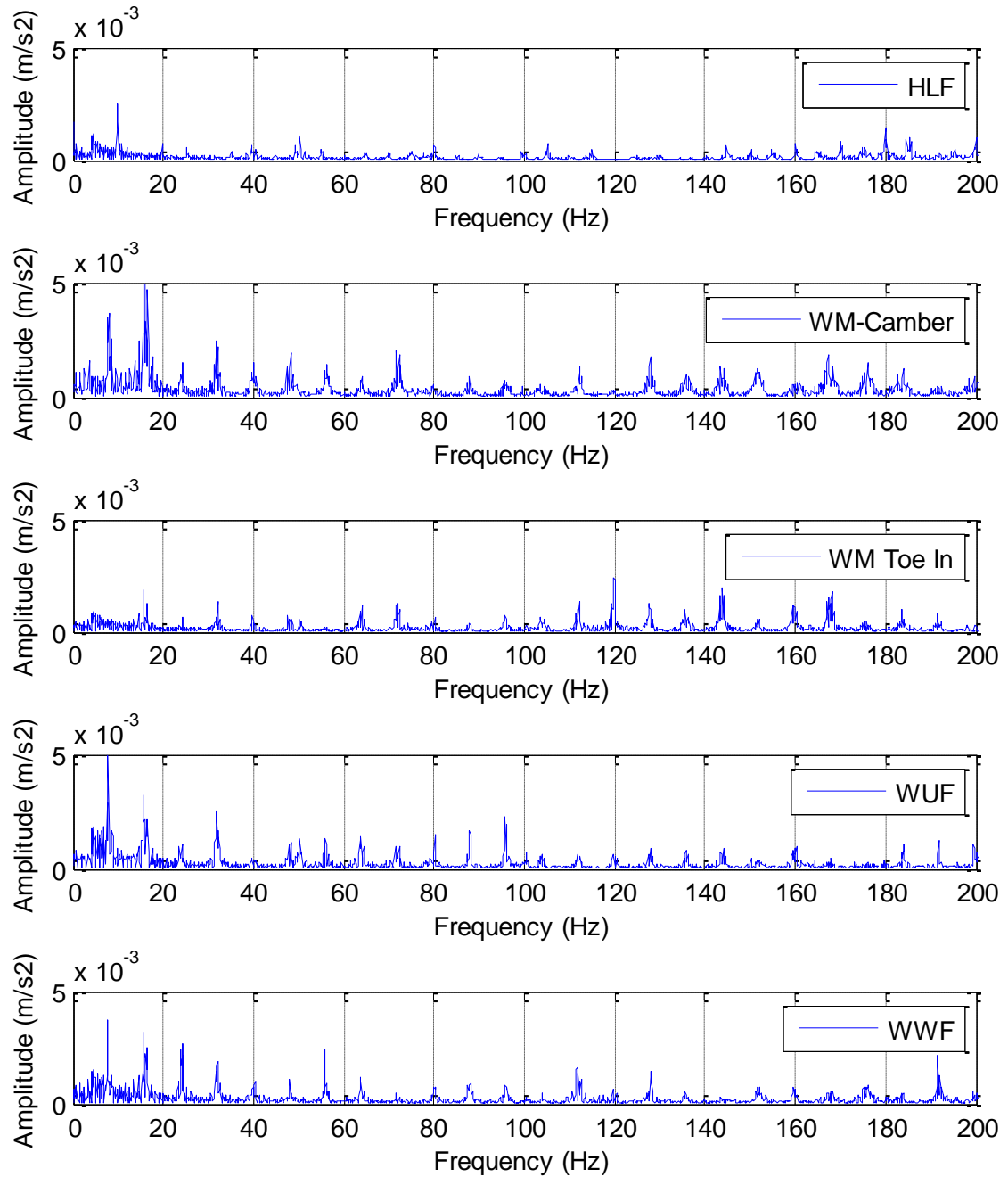


**Figure 4.12 FFT plots at 50 Km/h (8 Hz) for Brake Caliper Sensor –Front Wheel**

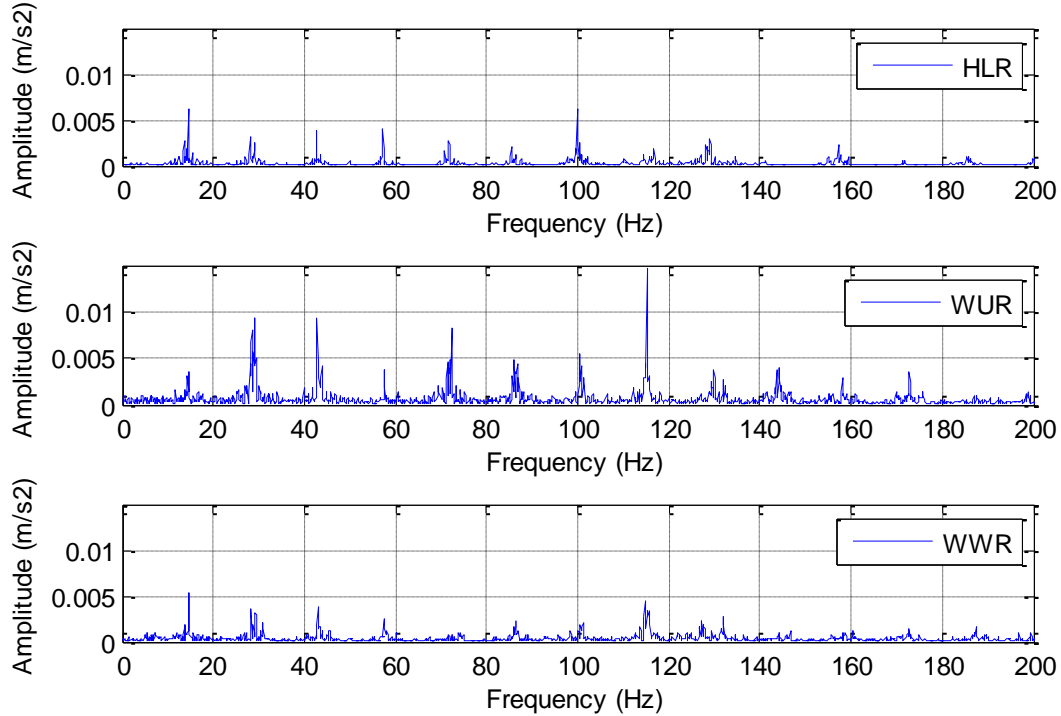


**Figure 4.13 FFT plots at 90 Km/h (15 Hz) for Sensor at Brake drum- Rear Wheel**

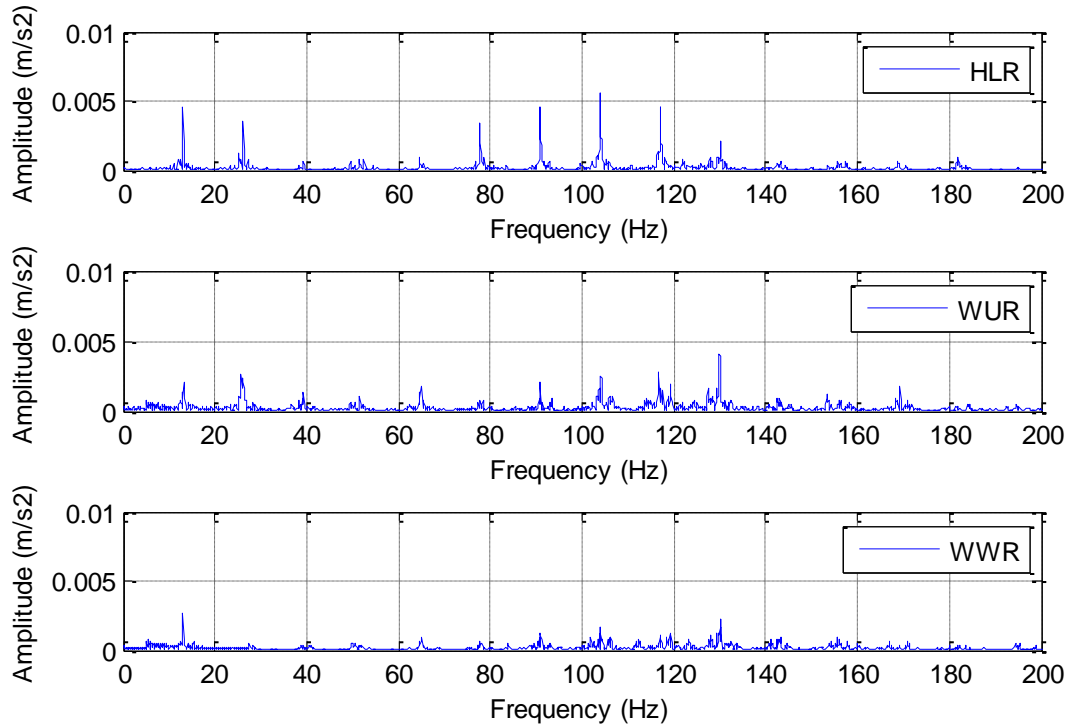


**Figure 4.14 FFT plots at 80 Km/h (13 Hz) for Sensor at Brake drum- Rear Wheel**

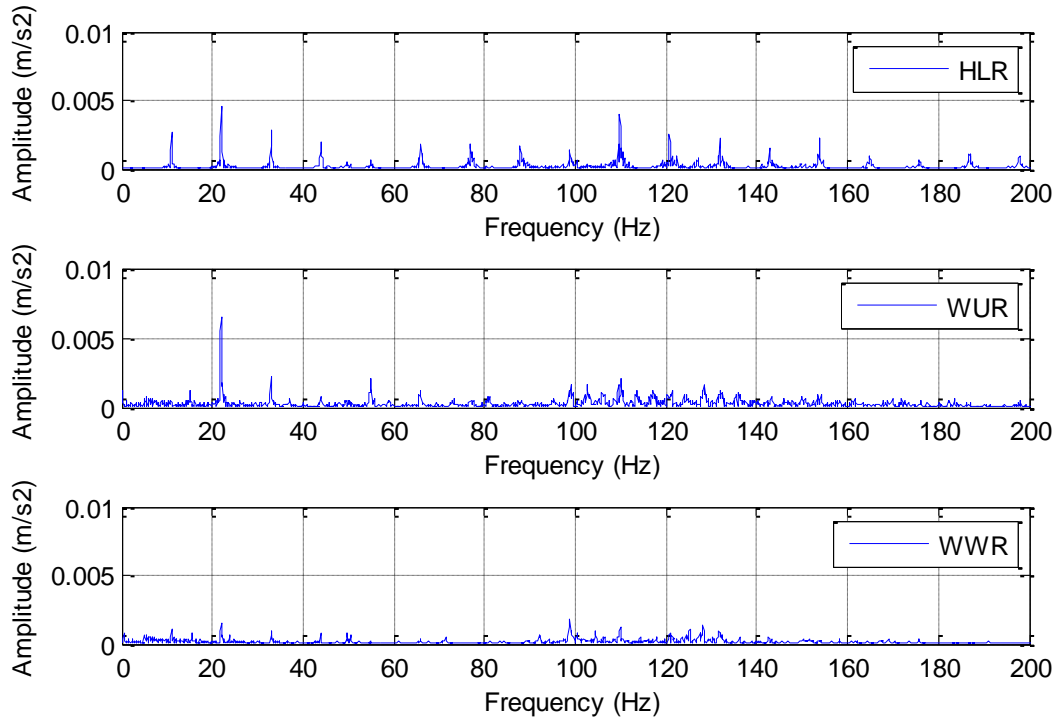


**Figure 4.15 FFT plots at 70 Km/h (11 Hz) for Sensor at Brake drum- Rear Wheel**

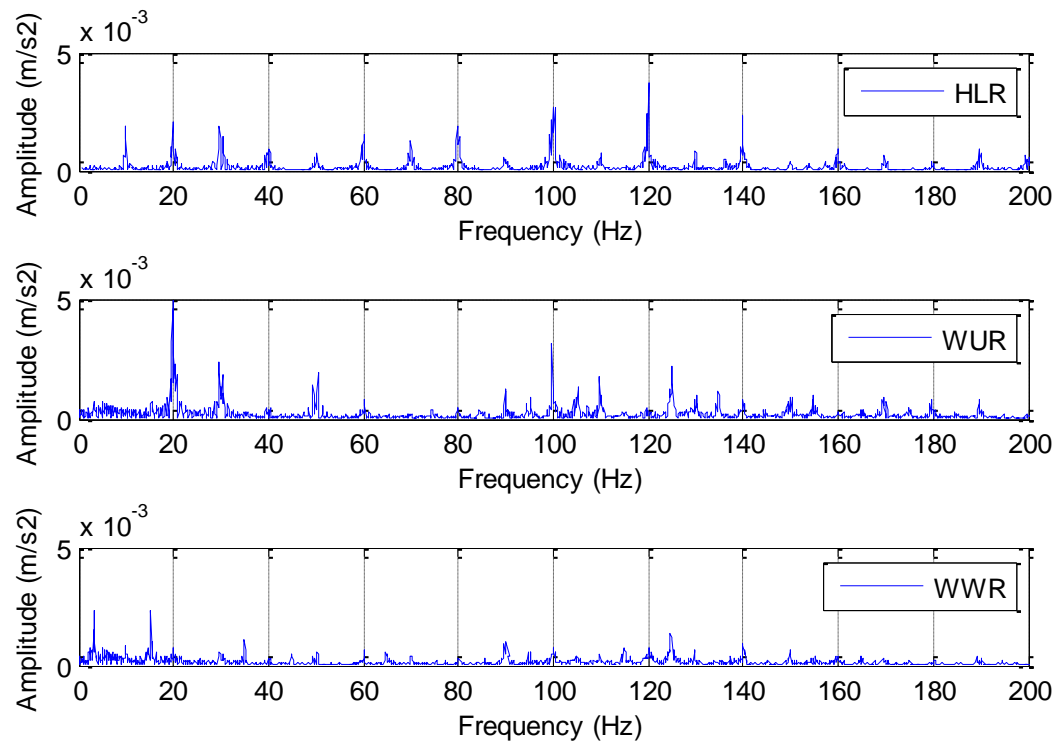


**Figure 4.16 FFT plots at 60 Km/h (10 Hz) for Sensor at Brake drum- Rear Wheel**

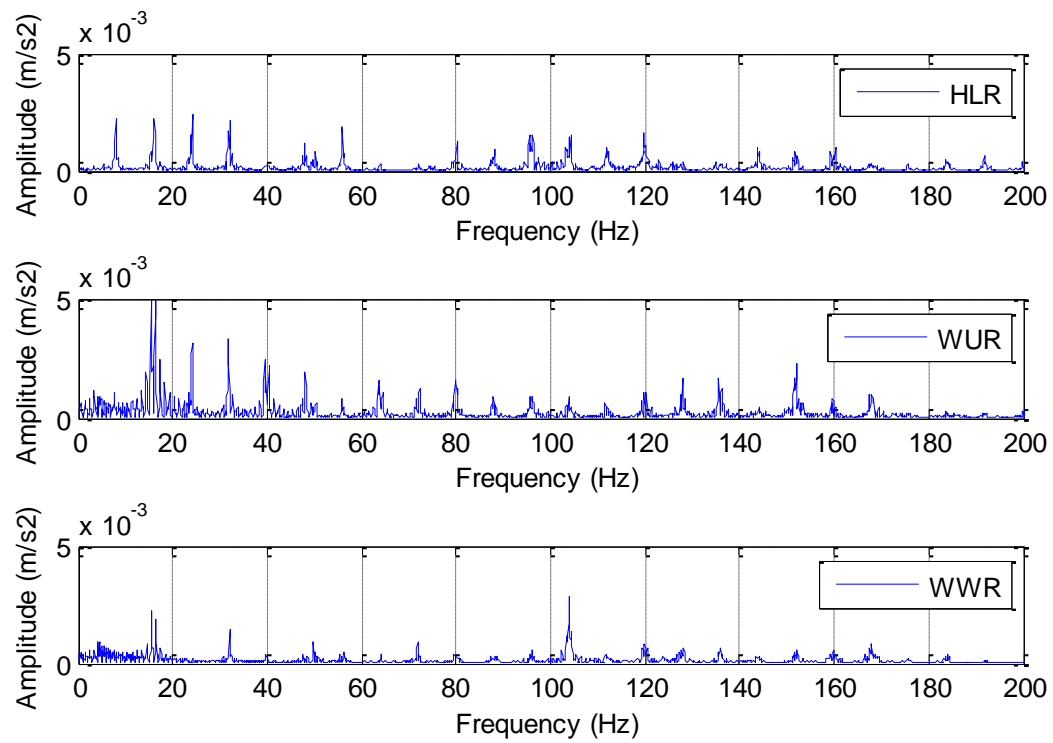


**Figure 4.17 FFT plots at 50 Km/h (8 Hz) for Sensor at Brake drum- Rear Wheel**

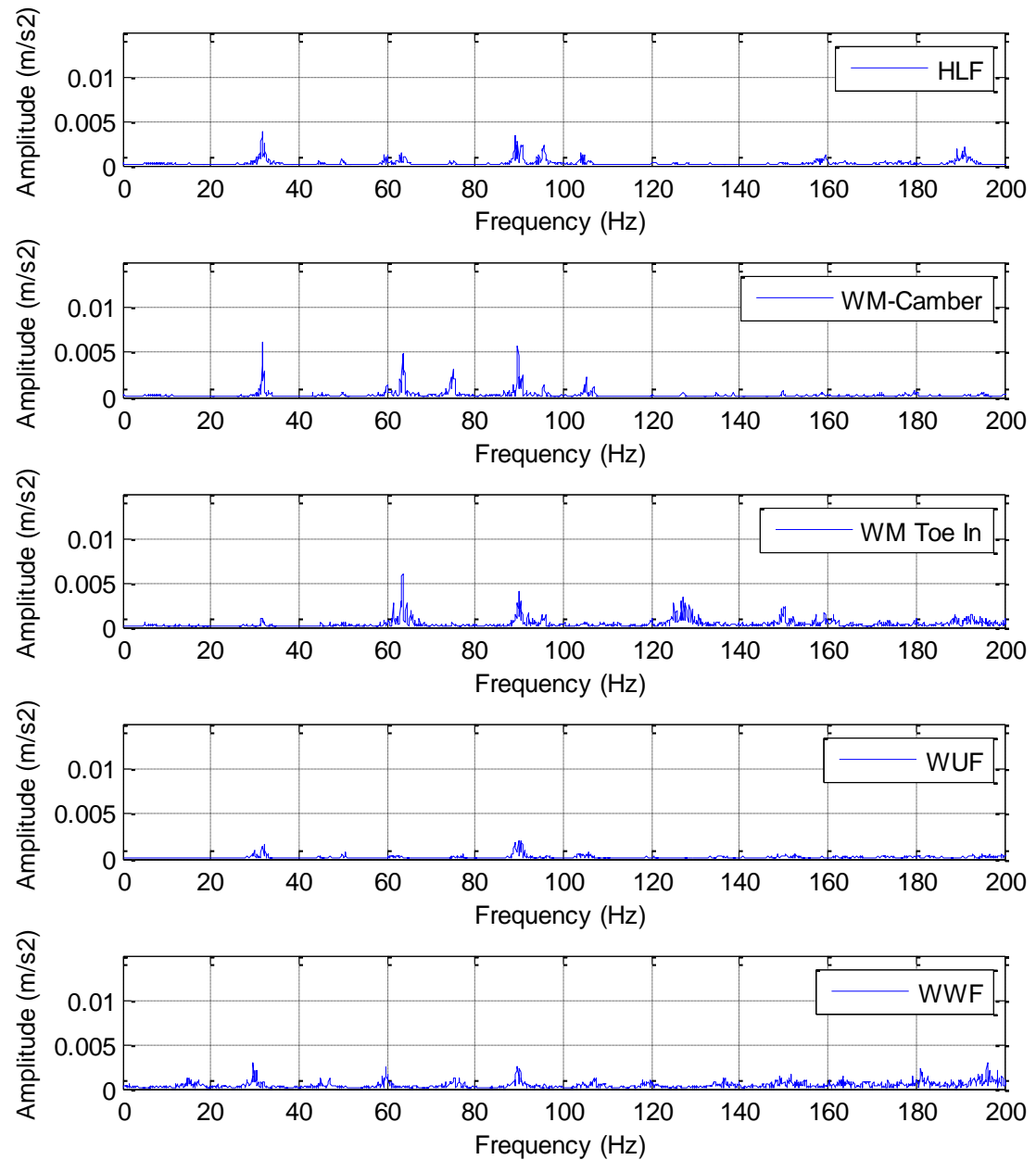


**Figure 4.18 FFT plots at 90 Km/h (15 Hz) for Sensor at LB Arm Front Wheel**

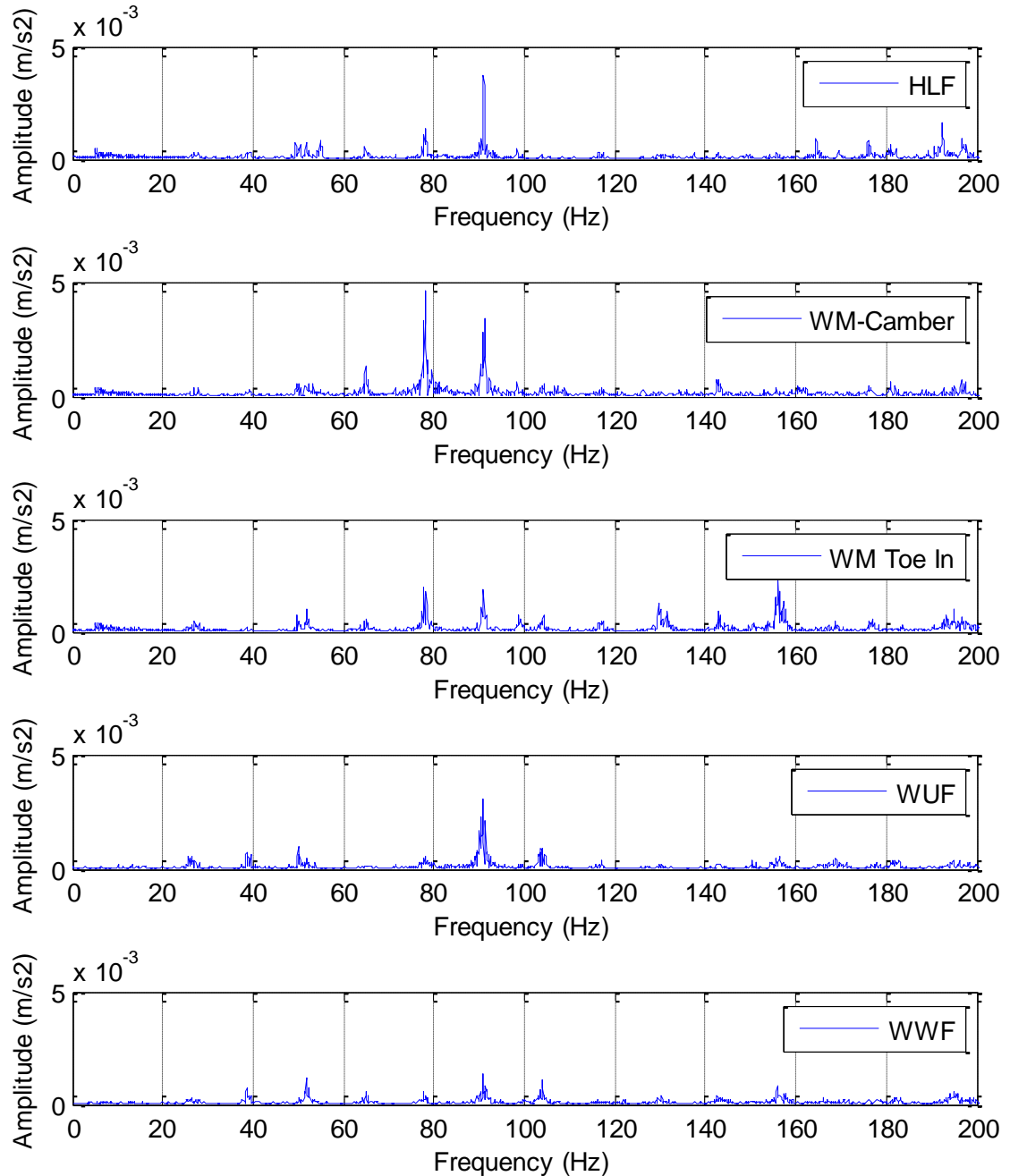


**Figure 4.19 FFT plots at 80 Km/h (13 Hz) for Sensor at LB Arm Front Wheel**

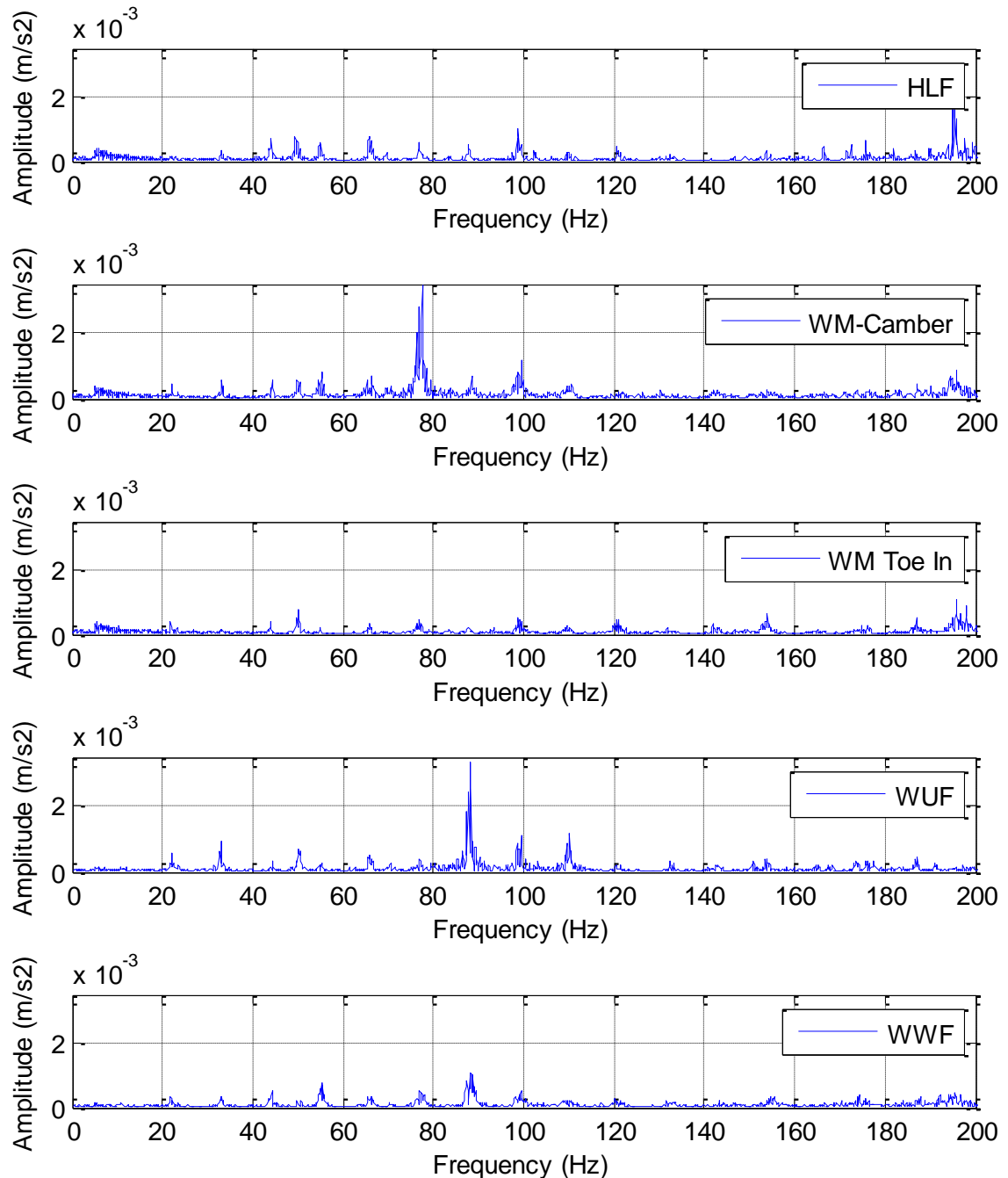


**Figure 4.20 FFT plots at 70 Km/h (13 Hz) for Sensor at LB Arm Front Wheel**

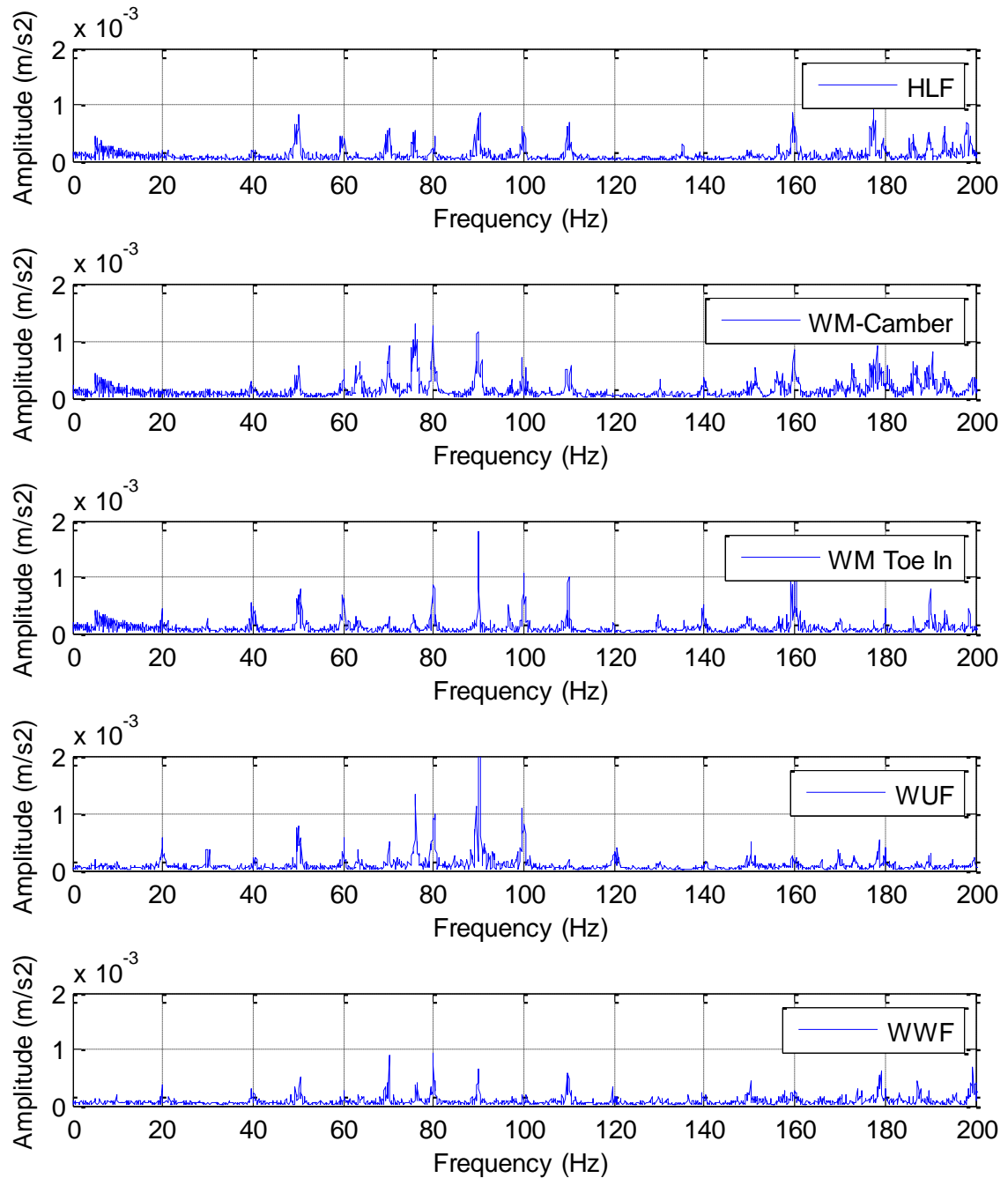


**Figure 4.21** FFT plots at 60 Km/h (10 Hz) for Sensor at LB Arm Front Wheel

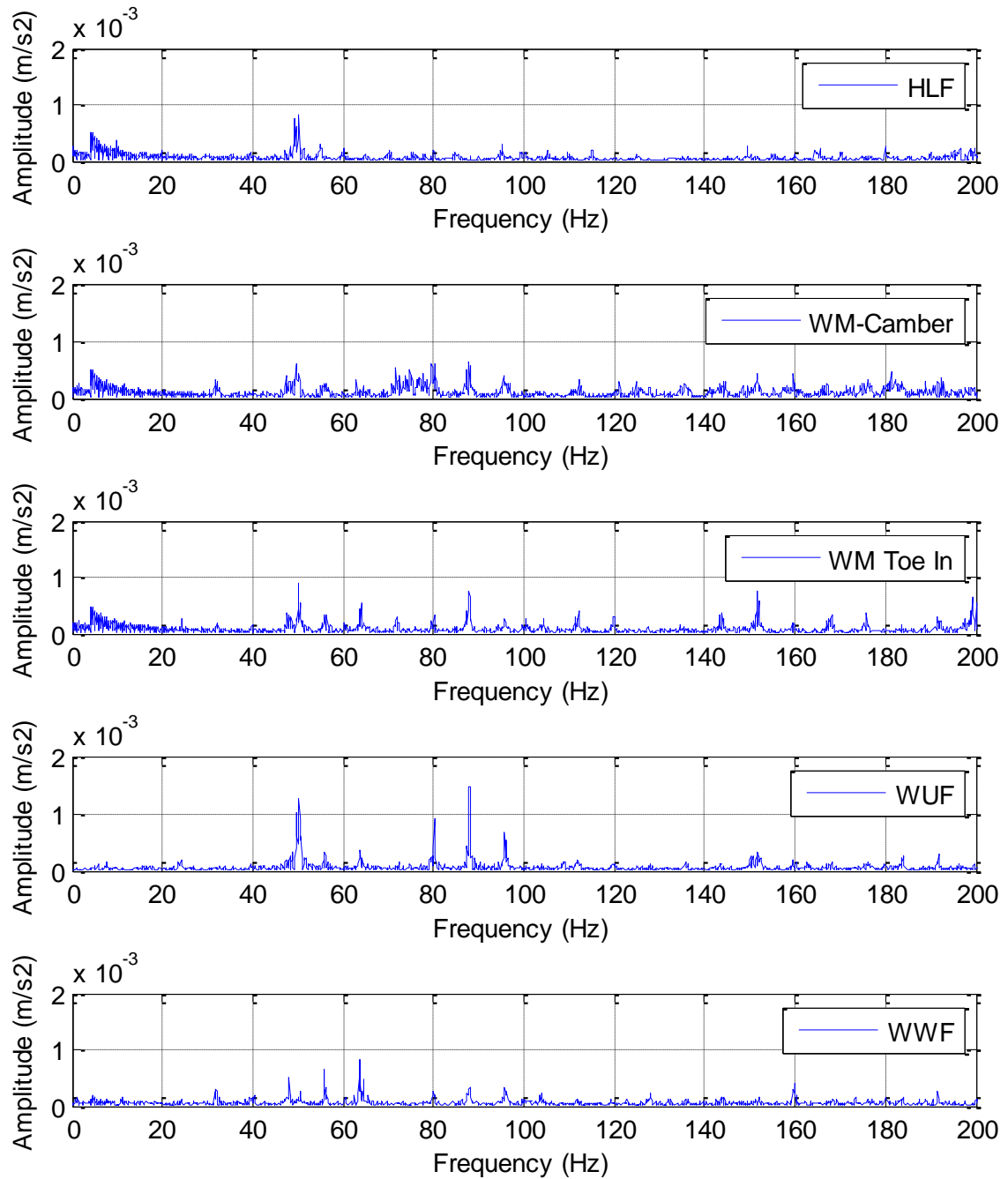


**Figure 4.22 FFT plots at 50 Km/h (8 Hz) for Sensor at LB Arm Front Wheel**

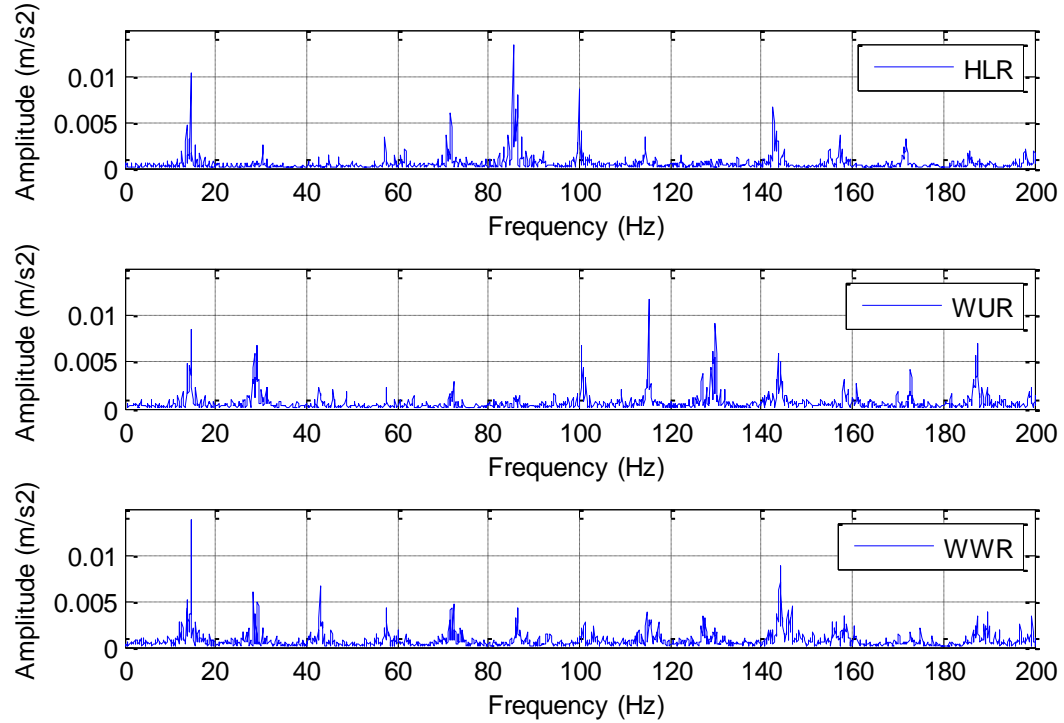


**Figure 4.23 FFT plots at 90 Km/h (15 Hz) for Sensor at Rear Wheel Axle**

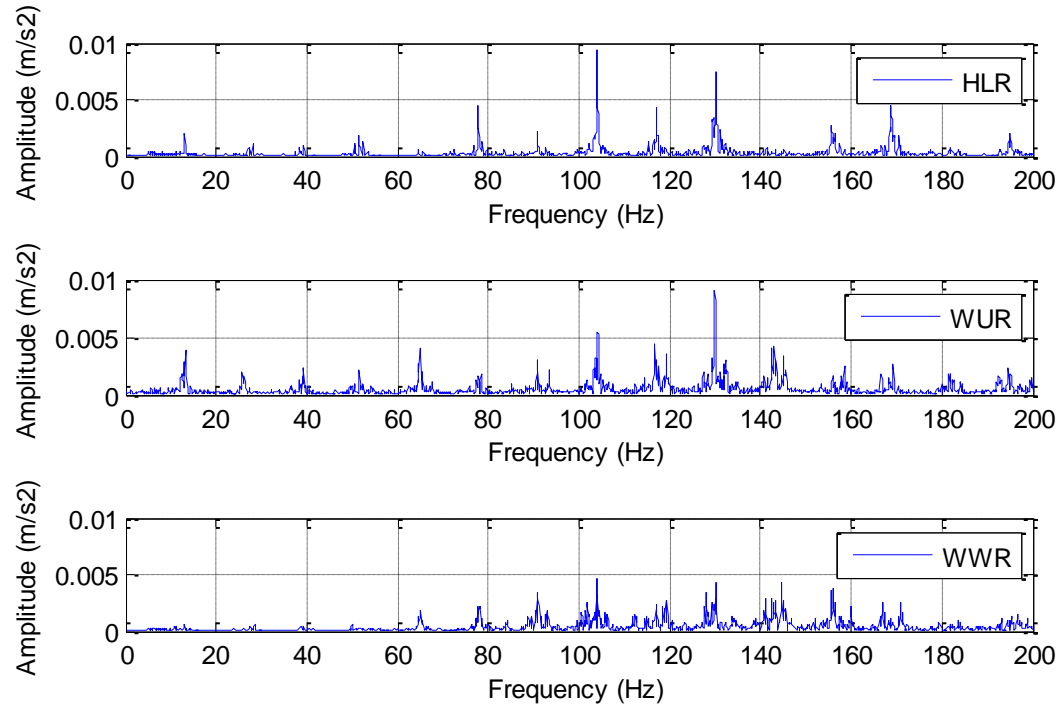


**Figure 4.24 FFT plots at 80 Km/h (13 Hz) for Sensor at Rear Wheel Axle**

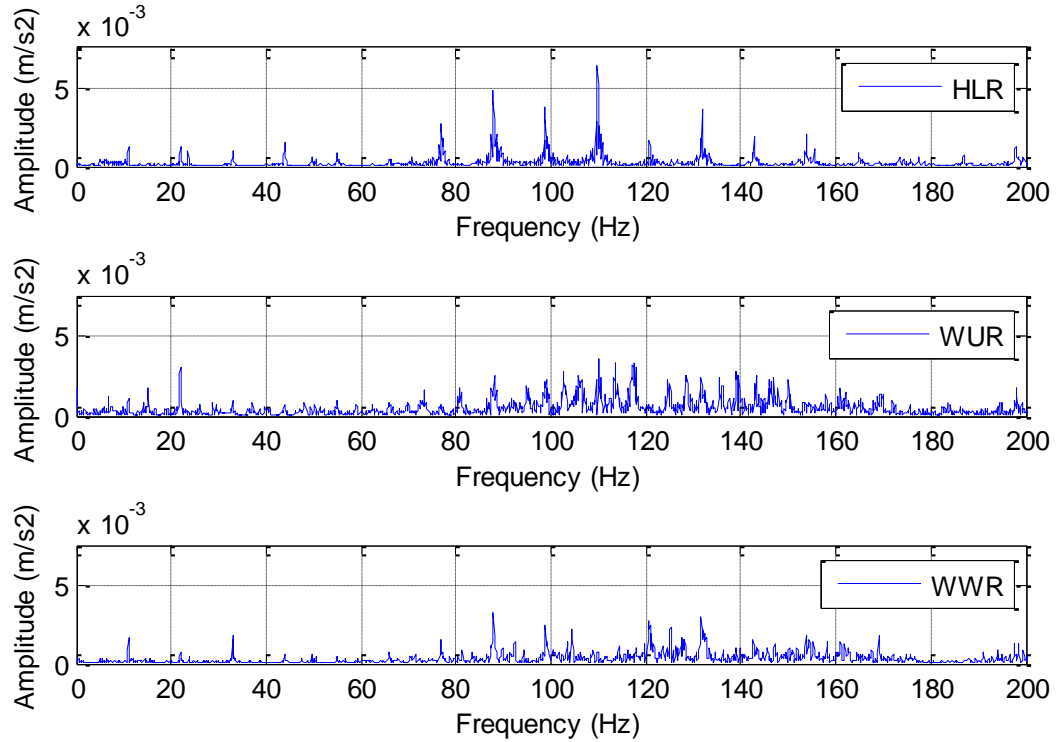


**Figure 4.25 FFT plots at 70 Km/h (11 Hz) for Sensor at Rear Wheel Axle**

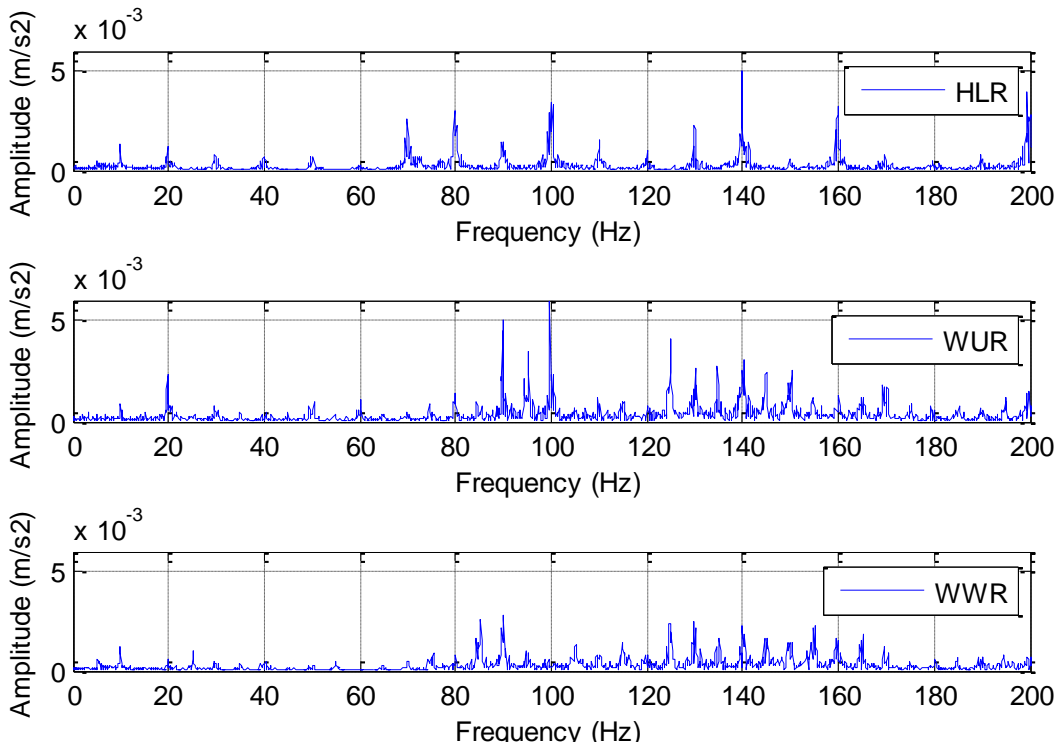


**Figure 4.26 FFT plots at 60 Km/h (10 Hz) for Sensor at Rear Wheel Axle**

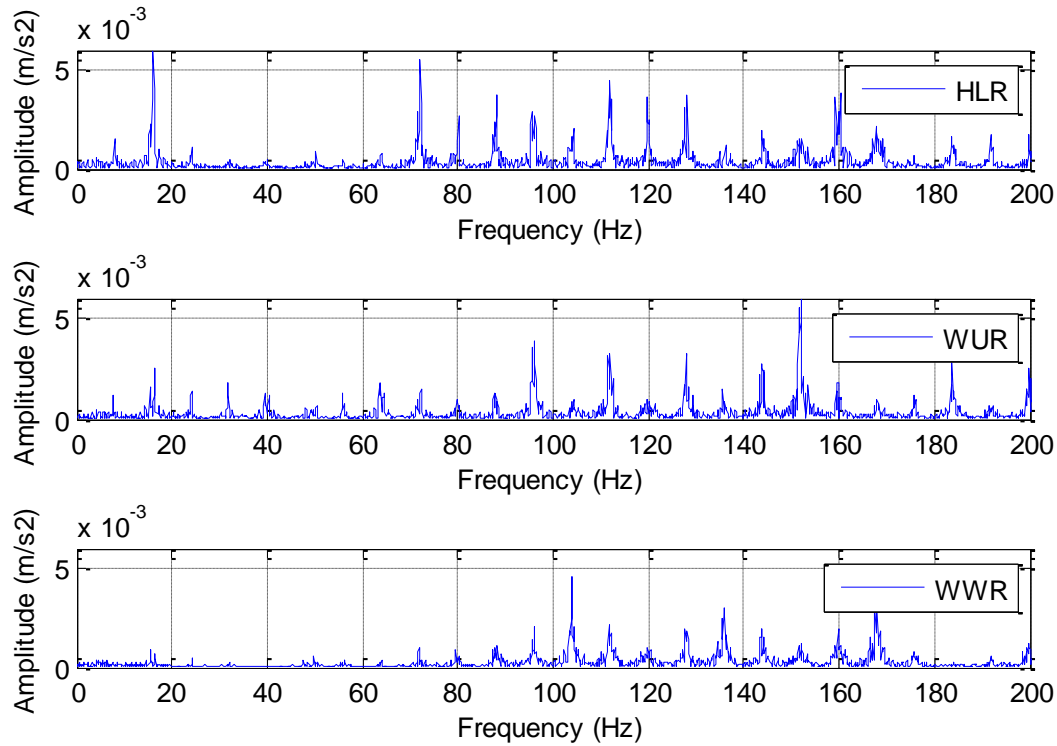


**Figure 4.27 FFT plots at 50 Km/h (8 Hz) for Sensor at Rear Wheel Axle**

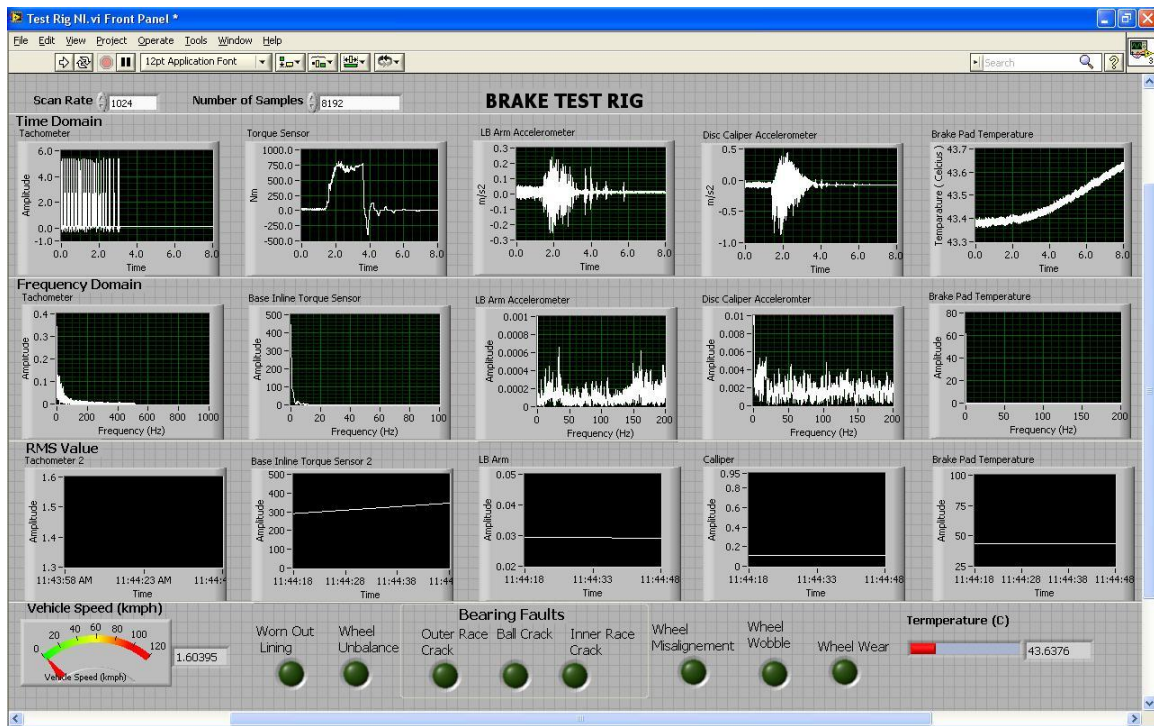
#### 4.4.2 Transient Case

In transient i.e. under braking condition, faults have been deliberately introduced in the quarter car model in the rig. For this case faults have been simulated at two wheel speeds 5 Hz and 10 Hz (i.e. 30 Km/h and 60 Km/h) with two different braking rates. Set of faulty pair of wheels and Brake pad/ Brake shoe supplied with test rig was used to produce these faulty conditions. Full Braking implies that full brake pressure is suddenly applied to the brake pad / drum. Partial Braking implies that only 50% of braking pressure is applied. Faults that have been simulated are listed in Table 4.3. Faults have been simulated for following four cases:

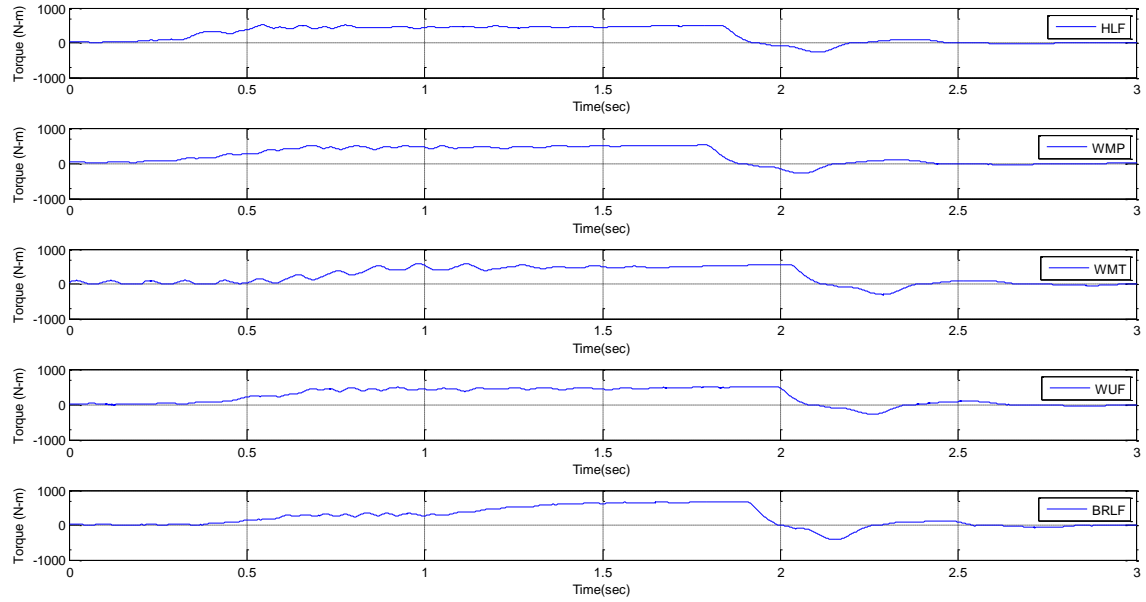
- i. 30 Km/h with Full Braking
- ii. 60 Km/h with Full Braking
- iii. 30 Km/h with Partial Braking
- iv. 60 Km/h with Partial Braking

**Table 4.3 Faults simulated for Transient Case**

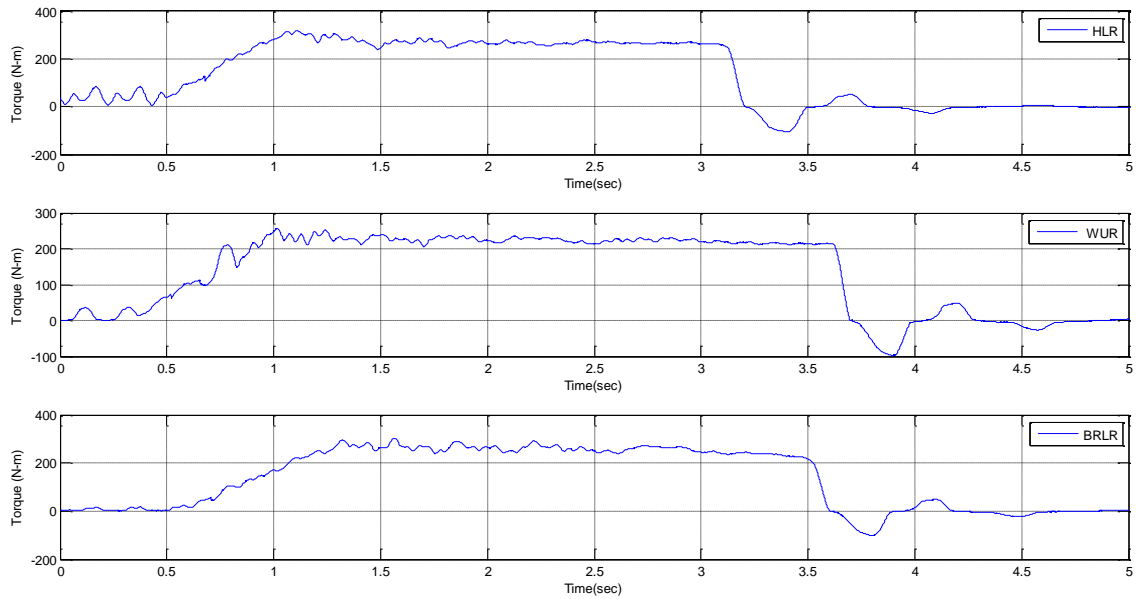
<b>Front Wheel</b>	<b>Rear Wheel</b>
a) Healthy System b) Wheel Misalignment due to Positive Camber c) Wheel Misalignment due to Toe-In d) Wheel Unbalance e) Brake Lining	a) Healthy System b) Wheel Unbalance c) Brake Lining

**Figure 4.28 Front Panel: Typical Vibration Signal at 60 Km/h (10 Hz) for transient**

The vibration signatures for the various faults of transient case were acquired and stored in Desktop PC. Time domain data of the transient signals for each fault are shown in Figure 4.29 – 4.32 for all sensors. A total of 10 sets of vibration signals were acquired for each of the fault for two different braking rates mentioned above. Wavelet transform (Scalogram) of the all signals have been taken and analysed further for the feature extraction.

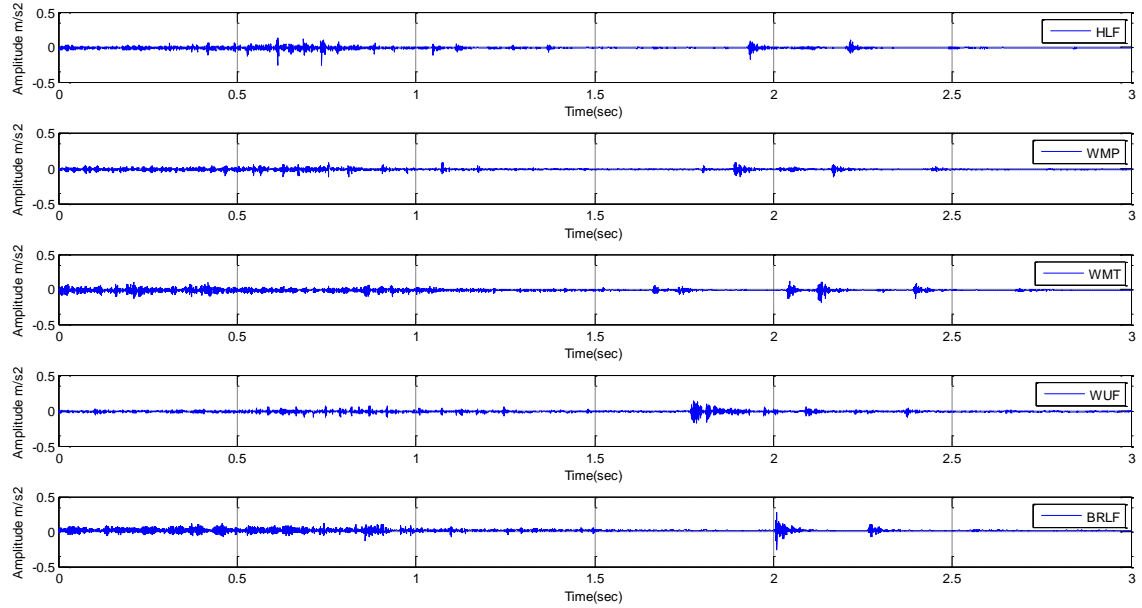


(a)

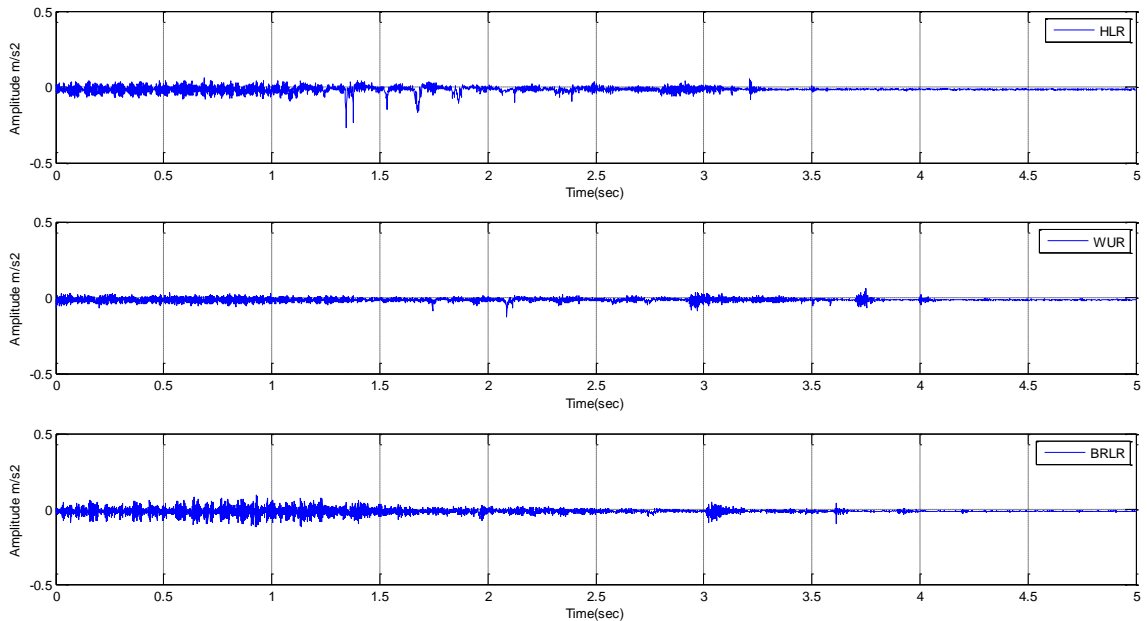


(b)

**Figure 4.29 Time domain data at 30 Km/h for Torque Sensor, Case -1 Full braking**  
**(a) Front Wheel, (b) Rear Wheel**

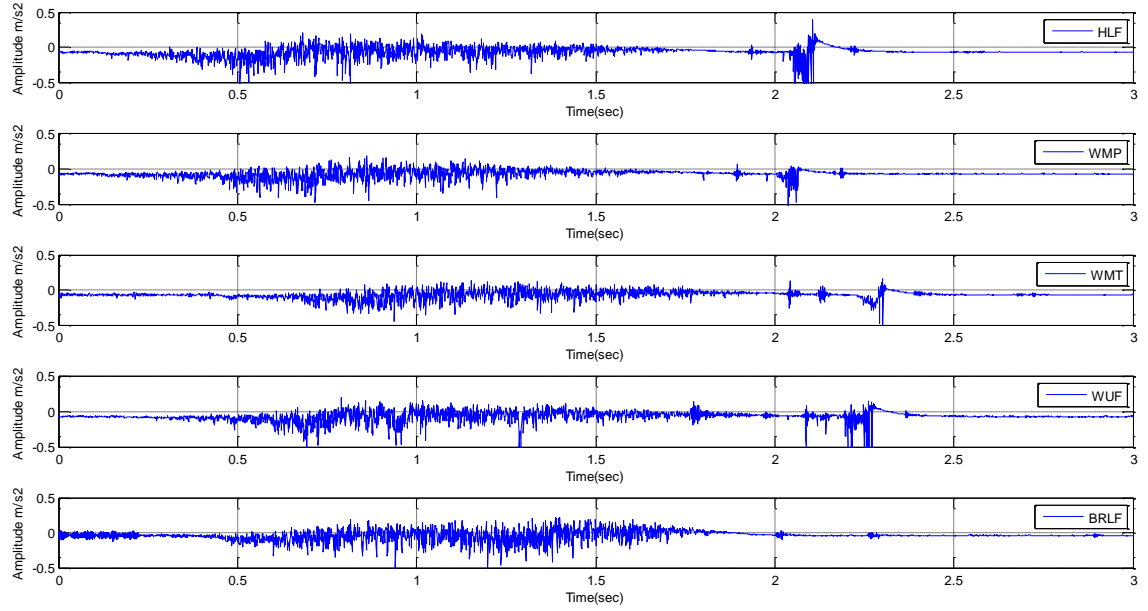


(a)

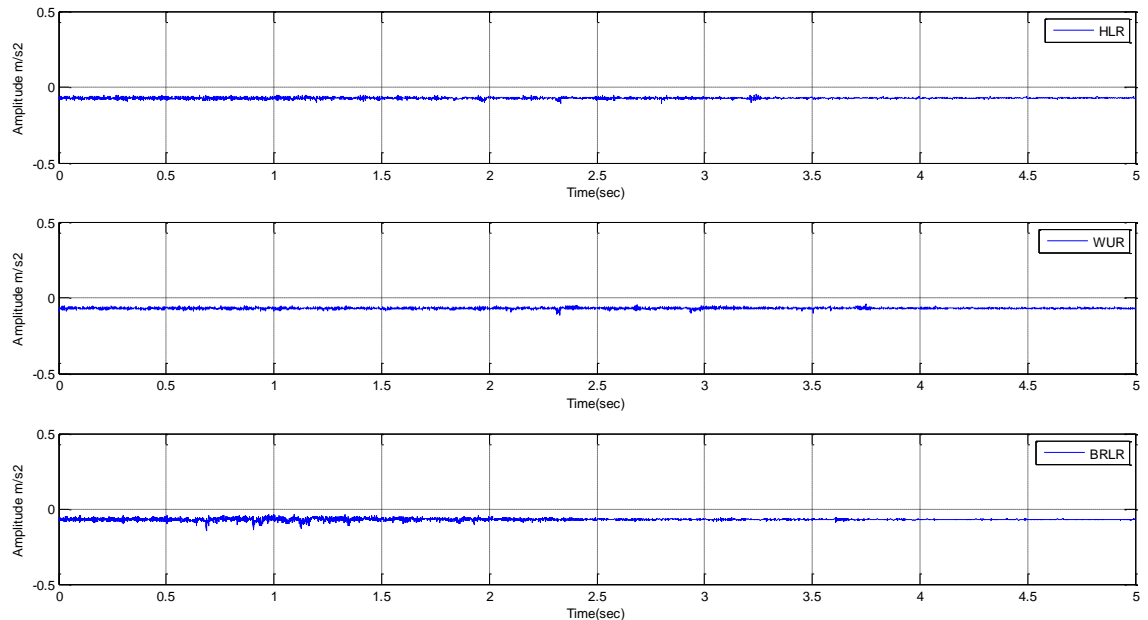


(b)

**Figure 4.30 Time domain data at 30 Km/h, Case -1 Full braking (a) Front Wheel-LB Arm Accelerometer, (b) Rear Wheel- Axle Accelerometer**



(a)



(b)

**Figure 4.31 Time domain data at 30 Km/h, Case -1 Full braking (a) Front Wheel-Brake Caliper Accelerometer, (b) Rear Wheel- Brake drum Accelerometer**

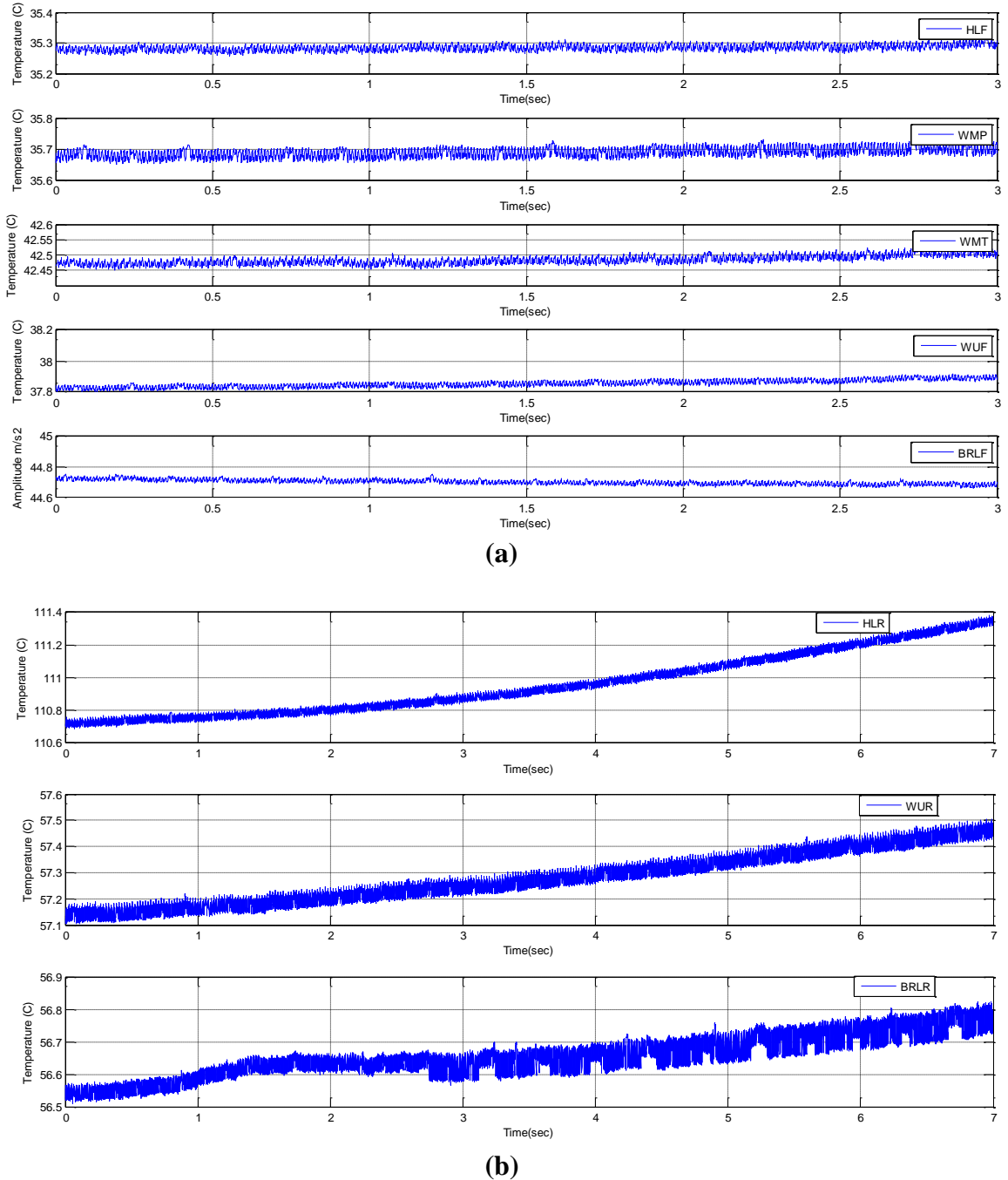


**Figure 4.32 Time domain data at 30 Km/h for Temperature Sensor, Case -1 Full braking (a) Front Wheel, (b) Rear Wheel**

## Analysis of Temperature and Torque Sensor Signal

It is seen that temperature is increasing steadily with the application of brake. For extracting useful information from the temperature signal the gradient of temperature with time have been calculated and observed simultaneously with the torque sensor signal. It has been observed from Figure 4.33 -4.34 that temperature gradient shows clear demarcation for the brake lining faults from the others. However, it is concluded that direct inferences from the temperature signal is complex and would require good digitisable data for appropriate signal processing. This exercise has not been further taken up in the present work and left to be undertaken in future, by subsequent researchers.

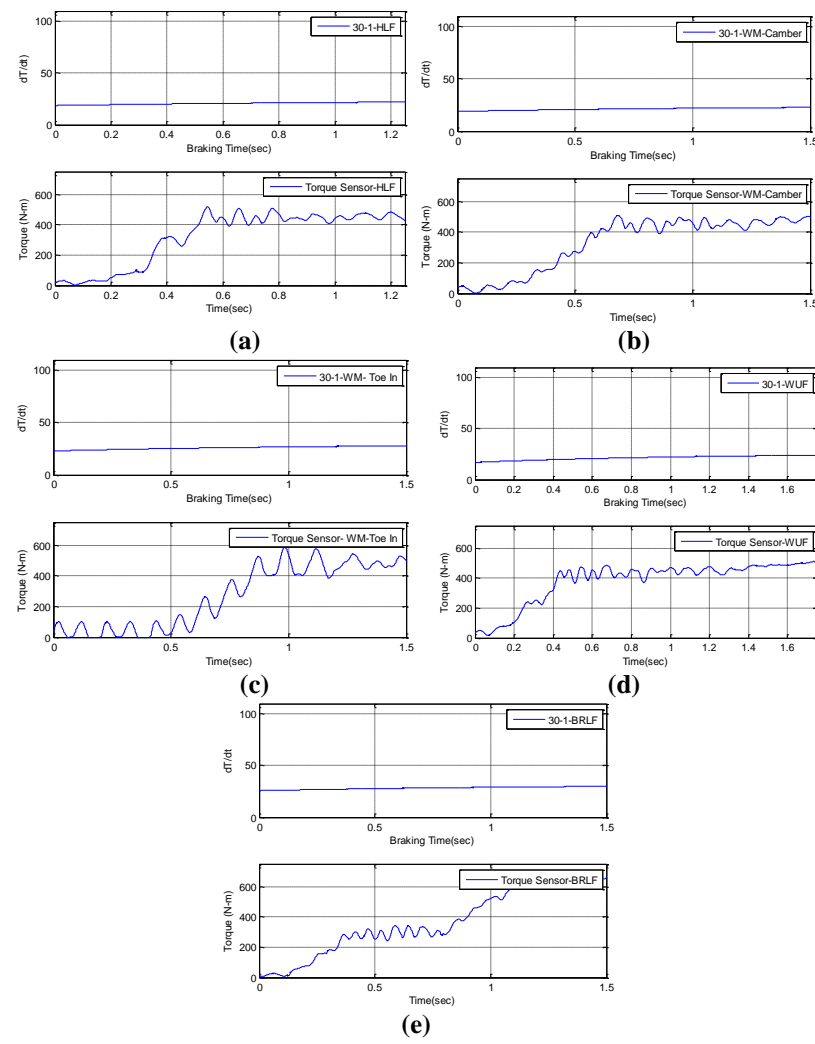


**Figure 4.33**  $dT/dt$  and Torque curves with braking time at 30 Km/h with Full Braking for Front wheel (a) Healthy system (b) WM- Camber (c) WM-Toe In (d) Wheel Unbalance (e) Brake Lining

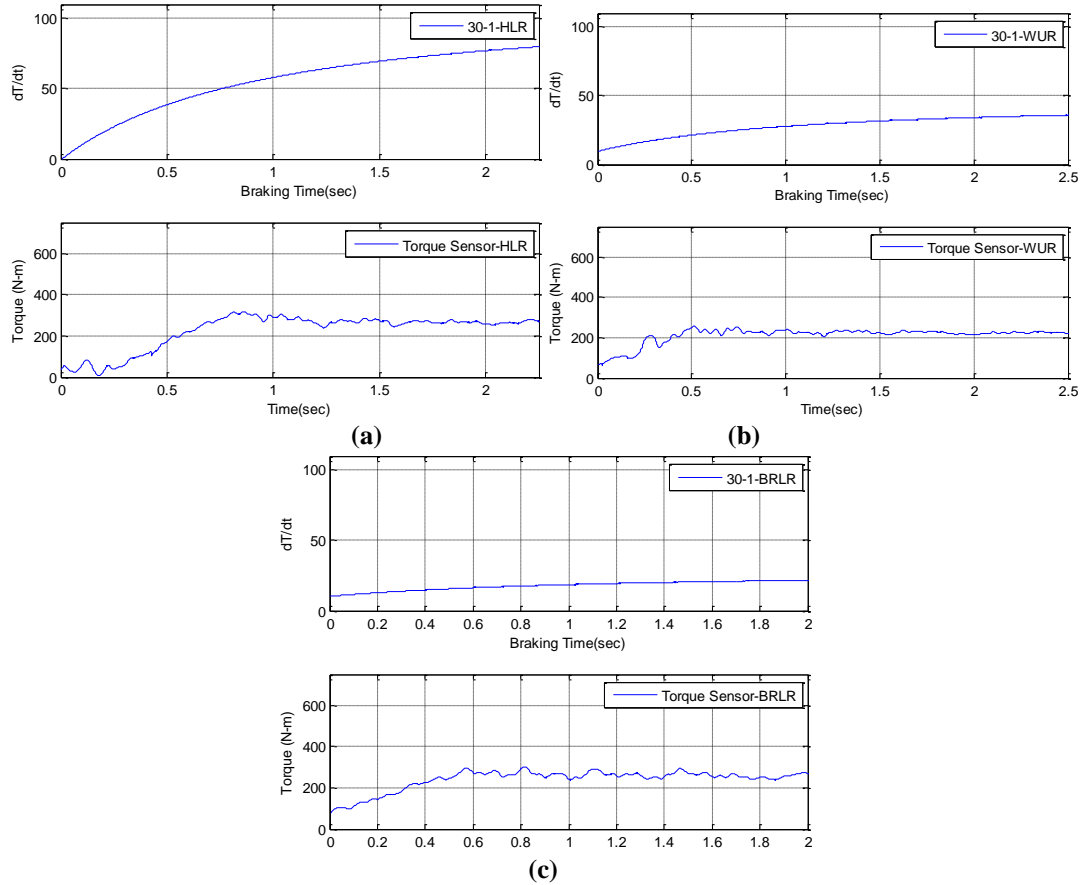


**Figure 4.34 dT/dt and Torque curves with braking time at 30 Km/h with Full Braking for Rear wheel (a) Healthy system (b) Wheel Unbalance (c) Brake Lining Wavelet Transforms of Signals**

Every wavelet function has different frequency scale variations resulting in different frequency resolutions for a fixed scale range. So, selection of an appropriate and best wavelet function is an important step in wavelet transform calculations. In the present work Morlet Wavelet functions has been used.

### Calculation of Wavelet Transform

The wavelet transform is calculated for a fixed scale ranging between 1 to  $S_{max}$  in steps of 0.5. The Transform is stored in the form of coefficient matrix  $[W]$ .

### Scalogram of Vibration Signals

For the purpose of wavelet transform calculation, a simple code is written in MATLAB which takes signal as an input and computes its wavelet transform. Before computing the wavelet transform time domain data have been analyzed thoroughly for each fault and

only braking time data have been taken for the consideration for wavelet transform, other part of the time domain data has been discarded as it contains unwanted information. The resultant transform is plotted as a scalogram. The scalograms of signals from LB Arm/Rear axle accelerometers with Speed-Time plots are shown in Figure 4.35 - 4.38. The scalograms shown are obtained with Morlet wavelet as the mother wavelet function.

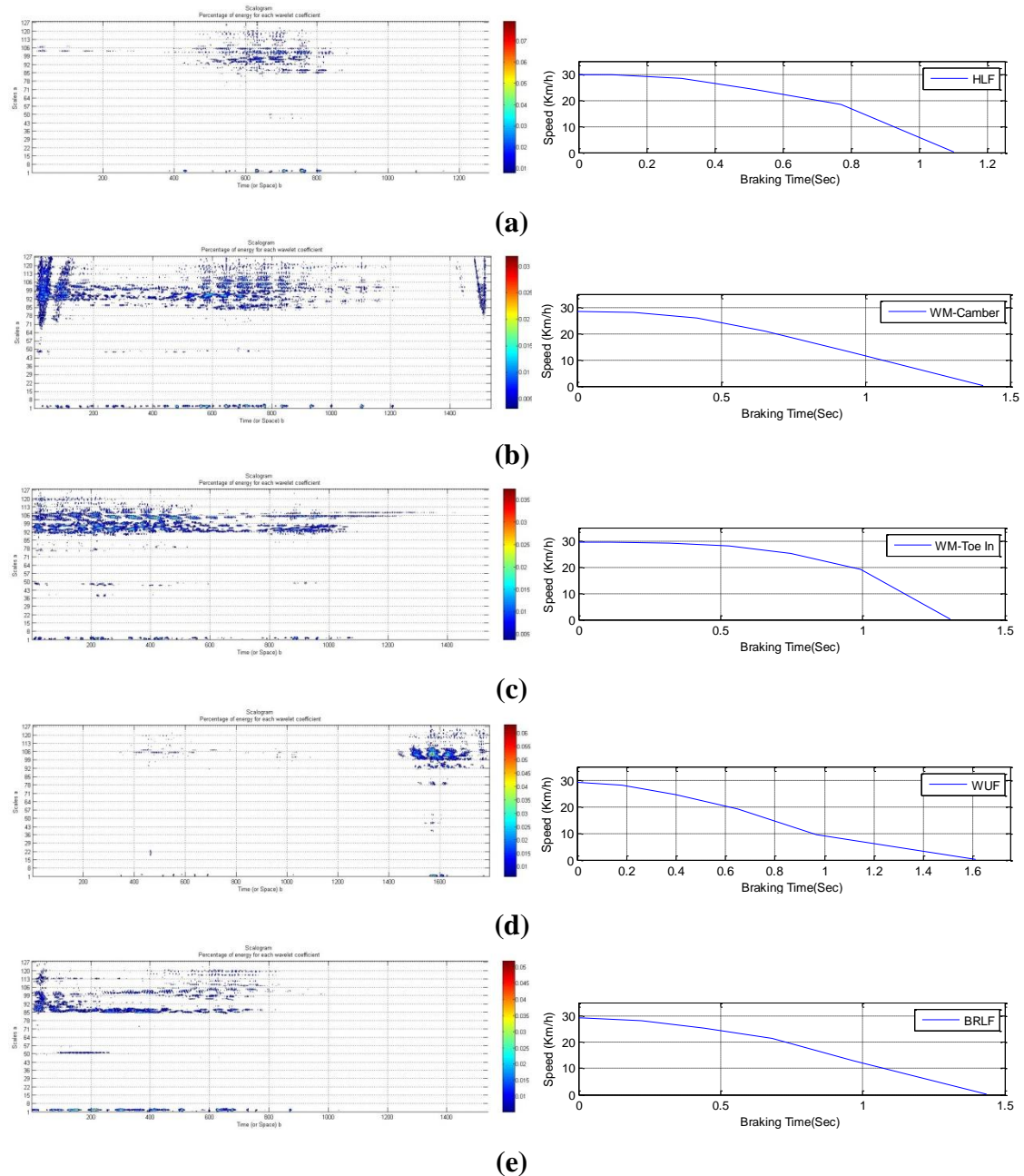


**Figure 4.35 Scalogram and Speed vs Time at 30 Km/h with full braking for front wheel (a) Healthy System (b) Wheel Misalignment- Camber (c) Wheel Misalignment – Toe In (d) Wheel Unbalance (e) Brake Lining**

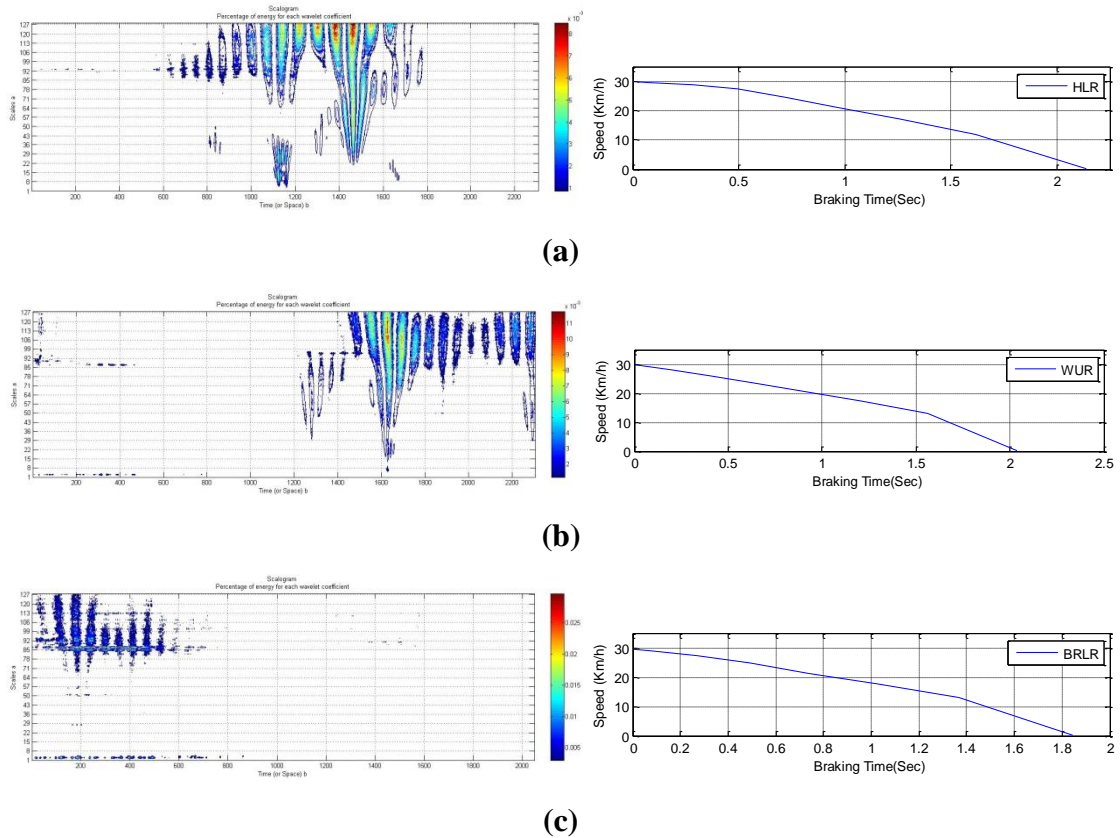


**Figure 4.36 Scalogram and Speed vs Time 30 Km/h with full braking for Rear wheel**

**(a) Healthy System (b) Wheel Unbalance (c) Brake Lining**

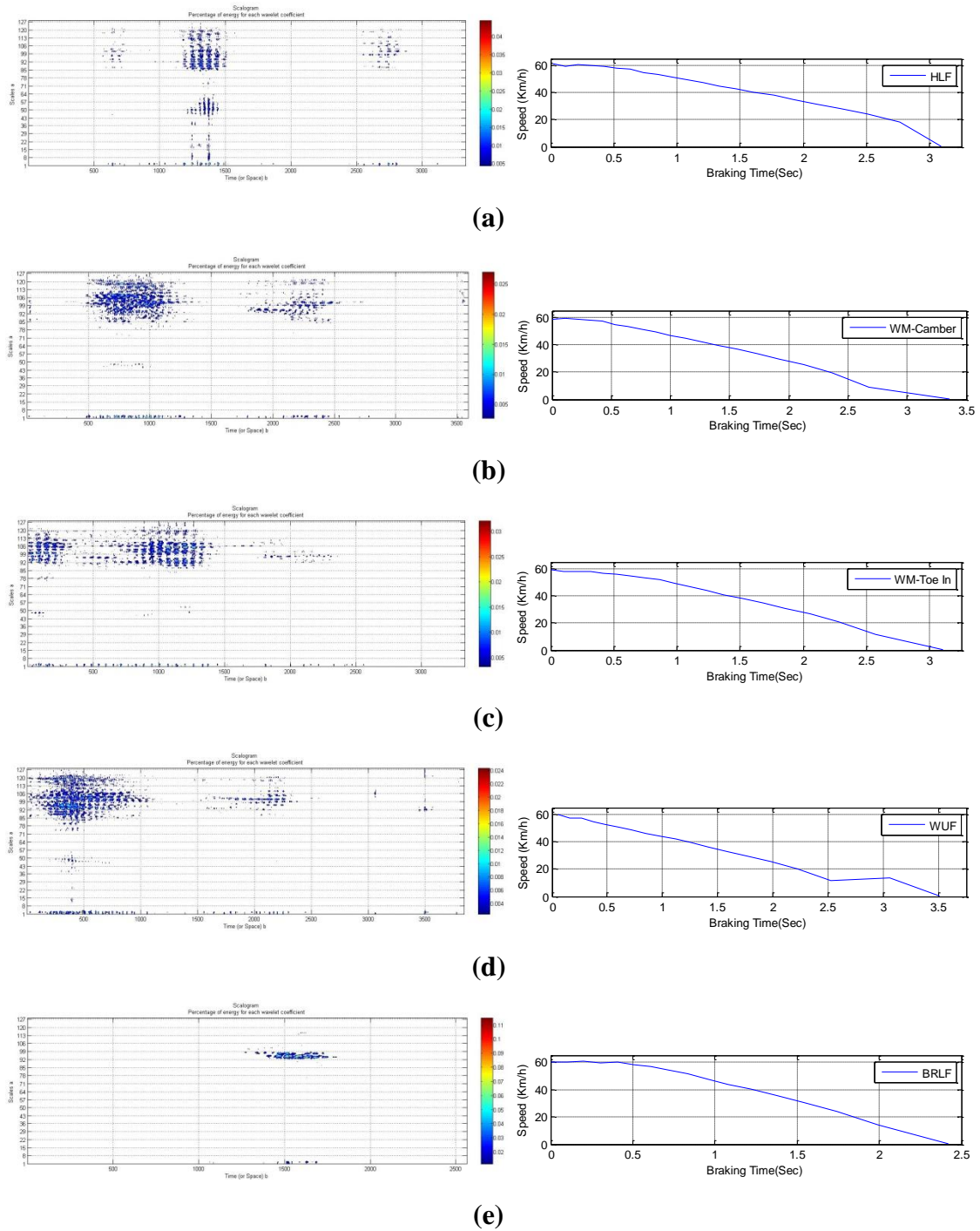


**Figure 4.37 Scalogram and Speed vs Time at 60 Km/h with full braking for front wheel**

**(a) Healthy System (b) Wheel Misalignment- Camber (c) Wheel Misalignment – Toe In (d) Wheel Unbalance (e) Brake Lining**

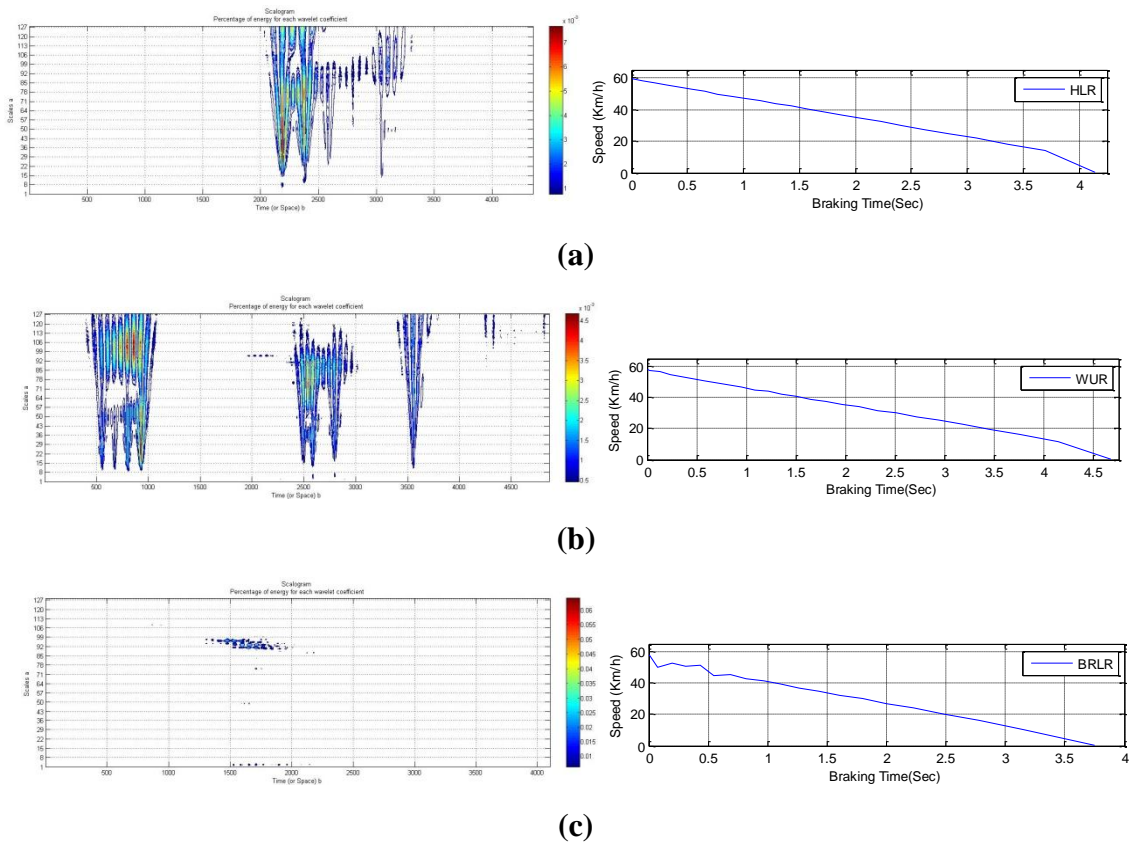


**Figure 4.38 Scalogram and Speed vs Time 60 Km/h with full braking for Rear wheel**  
**(a) Healthy System (b) Wheel Unbalance (c) Brake Lining**

### Feature Extraction from Transform Coefficients

Apart from the original intention of the wavelet transform for the analysis of non-stationary signals, another very important and successful application of the wavelet in machine fault diagnostics is fault feature extraction. Due to the compact support of the basis functions used in the wavelet transforms, wavelets have good energy concentration properties. Most coefficients are usually very small, and can be discarded without causing a significant error for signal's presentation. Therefore, the wavelet transform can present the signal with a limited number of coefficients. These coefficients usually can be directly used as the fault features. The key problem is which coefficients should be selected as the fault features and can best describe the fault.

## **Feature Extraction**

For the purpose of extracting features, wavelet transforms of the signals from two accelerometers have been taken. An algorithm has been developed to automatically extract features from wavelet transforms of the signatures. Calculation of wavelet transforms has already been described in previous sections. The size of the resultant wavelet transform coefficient matrix is practically too large to search for features. Hence, it is to be further reduced. For this, five prominent energy components with scale information from the wavelet transform have been extracted for all listed faults. So, 10 (5 x2) features are extracted for each fault which are stored as a vector.

## **Fault Diagnosis**

The features extracted here need to be processed further to diagnose the faults. It is mainly due to the absence of any clear visual pattern in the features. So, an expert system is developed to recognize the typical pattern associated with the extracted features. Neural networks are employed to develop the expert system. The details associated with neural networks and trainings are described in next chapter.

## **4.5 Remarks**

In this chapter fault simulation, instrumentation and data acquisition have been discussed. Characteristics of the acquired signatures in terms of their harmonics have been identified for steady speed cases. Similarly characteristic features for transient cases have also been identified and extracted, which can be fed to the neural network as inputs.

# CHAPTER 5

## NETWORK TRAINING AND FAULT IDENTIFICATION

In the process of fault diagnosis, once the vibration data is acquired and analysed, it comes to the stage of network training and validation. It is followed by extraction of relevant features from data, selection of neural network architecture and selection of training algorithm. In the present study, an algorithm for automatic feature extraction is developed using MATLAB R2011a. Various architectures of Back Propagation Network are explored. Trained networks are finally tested and validated for fault identification.

### **5.1 Feature Extraction**

As discussed in chapter 1 and chapter 3, ANN has been used as fault classifier in this study. ANN learns by training on observed data with known inputs and outputs. It is impractical to feed whole waveform as input to the ANN due to its large size and it may contain unnecessary frequencies which may confuse the neural network. Thus it is important to give relevant inputs only to the neural network. This process of separating characteristic information from raw data is called as feature extraction. Effective feature extraction techniques are very critical for the success of fault diagnosis. Many researchers have used time domain features as well as frequency domain features. In present work amplitudes of spectrum at particular harmonics (for steady case) and wavelet transform coefficients corresponding to high energy content for braking time (for transient case) have been used as input features to ANN. Separate algorithms have been developed to automatically extract features from frequency spectrum and wavelet transform coefficient to generate training vector for ANN for steady and transient case respectively.

ANN training and fault identification can be explained by flow chart shown in Figure 5.1. Sensors pick the vibration signature from the test rig. Features are then extracted from acquired data which form input vector to the neural network. Input vectors are divided in two groups namely, Training data sets and Validation / Test data sets. Training data sets are fed to network during training, with respect to which, weights and

biases are updated. Learning continues until desired goal is achieved. Once trained, even though the network is ready for actual application, it is validated using remaining data sets.

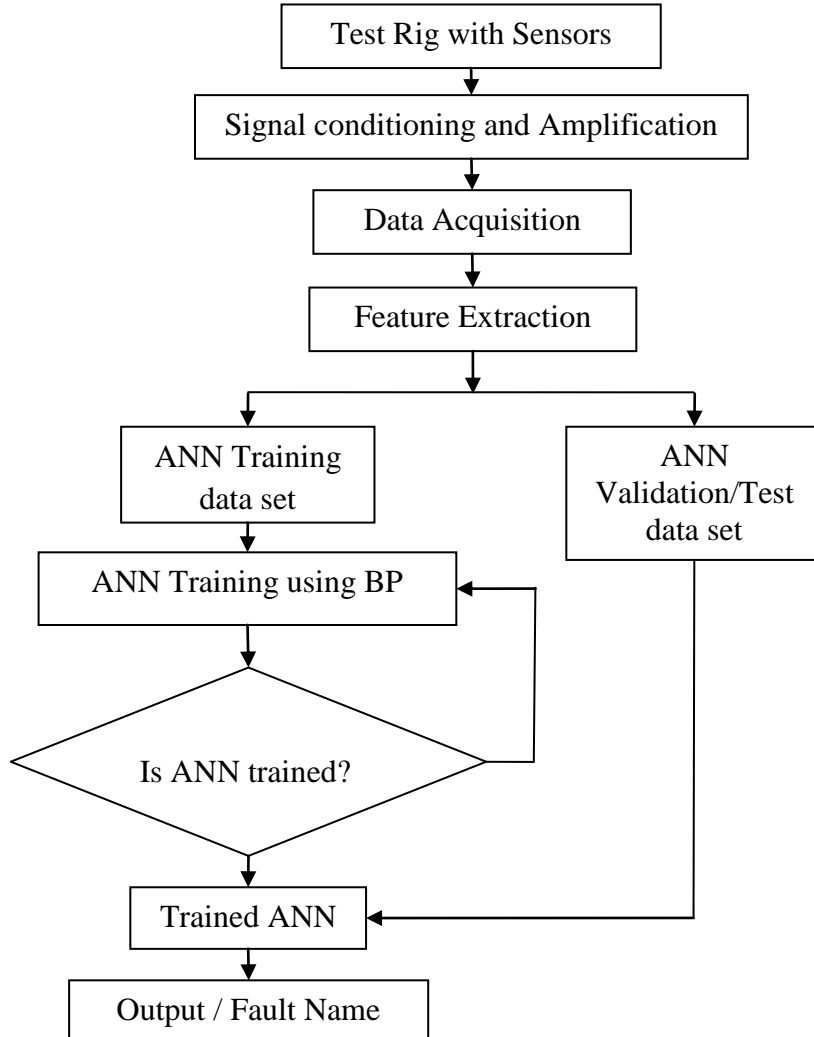


**Figure 5.1 Fault diagnosis algorithm**

### 5.1.1 Selection of Features

As discussed in previous chapter, amplitudes of vibration and energy associated with the signals changes due to introduction of faults.

Experiments have been conducted in two parts:

a) **Steady State operations:**

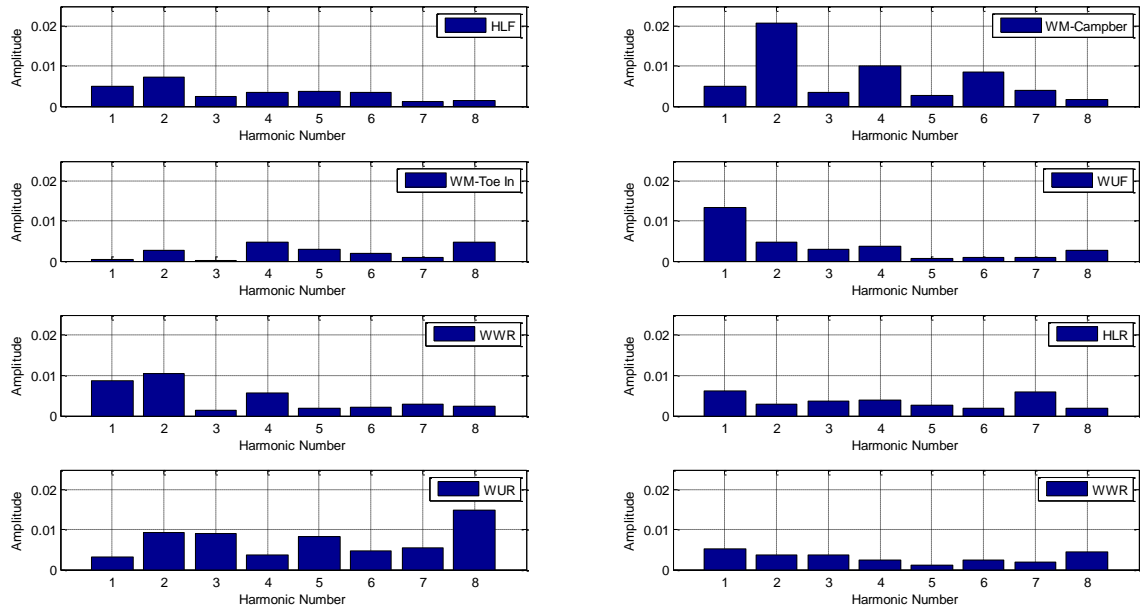
Vibration signals have been recorded for motor operating frequency ranging from 8 Hz to 15 Hz (corresponding to 50 Km/ to 90 Km/h i.e. at five different speeds

at interval of 10). It has been observed in the frequency spectrum that, frequency components beyond 800 Hz indicate very less alteration due to introduction of faults. As the running frequencies are from 8 Hz to 15 Hz, and higher frequency components (beyond 200 Hz) might be associated with some unidentified natural frequencies of test rig structure and sub-components; hence higher frequency range beyond 200 Hz can be neglected without any significant information loss. For such fault identification generally, first 5 harmonics are considered sufficient, but it was observed in the frequency spectrum that some higher harmonics also excited for some faults. Thus amplitudes corresponding to first eight harmonics have been extracted from FFT spectrum of each sensor signal. In total 16 (8x2) features have been extracted to form the input training vector for fault diagnosis. Sets of faults simulated were organized of eight individual faults shown in Table 5.1.

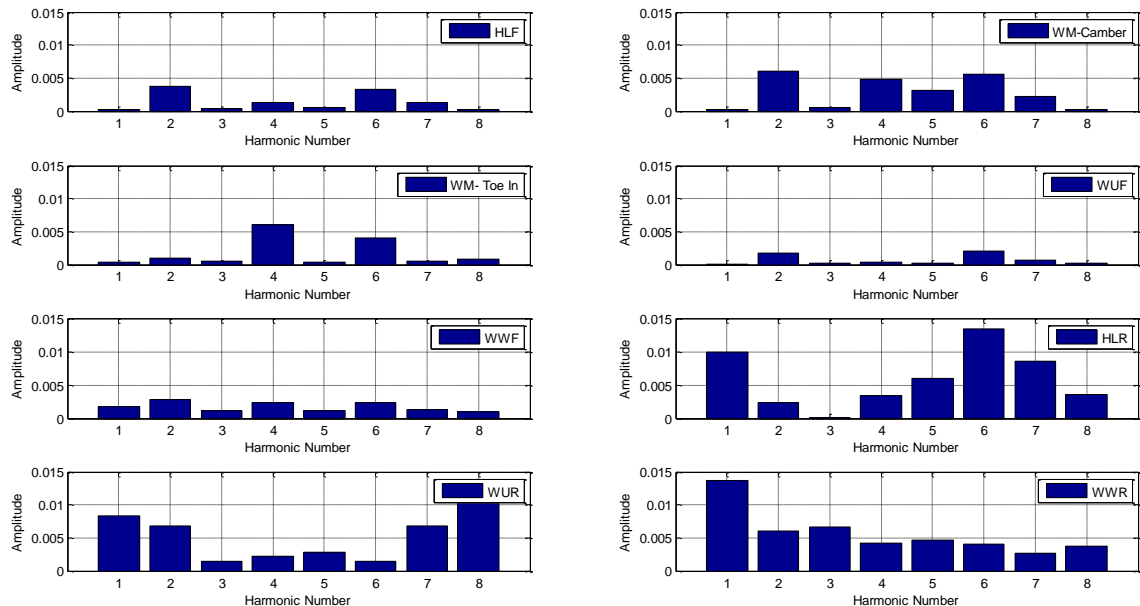
**Table 5.1 Numbering of Faults for Steady Case**

S. No	Fault No	Fault
1	1	HLF- Healthy System Front
2	2	HLR- Healthy System Rear
3	3	WUF- Wheel Unbalance Front
4	4	WUR- Wheel Unbalance Rear
5	5	WMP- Wheel Misalignment due to Camber
6	6	WMT- Wheel Misalignment due to Toe In
7	7	WWF- Worn Wheel Front
8	8	WWR- Worn Wheel Rear

Features extracted have been shown in Figure 5.2 – 5.6 for two accelerometers at above mentioned speed. It has been observed as the speed decreases the amplitudes of the harmonics also decreases. At low vehicle speed i.e. at 30 Km/h and 40 Km/h energy associated with the system is apparently, too less to excite the harmonics.

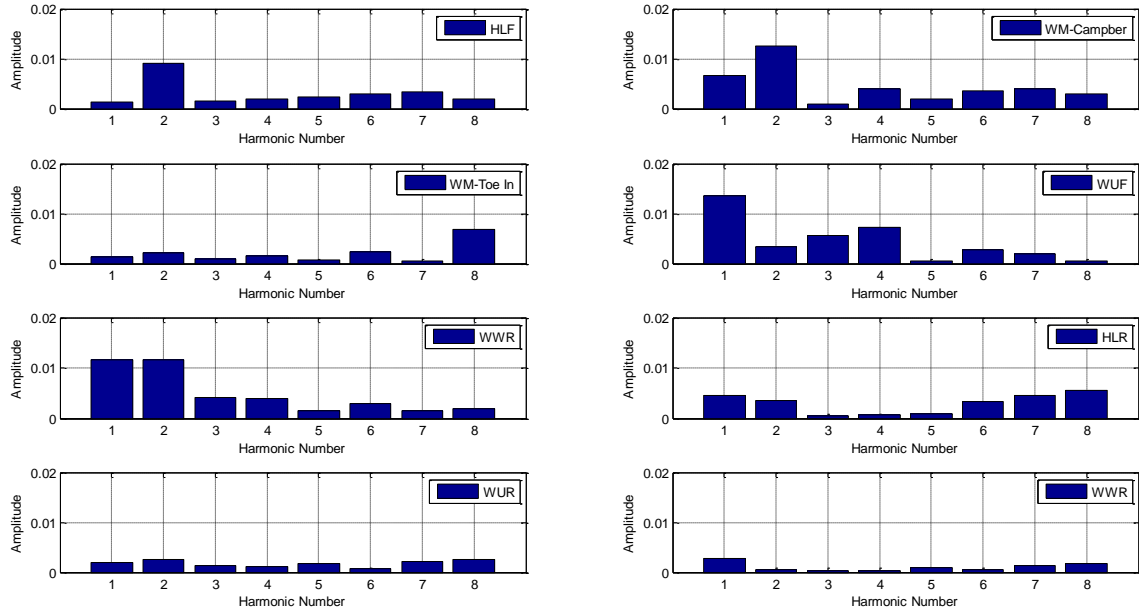


(a)

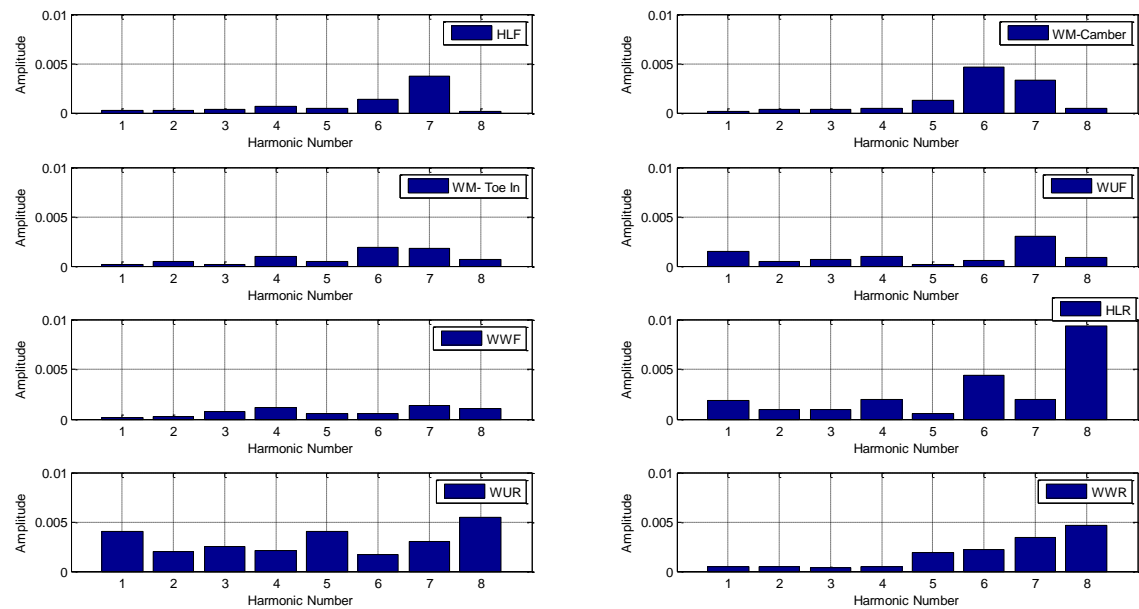


(b)

**Figure 5.2 Feature extraction: Speed 90 Km/h (a) Brake Pad Sensor (b) LB Sensor**

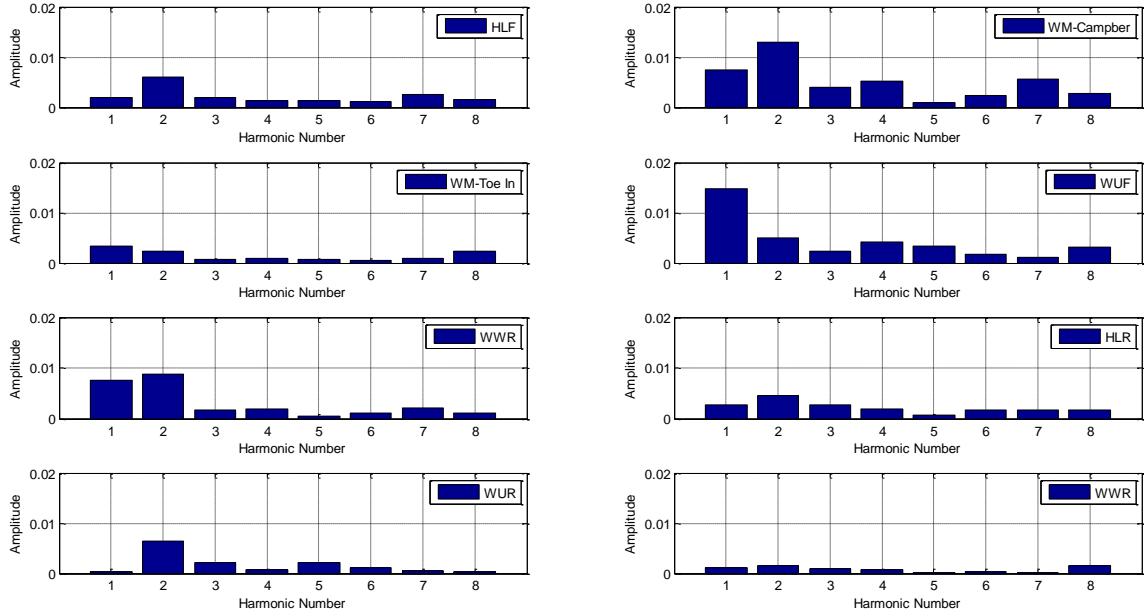


(a)

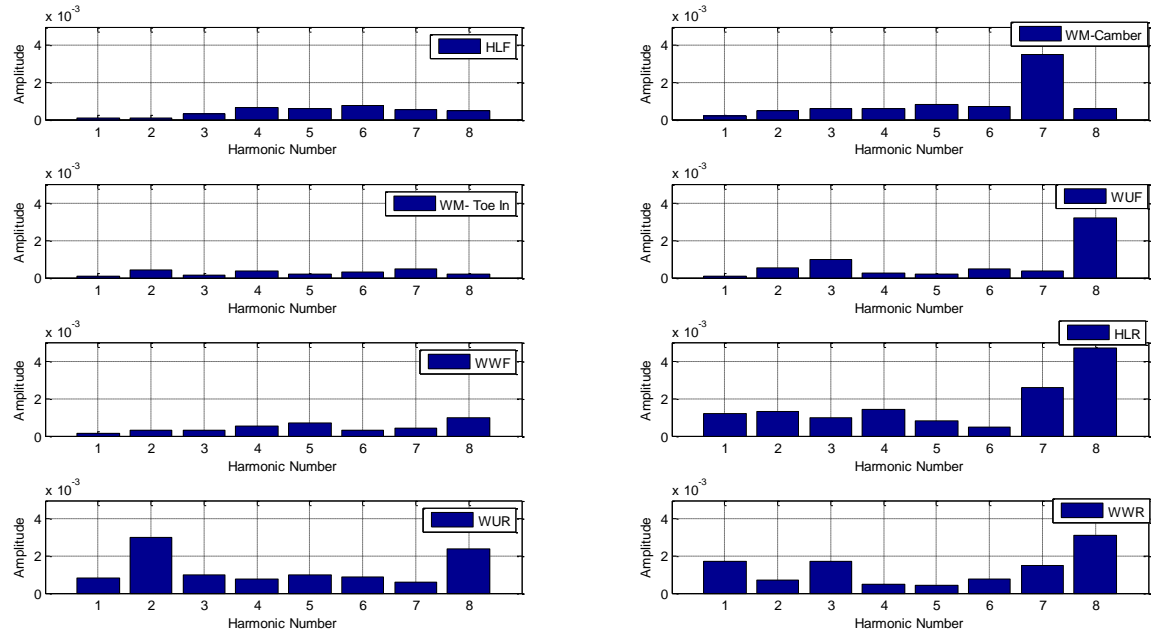


(b)

**Figure 5.3 Feature extraction: Speed 80 Km/h (a) Brake Pad Sensor (b) LB Arm Sensor**

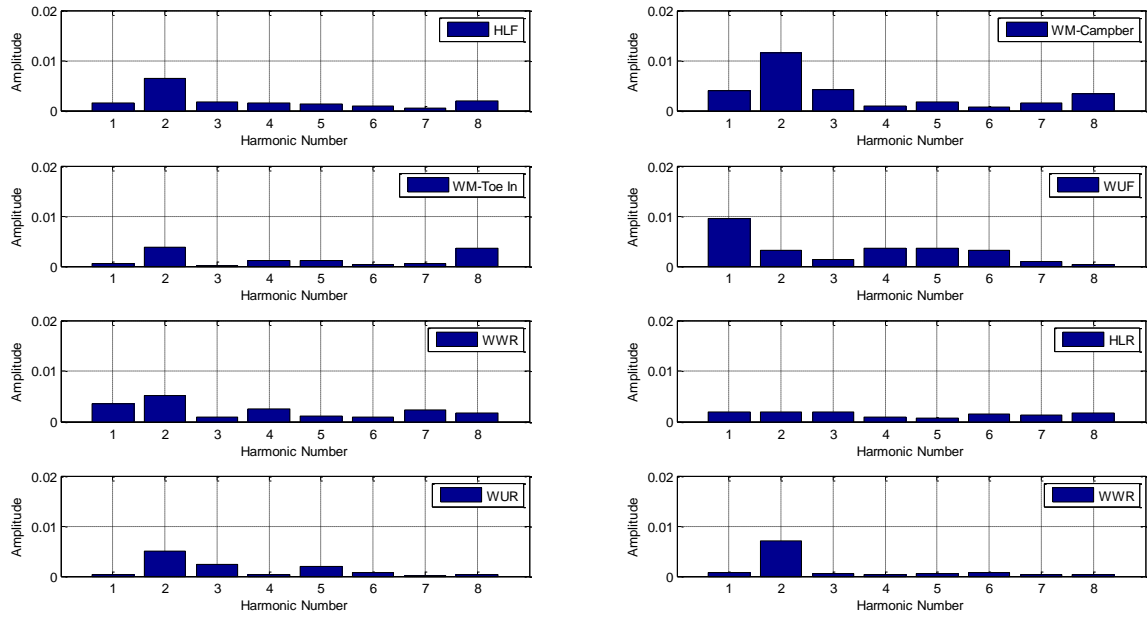


(a)

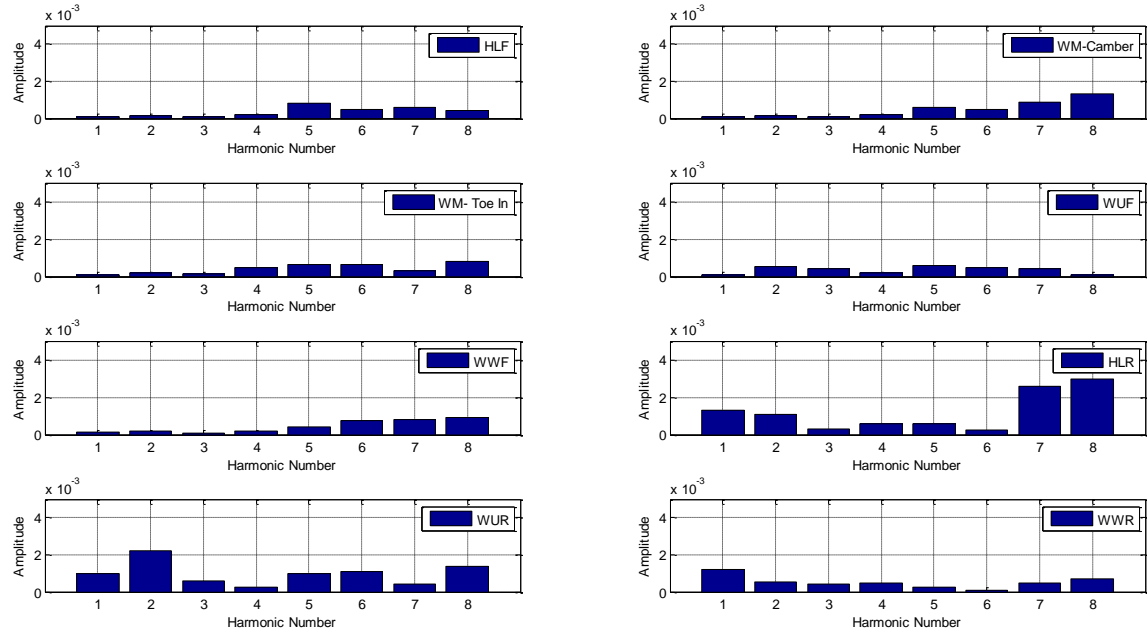


(b)

**Figure 5.4 Feature extraction: Speed 70 Km/h (a) Brake Pad Sensor (b) LB Arm Sensor**

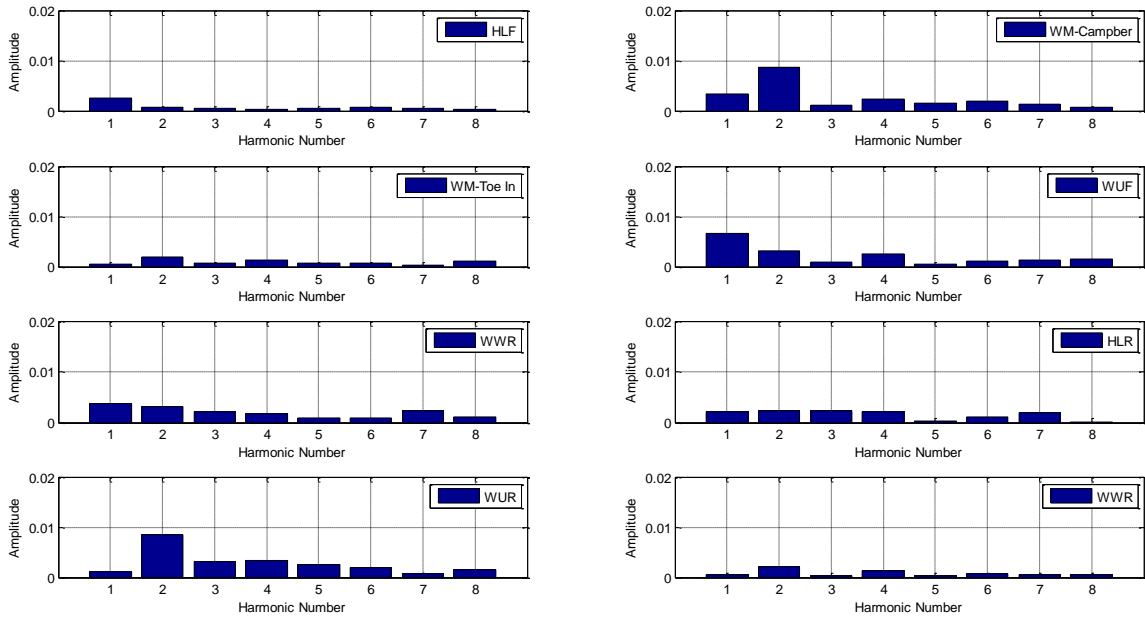


(a)

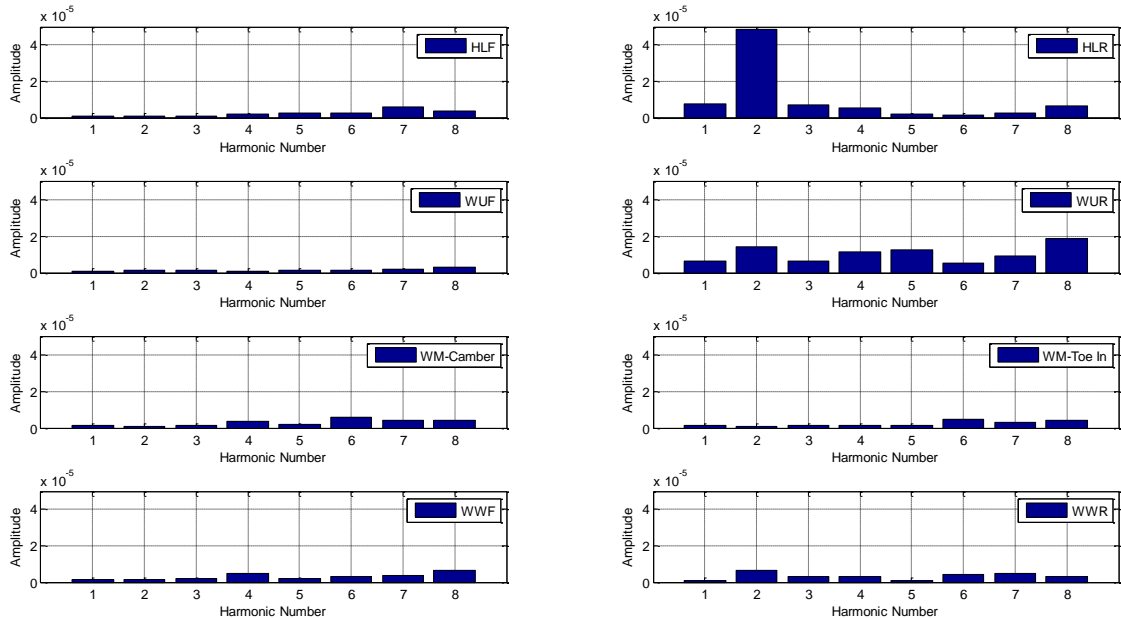


(b)

**Figure 5.5 Feature extraction: Speed 60 Km/h (a) Brake Pad Sensor (b) LB Arm Sensor**



(a)



(b)

**Figure 5.6 Feature extraction: Speed 50 Km/h (a) Brake Pad Sensor (b) LB Arm Sensor**

b) **Transient Operations:**

As mentioned earlier, vibration signals for the transient case have been recorded for motor operating frequency at 5 Hz and 10 Hz (corresponding to 30 Km/ and 60 Km/h) with two different braking rates i.e. for following four cases:

- i. 30 Km/h with Full Braking
- ii. 60 Km/h with Full Braking
- iii. 30 Km/h with Partial Braking
- iv. 60 Km/h with Partial Braking

Wavelets transforms (Scalogram) for the recorded vibration signals have been taken and wavelet transform coefficients on the basis of energy coefficient amplitudes have been extracted for the feature vector. Here, for identification of faults 5 energy coefficients with higher amplitudes for each fault have been extracted for ANN. In all 40 (five for each accelerometer i.e.  $(5 \times 2 = 10)$ ; for four case  $(10 \times 4 = 40)$ ) features have been extracted to form the input training vector for fault diagnosis. Sets of faults simulated were organized of eight individual faults shown in Table 5.2.

**Table 5.2 Numbering of Faults for Transient Case**

S. No	Fault No	Fault
1	1	HLF- Healthy System Front
2	2	WMP- Wheel Misalignment due to Camber
3	3	WMT- Wheel Misalignment due to Toe In
4	4	WUF- Wheel Unbalance Front
5	5	BRLF- Brake Lining Front
6	6	HLF- Healthy System Rear
7	7	WUR- Wheel Unbalance Rear
8	8	BRLR- Brake Lining Rear

Extracted features have been shown in Figure 5.7 – 5.10 for the four cases discussed above. It has been observed that extracted features shows clear demarcation for individual faults, though for some faults, features overlap partially with each other. (for example in Figure 5.7 (a) HLF, WM-Camber, BRLF and HLR can be identified easily

whereas WM-Toe In, WUF, WUR and BRLR are seen to partially overlap). Similar inferences can be drawn from other figures.

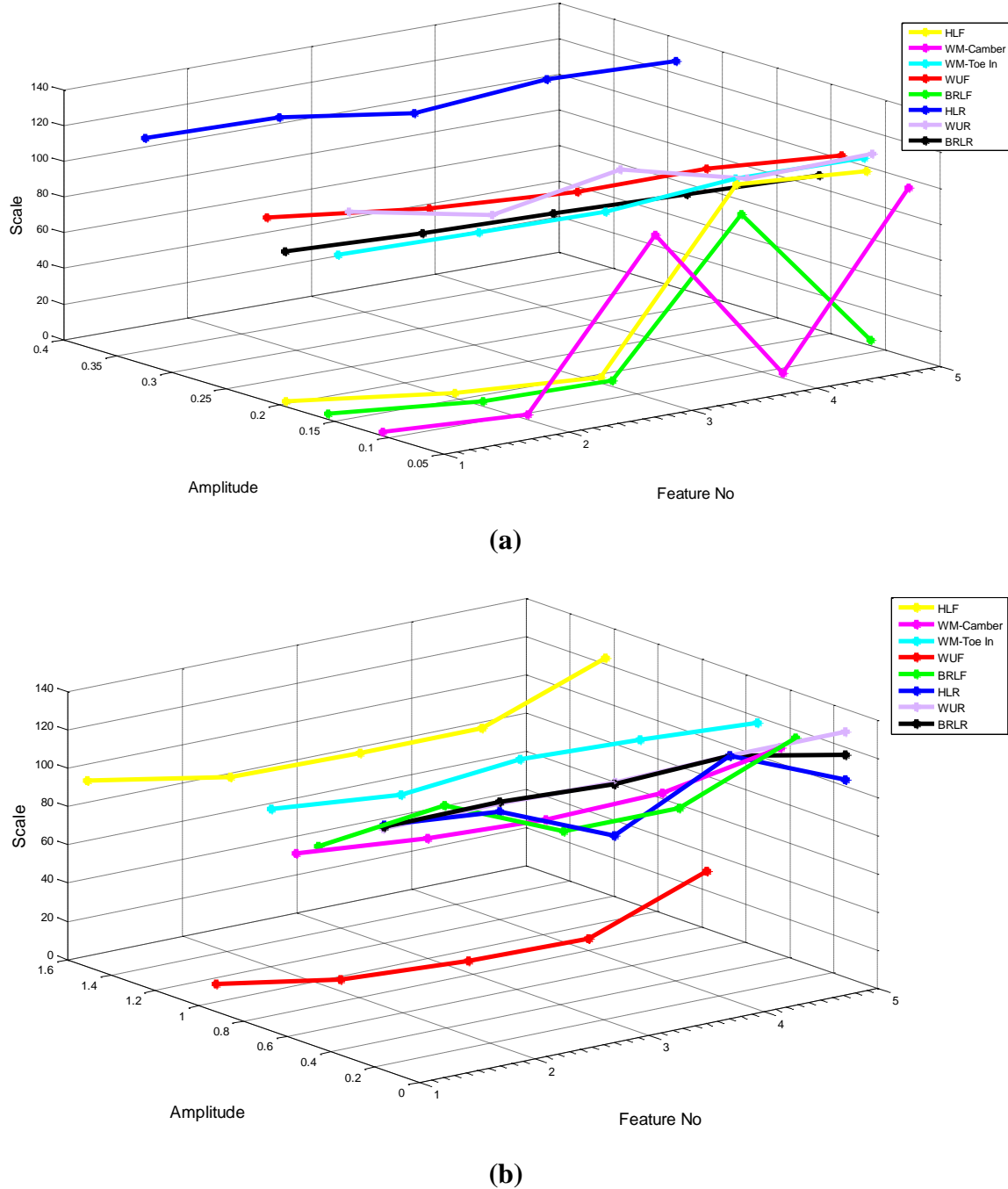


**Figure 5.7 Feature Extract at 30 Km/h with full braking: (a) LB Arm Sensor (b) Brake Pad Sensor**

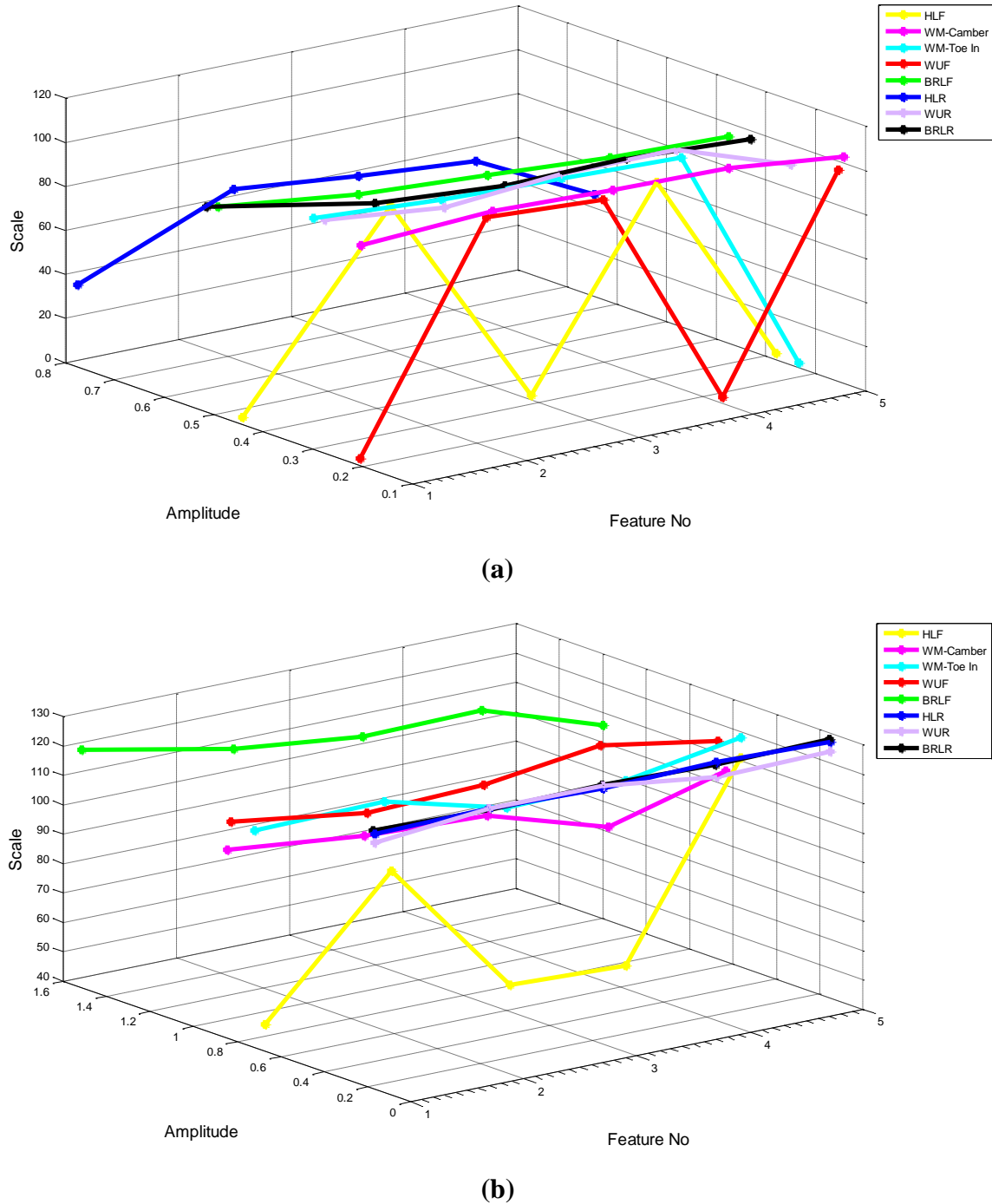


**Figure 5.8 Feature Extract at 60 Km/h with full braking: (a) LB Arm Sensor (b) Brake Pad Sensor**

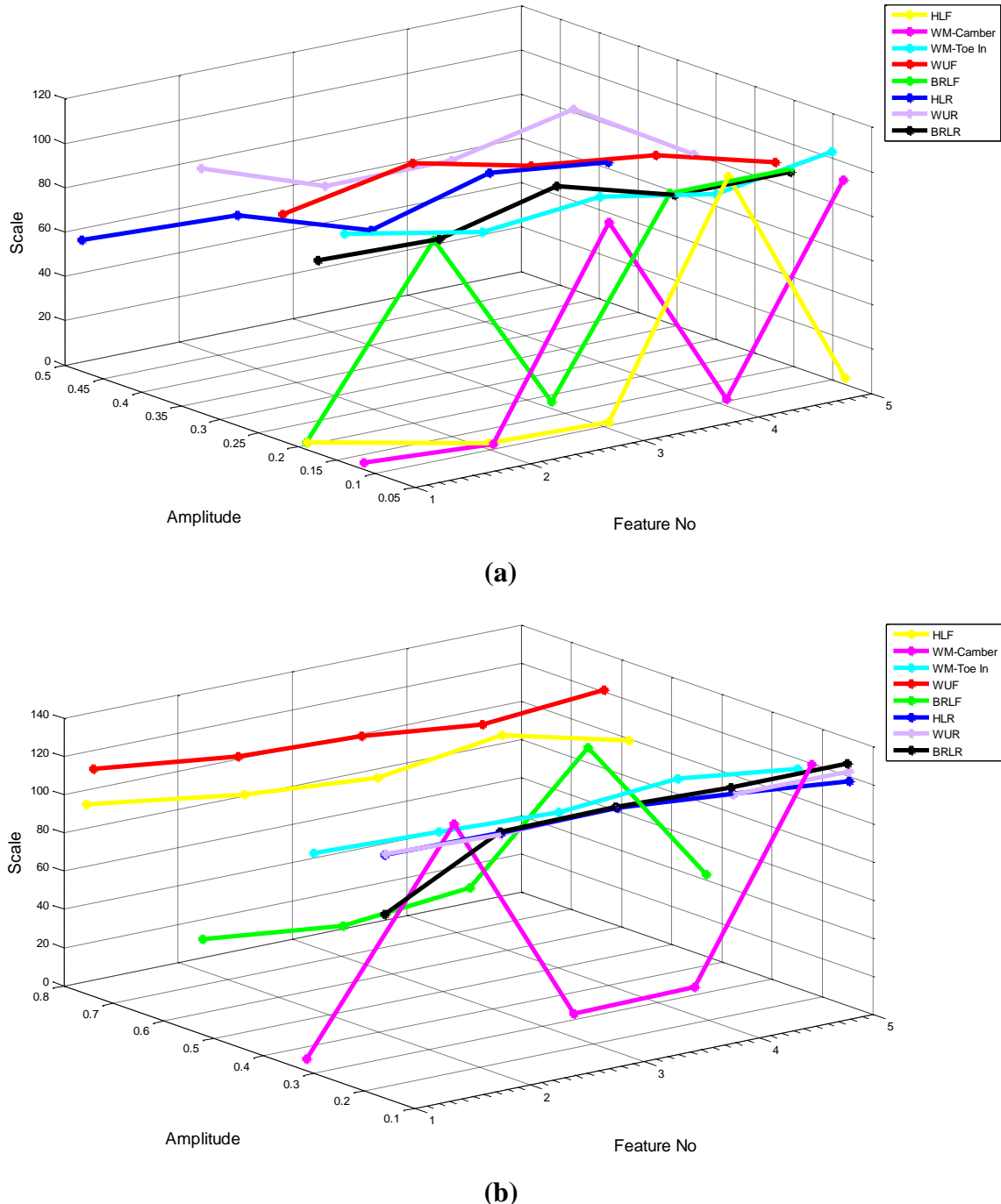


**Figure 5.9 Feature Extract at 30 Km/h with partial braking: (a) LB Arm Sensor (b) Brake Pad Sensor**

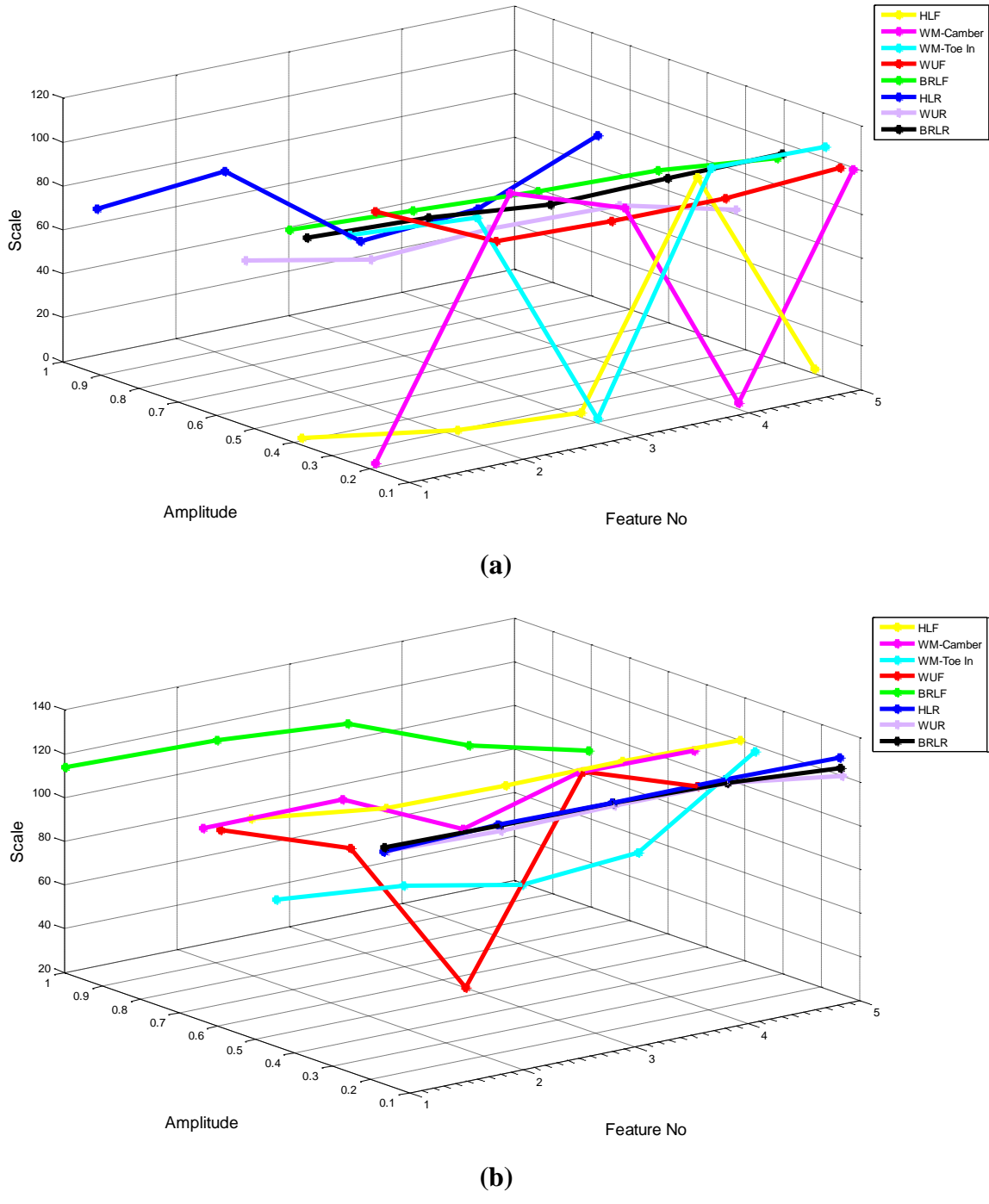


**Figure 5.10 Feature Extract at 60 Km/h with partial braking:** (a) LB Arm Sensor  
(b) Brake Pad Sensor

## 5.2 ANN Input Vector Generation

Input vector for ANN contains the features extracted from each sensor. 16 (8x2) features have been extracted for each fault from two sensor's frequency spectrum for steady case whereas 40((5x2) x4) for the transient case. A total of 96 sets, each containing 16 and 40 feature vectors have been generated and fed to the ANN for steady and transient case respectively. Table 5.3 and Table 5.4 show such a sample set of features for the brake pad accelerometer for steady and transient operation respectively.

**Table 5.3 Sample Training sets extracted for one Accelerometer for steady case**

Feature No	Fault No							
	1	2	3	4	5	6	7	8
1	0.0049	0.0049	0.0004	0.0135	0.0087	0.0061	0.0033	0.0053
2	0.0072	0.0207	0.0028	0.0046	0.0106	0.003	0.0093	0.0036
3	0.0024	0.0034	0.00011	0.003	0.0015	0.0037	0.009	0.0037
4	0.0034	0.01	0.00468	0.0036	0.0058	0.0039	0.0038	0.0024
5	0.0036	0.0027	0.003	0.0006	0.0018	0.0027	0.0083	0.00105
6	0.0035	0.0085	0.002	0.001	0.0022	0.002	0.0047	0.0023
7	0.0011	0.0039	0.0009	0.0009	0.003	0.006	0.0054	0.002
8	0.0015	0.0017	0.0048	0.0026	0.0025	0.0018	0.015	0.0044

**Table 5.4 Sample Training sets extracted for one Accelerometer for Transient Case**

Feature No	Fault No							
	1	2	3	4	5	6	7	8
1	0.19546	0.10637	0.14726	0.21324	0.15620	0.32475	0.13746	0.19623
2	0.15397	0.08702	0.13220	0.17735	0.12807	0.31543	0.11969	0.18351
3	0.13365	0.08378	0.12910	0.15527	0.12345	0.30539	0.11583	0.17717
4	0.12339	0.08046	0.12380	0.15038	0.11838	0.29748	0.11309	0.16887
5	0.11753	0.07878	0.11978	0.14030	0.11356	0.29266	0.11196	0.16111

## 5.3 Target Vector formation

The Target vector has been chosen such that it consists of combination of binary digits. Size of target vector has been kept equal to the number of faults simulated. Each element of target vector corresponds to the respective fault number. Here healthy condition itself is considered as fault number 1 condition. Thus target vector for healthy condition consists of first element as 1 and remaining all elements will be zeros. Similarly, for

second fault, second element will be 1 and rest all zeros. For sample inputs have shown in Table 5.3 and Table 5.4 which includes two healthy and six faulty operating conditions. The target for such inputs will be a unit matrix of order eight as shown in Table 5.5.

**Table 5.5 Sample Target vectors for both Cases**

	Fault Numbers							
	<b>1</b>	<b>2</b>	<b>3</b>	<b>4</b>	<b>5</b>	<b>6</b>	<b>7</b>	<b>8</b>
<b>Output Vector</b>	<b>1</b>	0	0	0	0	0	0	0
	0	<b>1</b>	0	0	0	0	0	0
	0	0	<b>1</b>	0	0	0	0	0
	0	0	0	<b>1</b>	0	0	0	0
	0	0	0	0	<b>1</b>	0	0	0
	0	0	0	0	0	<b>1</b>	0	0
	0	0	0	0	0	0	<b>1</b>	0
	0	0	0	0	0	0	0	<b>1</b>

## 5.4 Network Architecture Selection

Neural network architecture selection is crucial in any ANN application. This step comprises selection number of layers, number of neurons in each layer, type of activation function used etc. For training, multi layered feed forward back propagation network has been employed with non linear transfer function in hidden layers. As output vector values lie between zero and one, PURELIN activation functions have been used at output layer. Since, each input vector contains 16 features for steady case; 40 features for transient case and number of outputs required is equal to number of fault conditions, the input and output layer neurons are kept as 16-8 and 40-8 for steady and transient case respectively. The nomenclature used for architecture is in the form of " $i - h_1 - h_2 - h_3 - \dots - h_k - O$ " in which number of neurons used in input layer is denoted by  $i$ ,  $h_k$  is number of neurons in  $k^{th}$  hidden layer and  $O$  indicates output neurons.

## 5.5 ANN Training and Validation

To build an efficient network it is required to optimize the architecture or topology, training algorithm and activation functions employed in the network. Investigations have been carried out with variety of architectures and transfer functions like PURELIN, TANSIG, and LOGSIG etc. Different back propagation algorithms were tried during

training of network. All synaptic weights were initialised to zero before starting the training. During training, these weights get updated so as to get desired output. The algorithm tries to minimise the mean square error between the actual network output and the target output.

During fault simulation total of 96 set of features have been generated for each fault. 72 sets were employed in network training and the remaining 24 sets were used to calculate accuracy of prediction of the network. Training input vectors were randomly divided into two sets for training, validation and testing. Learning rate is kept constant at 0.05 and performance goal was kept at 1e-6. Architectures have been used for the comparison of performance for the steady and transient cases are shown in Table 5.6.

**Table 5.6 Different Architectures simulated for the ANN for the two cases**

<b>Case/ S. No.</b>	<b>Steady Architectures</b>	<b>Transient Architectures</b>
A	16-12-8	40-40-8
B	16-14-12-8	40-40-25-8
C	16-14-12-10-8	40-40-25-20-8
D	16-30-20-12-10-8	40-40-25-20-15-8

During network training, based on preliminary trials, TANSIG transfer function has been used though the network and TRAINLM (Levenberg-Marquardt) learning algorithm was employed for training. Performance diagrams are obtained during training for various network architectures and studied. The convergence patterns are shown in Figure 5.11 – 5.15 and described below.

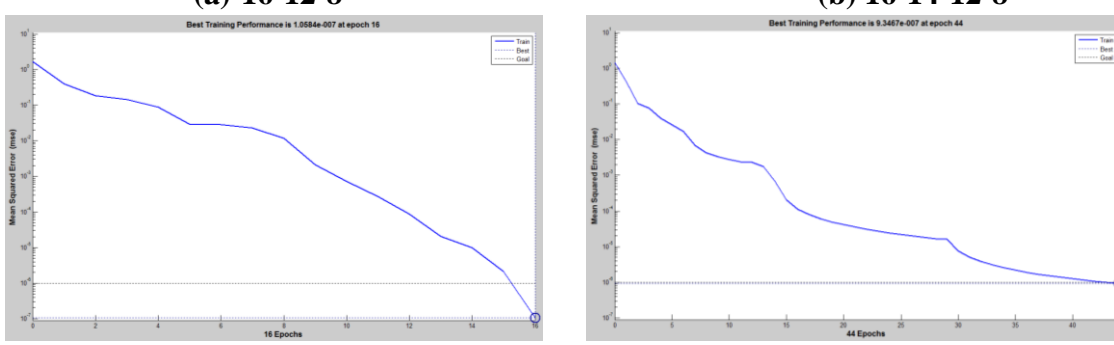
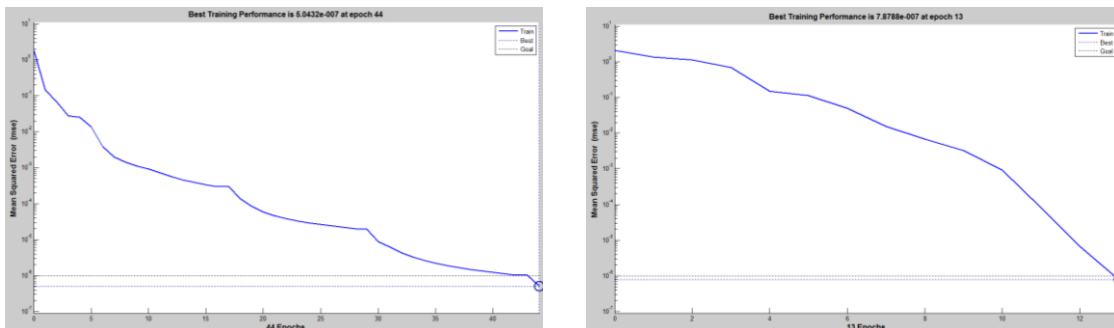
All the architectures investigated yield a very high percentage of correct predictions, the best results, as expected being by the one which gives minimum mean square error with fastest convergence. For the steady case architecture 16-14-12-8 shows better results at all speed. The same is tabulated for steady case in Table 5.7 – 5.15 (only odd table numbers). Table 5.8 – 5.16 (only even table numbers) shows the sample output patterns obtained from trained network for 16-14-12-8 network architecture. Further observations on these plots and tables are discussed in next section.

**Table 5.7 Comparison of various architectures for Steady case at 90 Km/h**

S.No	Network Architecture	Min. Error Achieved (x10-7)	Epochs	Time Taken (sec)
A	16-12-8	5.04	44	21
B	16-14-12-8	7.88	13	9
C	16-14-12-10-8	1.06	16	14
D	16-30-20-12-10-8	9.35	44	140

**Table 5.8 Sample output for test data for architecture 16-14-12-8**

Fault Numbers							
1	2	3	4	5	6	7	8
0.9993	0.0003	0.0013	-0.0002	-0.0001	0.0003	0.0000	0.0002
-0.0008	1.0004	-0.0003	-0.0002	0.0002	-0.0006	-0.0001	-0.0002
0.0000	-0.0016	0.9992	-0.0004	0.0010	0.0009	-0.0004	0.0002
0.0000	-0.0005	0.0005	0.9999	0.0001	0.0010	0.0000	-0.0004
0.0009	0.0015	0.0000	-0.0006	0.9995	-0.0022	0.0001	-0.0007
-0.0003	0.0000	-0.0011	0.0009	-0.0029	1.0000	0.0005	-0.0003
0.0005	0.0006	0.0007	0.0019	0.0022	-0.0009	1.0003	-0.0005
0.0005	-0.0007	-0.0003	-0.0013	0.0000	0.0014	-0.0004	1.0018
The output required is identity matrix of 8x8							

**Figure 5.11 Convergence patterns of various architectures at 90 Km/h**

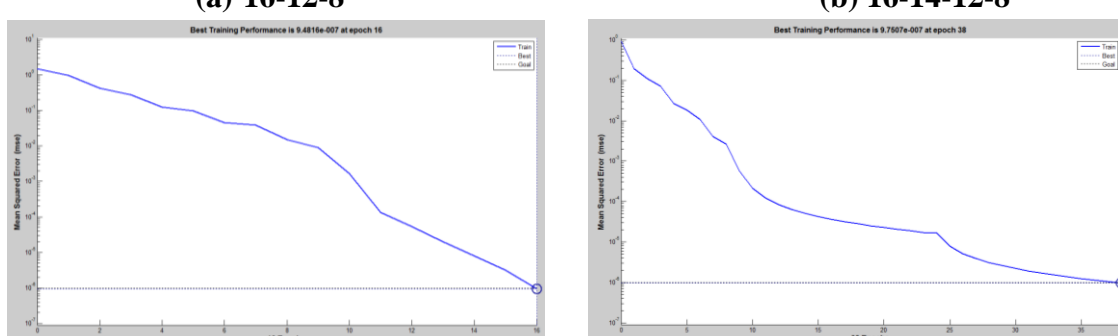
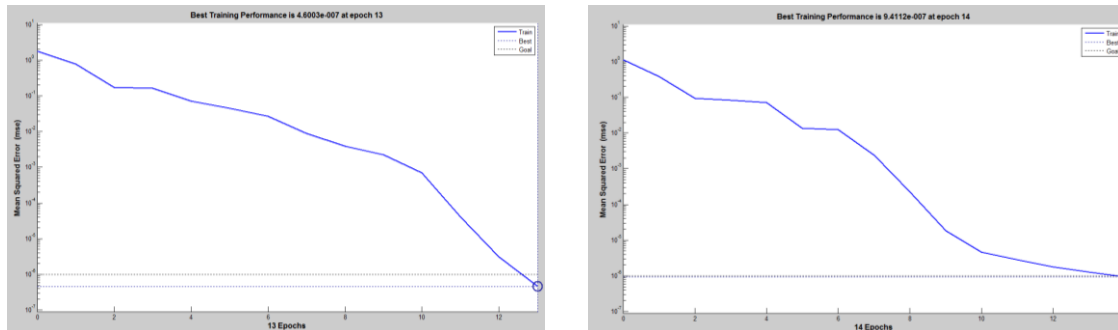
**Table 5.9 Comparison of various architectures for Steady case at 80 Km/h**

S.No	Network Architecture	Min. Error Achieved (x10-7)	Epochs	Time Taken (sec)
A	16-12-8	4.60	13	7
B	16-14-12-8	9.41	14	10
C	16-14-12-10-8	9.48	16	14
D	16-30-20-12-10-8	9.75	38	120

**Table 5.10 Sample output for test data for architecture 16-14-12-8**

Fault Numbers							
1	2	3	4	5	6	7	8
0.9997	0.0013	-0.0016	0.0001	0.0002	-0.0005	0.0004	0.0000
0.0000	1.0000	0.0004	0.0003	0.0000	0.0000	0.0000	0.0003
-0.0001	0.0000	0.9988	0.0000	0.0000	0.0000	-0.0010	0.0000
-0.0002	-0.0013	0.0004	0.9996	-0.0001	0.0005	-0.0044	0.0000
0.0002	-0.0006	0.0018	-0.0001	0.9996	0.0005	0.0025	0.0000
0.0003	0.0005	-0.0010	0.0001	-0.0003	0.9995	0.0015	-0.0002
0.0001	0.0000	0.0012	0.0000	0.0000	0.0000	1.0010	0.0000
0.0000	0.0002	0.0000	0.0000	0.0005	0.0000	0.0000	0.9998

**The output required is identity matrix of 8x8**

**Figure 5.12 Convergence patterns of various architectures at 80 Km/h**

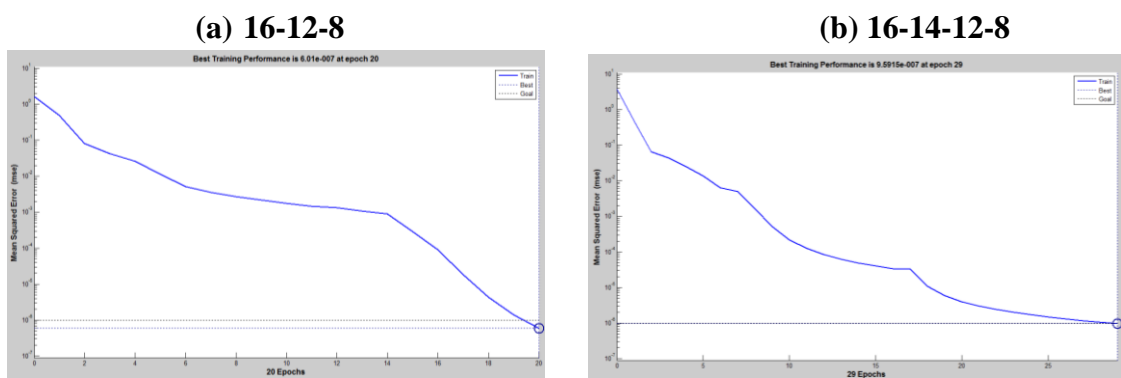
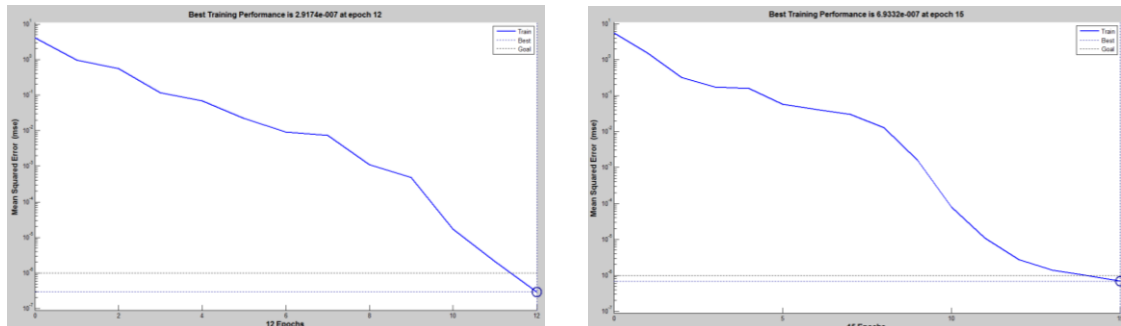
**Table 5.11 Comparison of various architectures for Steady case at 70 Km/h**

S.No	Network Architecture	Min. Error Achieved (x10-7)	Epochs	Time Taken (sec)
A	16-12-8	2.92	12	6
B	16-14-12-8	6.93	15	11
C	16-14-12-10-8	6.01	20	18
D	16-30-20-12-10-8	9.59	29	91

**Table 5.12 Sample output for test data for architecture 16-14-12-8**

Fault Numbers							
1	2	3	4	5	6	7	8
0.9999	0.0005	0.0003	0.0003	-0.0001	0.0002	0.0066	0.0000
0.0000	0.9998	0.0000	0.0000	0.0000	0.0000	0.0000	0.0001
0.0000	0.0000	0.9995	0.0000	0.0000	0.0000	0.0002	0.0000
0.0000	-0.0007	-0.0005	0.9990	0.0000	-0.0004	0.0109	-0.0001
0.0000	0.0003	0.0002	0.0002	1.0000	0.0001	0.0024	0.0000
0.0001	-0.0003	-0.0002	-0.0002	0.0000	0.9999	-0.0022	0.0000
0.0001	0.0005	0.0008	0.0008	0.0000	0.0003	0.9844	0.0000
0.0001	-0.0003	-0.0002	-0.0002	0.0000	-0.0001	-0.0024	1.0000

**The output required is identity matrix of 8x8**

**Figure 5.13 Convergence patterns of various architectures at 70 Km/h**

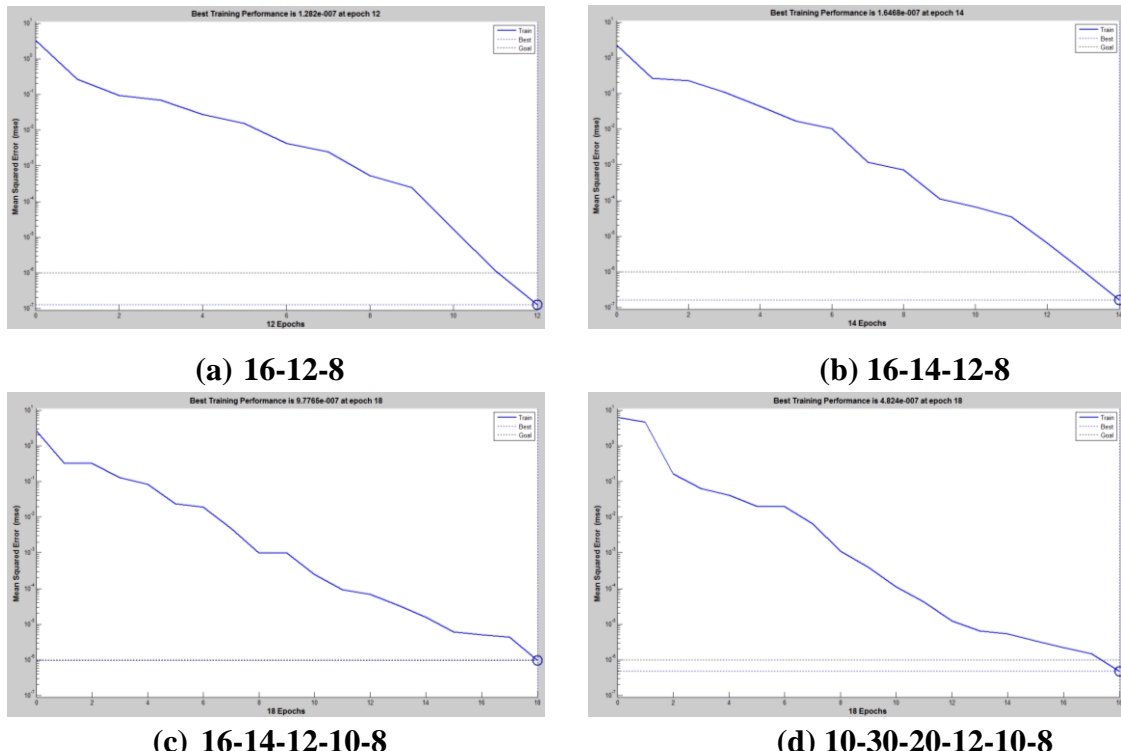
**Table 5.13 Comparison of various architectures for Steady case at 60 Km/h**

S.No	Network Architecture	Min. Error Achieved (x10-7)	Epochs	Time Taken (sec)
A	16-12-8	1.28	12	6
B	16-14-12-8	1.65	14	11
C	16-14-12-10-8	9.78	18	24
D	16-30-20-12-10-8	4.82	18	85

**Table 5.14 Sample output for test data for architecture 16-14-12-8**

Fault Numbers							
1	2	3	4	5	6	7	8
1.0001	0.0001	0.0000	-0.0001	-0.0002	0.0000	0.0000	-0.0002
0.0009	1.0000	0.0002	0.0001	0.0004	0.0000	0.0000	-0.0002
-0.0001	0.0000	0.9999	0.0000	0.0002	-0.0001	0.0000	0.0000
-0.0008	-0.0001	0.0002	1.0000	0.0004	0.0001	0.0000	0.0000
-0.0003	0.0000	-0.0001	0.0000	0.9992	0.0000	0.0000	0.0000
-0.0003	0.0000	-0.0002	0.0000	0.0003	1.0000	0.0000	0.0001
-0.0001	0.0000	0.0000	0.0000	0.0000	0.0000	1.0000	0.0003
0.0003	0.0000	-0.0002	0.0000	-0.0002	0.0001	0.0000	1.0000

**The output required is identity matrix of 8x8**

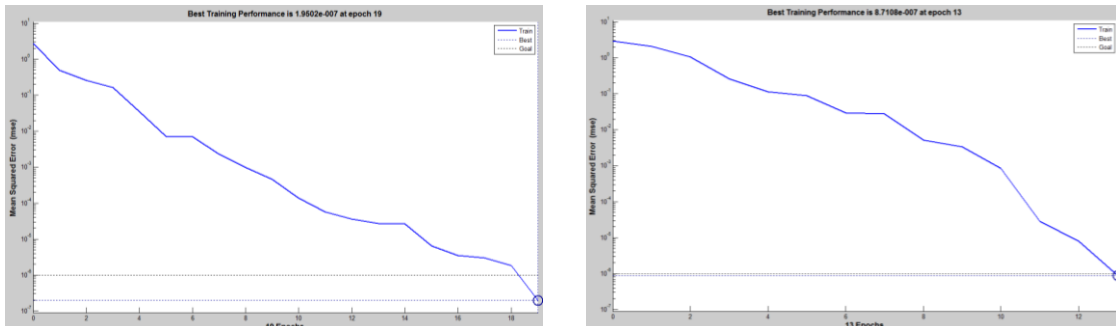
**Figure 5.14 Convergence patterns of various architectures at 60 Km/h**

**Table 5.15 Comparison of various architectures for Steady case at 50 Km/h**

S.No	Network Architecture	Min. Error Achieved (x10-7)	Epochs	Time Taken (sec)
A	16-12-8	1.95	19	10
B	16-14-12-8	8.71	13	10
C	16-14-12-10-8	9.69	24	22
D	16-30-20-12-10-8	4.73	18	58

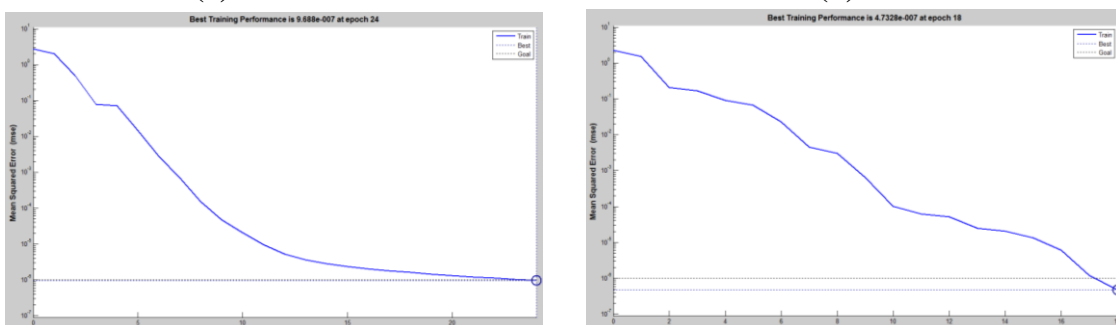
**Table 5.16 Sample output for test data for architecture 16-14-12-8**

Fault Numbers							
1	2	3	4	5	6	7	8
0.9999	0.0001	0.0021	0.0000	0.0001	0.0001	0.0000	-0.0001
0.0000	0.9996	-0.0004	0.0000	0.0000	0.0002	0.0000	0.0001
0.0004	0.0001	1.0002	0.0000	0.0000	0.0003	0.0000	0.0001
0.0000	0.0007	0.0007	0.9999	0.0002	-0.0013	-0.0001	-0.0004
0.0002	0.0000	0.0005	0.0000	0.9999	0.0001	0.0000	0.0000
-0.0003	-0.0001	-0.0015	0.0000	0.0000	0.9996	0.0000	0.0000
0.0000	-0.0003	-0.0014	0.0000	-0.0001	0.0010	1.0000	0.0002
-0.0001	0.0001	-0.0001	0.0000	0.0000	0.0000	0.0000	1.0000
The output required is identity matrix of 8x8							



(a) 16-12-8

(b) 16-14-12-8



(c) 16-14-12-10-8

(d) 10-30-20-12-10-8

**Figure 5.15 Convergence patterns of various architectures at 50 Km/h**

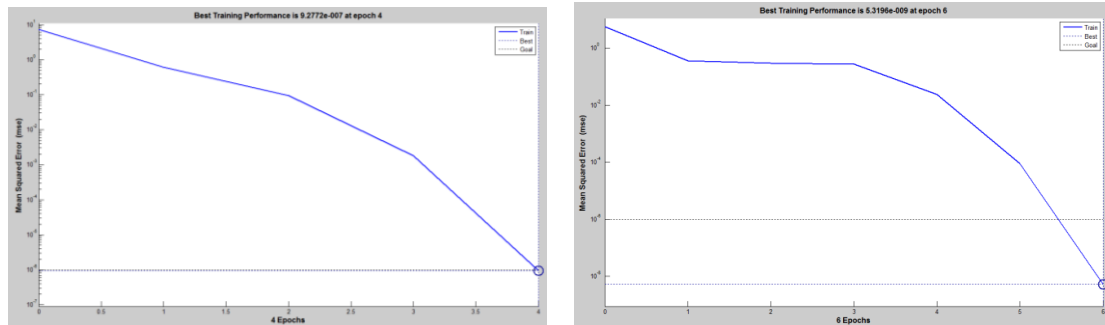
**Table 5.17 Comparison of various architectures for transient case**

S.No	Network Architecture	Min. Error Achieved (x10-7)	Epochs	Time Taken (sec)
A	40-40-8	9.277	4	9
B	40-40-25-8	0.0531	6	56
C	40-40-25-20-8	2.996	7	82
D	40-40-25-20-15-8	4.378	6	88

**Table 5.18 Sample output for test data for architecture 40-40-25-8**

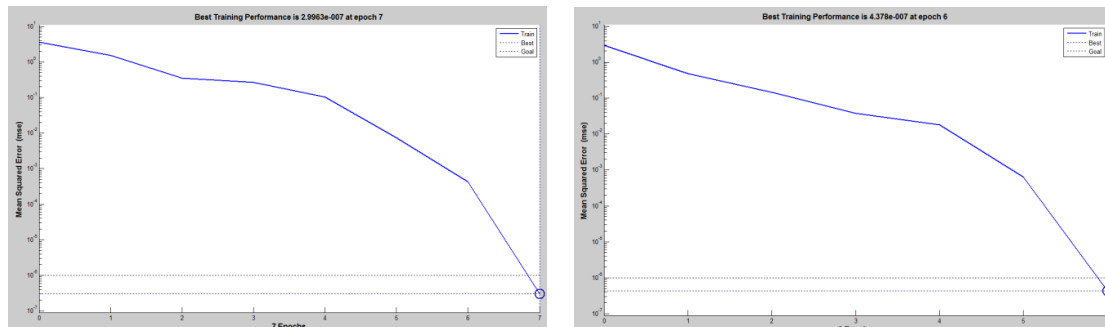
Fault Numbers							
1	2	3	4	5	6	7	8
1.0001	0.0002	0.0003	0.0001	-0.0001	0.0001	0.0002	0.0002
-0.0001	1.0006	0.0003	0.0000	0.0001	0.0000	0.0001	0.0001
0.0000	-0.0005	0.9997	0.0000	-0.0001	0.0000	-0.0001	0.0000
0.0000	-0.0001	0.0000	1.0000	0.0000	0.0000	0.0001	0.0001
0.0000	0.0002	0.0002	0.0000	1.0000	0.0001	-0.0001	-0.0001
-0.0001	-0.0002	-0.0001	0.0000	0.0002	1.0000	0.0000	0.0001
0.0002	0.0003	0.0002	0.0001	0.0001	0.0000	1.0000	0.0001
0.0001	0.0001	0.0000	0.0000	-0.0001	0.0000	0.0001	1.0001

**The output required is identity matrix of 8x8**



(a) 40-40-8

(b) 40-40-25-8



(c) 40-40-25-20-8

(d) 40-40-25-20-15-8

**Figure 5.16 Convergence patterns of various architectures for Transient Case**

For the transient case architecture 40-40-25-8 gives lowest value for the error. The same is tabulated in Table 5.17. Table 5.18 shows the sample output patterns obtained from trained network for 40-40-25-8 network architecture. Further observations on these plots and tables are discussed in next section.

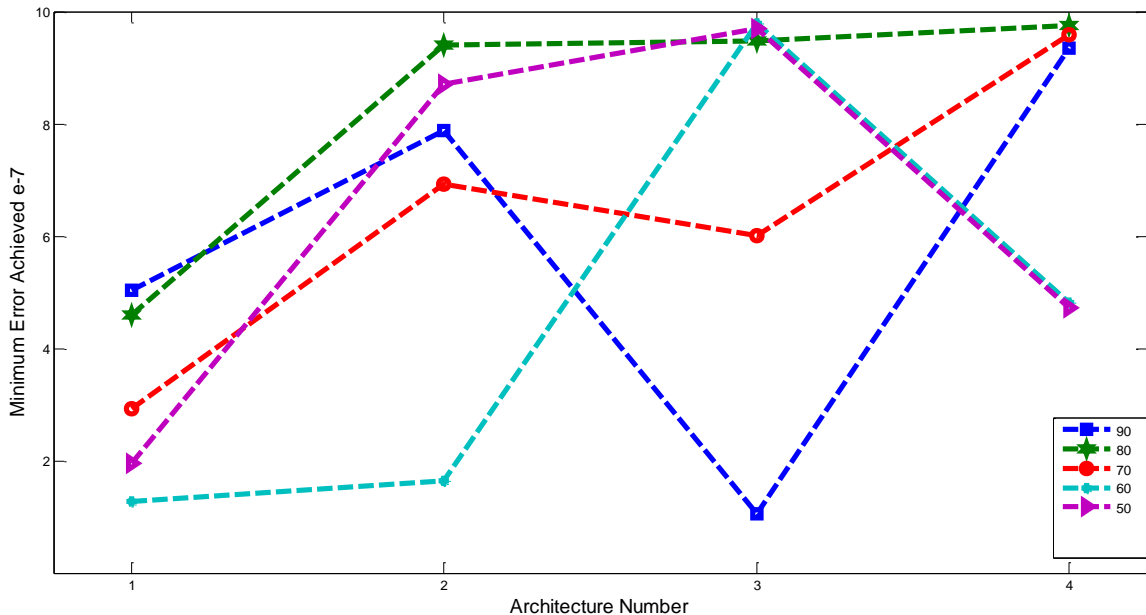


**Figure 5.17 Plot of minimum error achieved by various network architectures for Steady Case for different speed**

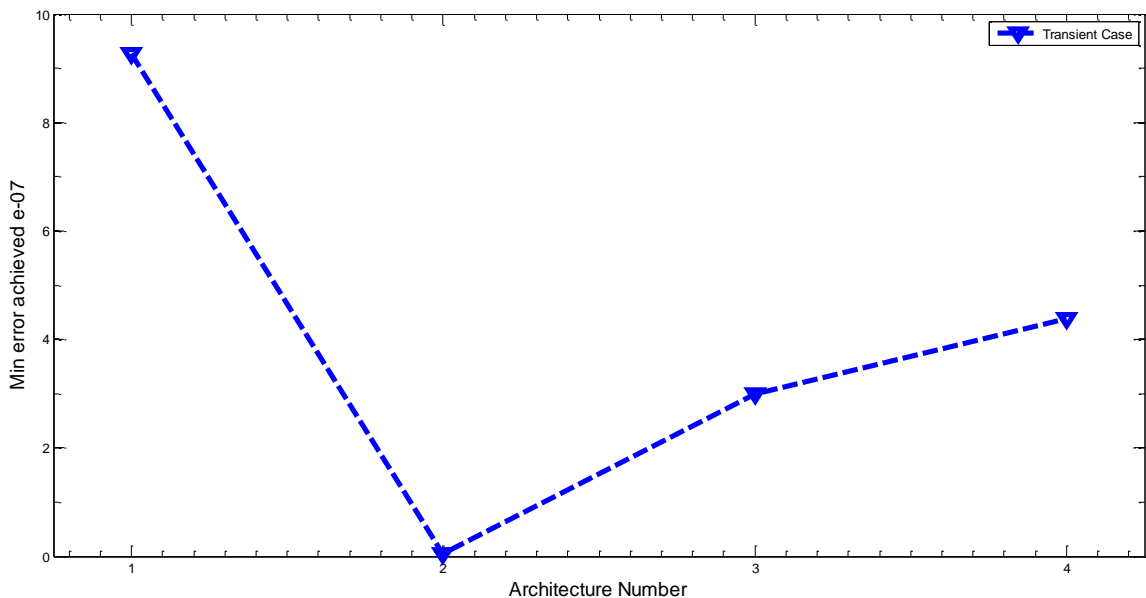


**Figure 5.18 Plot of minimum error achieved by various network architectures for Transient Case**

Figure 5.17 and Figure 5.18 shows plots for minimum error achieved during neural network training for steady and transient case respectively. In present study four network architectures have been employed in training and validation of network for each case. Architecture numbers are assigned to x-axis where as mean squared errors have been plotted on y axis.

## 5.6 Remarks

It can be said on the basis of present study based on data from two sensors

Table 5.7 to 5.15 (only odd table numbers) and Table 5.17 that

- near perfect prediction accuracy has been achieved for two sensors used for training networks for both cases.
- when large numbers of sets were used for training, performance for training found satisfactory for sensors under all conditions.
- in both cases, it is observed that, for less number of neurons training becomes faster but at expense of increased epochs.
- 16-30-20-12-10-8 architecture gives poor performance for most of the speed whereas 16-14-12-8 leads to consistent results for mean square error, epochs and time at each speed for steady case.
- 40-40-25-8 architecture gives better performance for the transient case, whereas 40-40-8 gives poor performance.

## CHAPTER 6

### CONCLUSIONS AND SCOPE FOR FUTURE WORK

The goal of present work was to develop a diagnostic scheme to identify faults in the automobile braking system and wheel/ tire assembly.

Present study has been carried out for two cases on the brake test rig which represents the quarter car model of a standard vehicle:

- 1) Steady case: when vehicle running on constant speed.
- 2) Transient case: with the application of brake.

Five commonly occurring vehicle faults were simulated on test rig. Diagnosis scheme used vibration sensors for data acquisition. Data acquisition by employing LabVIEW 2010 has been developed.

Frequency spectrum and wavelet transform of the vibration signals have been taken. Artificial neural network based on back propagation algorithm has been used as a diagnosis tool. For automatic extraction of features and training in ANN codes were written in MATLAB R2011a. ANN trainings were conducted for optimal frequency domain features and wavelet transform coefficient features by employing variety of algorithms. Levenberg-Marquardt (trainlm) algorithm has been found to be robust and fast converging for present study.

In this work only amplitudes corresponding to characteristic frequencies were used in formation of feature vector for steady case, whereas wavelet transform coefficients with scale information have been used in transient case. The feature extraction from the wavelet coefficient contains prominent energy amplitudes with scale information. However, if ridge extraction can be incorporated to be fed as input to the identification algorithm, it may yield better and still faster diagnosis, in the transient case.

ANN training for the steady case has been carried out at different steady speeds. Since the vehicle covers a range of speeds during its travel and if algorithms can be based on signatures not necessarily collected at identical speeds, it may be of better utility. For this

wheel speed information may also need to be fed as an ingredient to the diagnosis algorithm.

At the simulation stage, data from two sensors have been used. However, attempt should be made to carry out diagnosis on signals from a single appropriately located sensor.

The present work was performed over the custom designed brake test rig, where it was assumed that the road profile is perfectly smooth. In future it is desirable that similar experiments be performed on fully instrumented vehicle/ car(s) while running on different road profiles for all possible speed ranges.

During the present study the emphasis was on qualitative classification of faults. Future work can be directed towards quantifying faults.

## REFERENCES

- [1] Williams, Z. Benefits of IVHM: an analytical approach. In Proceedings of the 2006 IEEE Aerospace Conference, Big Sky, Montana, USA, 4–11 March 2006, paper no. 1507.
- [2] Janasak, K. M. and Beshears, R. R. Diagnostics to prognostics – a product availability technology evolution. In Proceedings of the 2007 Reliability and Maintainability Symposium – RAMS’07, Orlando, Florida, USA, 22–25 January 2007, pp. 113–118.
- [3] Byer, B., Hess, A., and Fila, L. Writing a convincing cost benefit analysis to substantiate autonomic logistics. In Proceedings of the 2001 IEEE Aerospace Conference, Big Sky, Montana, USA, 10–17 March 2001, vol. 6, pp. 3095–3103.
- [4] Hess, A., Calvello, G., and Dabney, T. PHM a key enabler for the JSF autonomic logistics support concept. In Proceedings of the 2004 IEEE Aerospace Conference, Big Sky, Montana, USA, 6–13 March 2004, vol. 6, pp. 3543–3550.
- [5] Zuniga, F. A., MacLise, D. C., Romano, D. J., Jize, N. N., Wysocki, P. F., and Lawrence, D. P. Integrated systems health management for exploration systems. In Proceedings of the 1st Space Exploration Conference, Orlando, Florida, USA, 30 January–1 February 2005, vol. 2, pp. 679–694.
- [6] Aaseng, G. B. Blueprint for an integrated vehicle health management system. In Proceedings of the 20th Digital Avionics Systems Conference, Daytona Beach, Florida, USA, 14–18 October 2001, vol. 1, pp. 3.C.1-1–3.C.1-11.
- [7] O Benedettini<sup>1,2,T</sup> S Baines<sup>2</sup>, H W Lightfoot<sup>2</sup>, and R M Greenough<sup>2</sup>, State-of-the-art in integrated vehicle health management, Proc. IMechE Vol. 223 Part G: J. Aerospace Engineering.
- [8] Hess, A. and Fila, L. The joint strike fighter PHM concept: potential impact on aging aircraft problems. In Proceedings of the 2002 IEEE Aerospace Conference, Big Sky, Montana, USA, 9–16 March 2002, vol. 6, pp. 3021–3026.
- [9] Bird, G., Christensen, M., Lutz, D., and Scandura, P. A. Use of integrated vehicle health management in the field of commercial aviation. In Proceedings of the 1st International Forum on System Health Engineering and Management in Aerospace – NASA ISHEM Forum 2005, Napa, California, USA, 7–10 November 2005, paper no. 12.
- [10] Baroth, E., Powers, W. T., Fox, J., Prosser, B., Pallix, J., Schweikard, K., and Zakrajsek, J. IVHM (Integrated Vehicle Health Management) techniques for future space vehicles. In Proceedings of the 37<sup>th</sup> AIAA/ASME/SAE/ASEE Joint Propulsion Conference Exhibit, Salt Lake City, Utah, USA, 8–11 July 2001, AIAA paper 2001-3523.

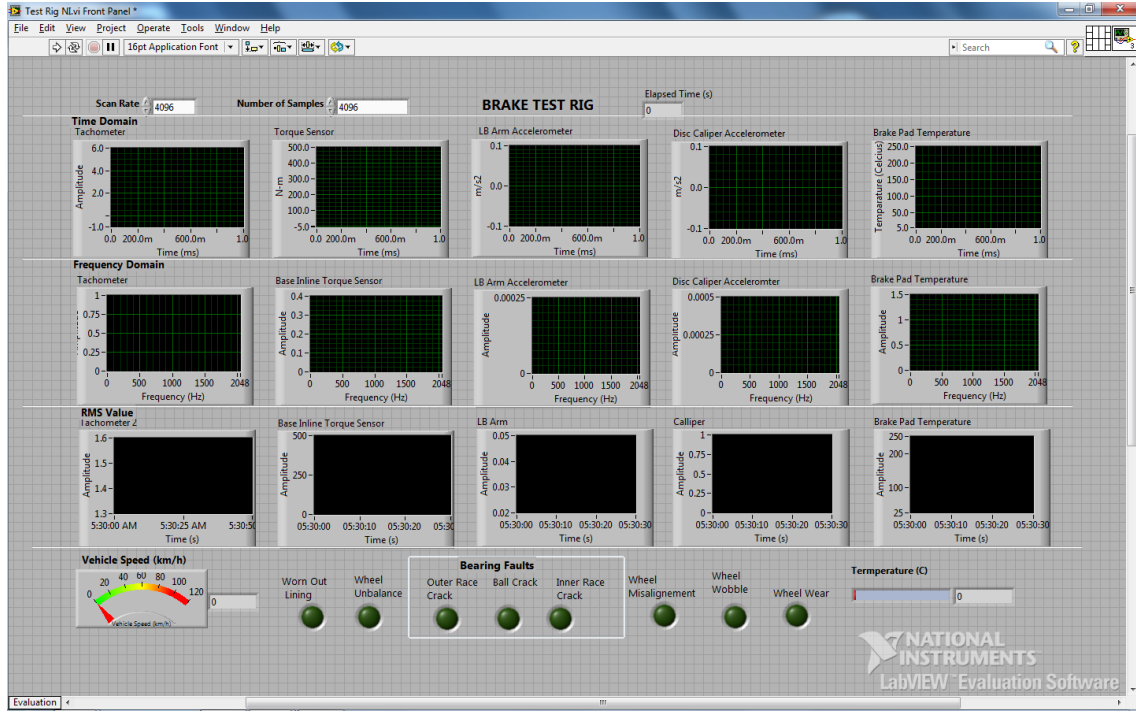
- [11] Vachtsevanos, G., Lewis, F. L., Roemer, M., Hess, A., and Wu, B. Intelligent fault diagnosis and prognosis for engineering systems, 2006 (John Wiley & Sons, New Jersey, USA).
- [12] Fox, J. J. and Glass, B. J. Impact of integrated vehicle health management (IVHM) technologies on ground operations for reusable launch vehicles (RLVs) and spacecrafts. In Proceedings of the 2000 IEEE Aerospace Conference, Big Sky, Montana, USA, 18–25 March 2000, vol. 2, pp. 179–186.
- [13] Schmalzel, J. L., Figueroa, F., Morris, J. A., and Shreekanth, A. A road map for integrated systems health management. In Proceedings of the 2008 IEEE International Instrumentation and Measurement Technology Conference, Victoria, Vancouver Island, Canada, 12–15 May 2008, pp. 522–524.
- [14] Ofsthun, S. Integrated vehicle health management for aerospace platforms. *IEEE Instrum. Meas. Mag.*, 2002, 5(N3), 21–24.
- [15] National Aeronautics and Space Administration (NASA). Research and technology goals and objectives for integrated vehicle health management (IVHM). Report NASA-CR-192656, October 1992.
- [16] Price, D. C., Scott, D. A., Edwards, G. C., Batten, A., Farmer, A. J., Hedley, M., Johnson, M. E., Lewis, C. J., Poulton, G. T., Prokopenko, M., Valencia, P., and Wang, P. An integrated health monitoring system for an ageless aerospace vehicle. In Structural health monitoring 2003: from diagnostics & prognostics to structural health management (Ed. F.-K. Chang), 2003, pp. 310–318 (DEStec Publications, Lancaster, Pennsylvania).
- [17] Paris, D. E., Trevino, L. C., and Watson, M. D. A framework for integration of IVHM technologies for intelligent integration for vehicle management. In Proceedings of the 2005 IEEE Aerospace Conference, Big Sky, Montana, USA, 5–12 March 2005, pp. 3843–3852.
- [18] Söderholm, P. Continuous improvement of complex technical systems: a theoretical quality management framework supported by requirements management and health management. *Total Qual. Manage. Bus.*, 2004, 15(N4), 511–525.
- [19] Scandura, P. A. Integrated vehicle health management as a system engineering discipline. In Proceedings of the 24th Digital Avionics Systems Conference – DASC 2005, Portland, Oregon, USA, 30 October–3 November 2005, vol. 2, pp. 7.D.1-1–7.D.1-10. 27 Banks, J., Reichard, K., Crow,
- [20] Lane, R. A. Sensors and sensing technologies for integrated vehicle health monitoring systems. *AMPTIAC Q.*, 2004, 8(3), 11–15.
- [21] Wilson, W. C., Perey, D. F., Atkinson, G. M., and Barclay, R. O. Passive wireless SAW sensors for IVHM. In Proceedings of the 2008 IEEE International Frequency Control Symposium, Honolulu, Hawaii, USA, 19–21 May 2008, pp. 273–277.

- [22] M.C. Pan, P. Sas, Transient analysis on machinery condition monitoring, International Conference on Signal Processing Proceedings, ICSP 2 (1996) 1723–1726.
- [23] P.C. Russell, J. Cosgrave, D. Tomtsis, A. Vourdas, L. Stergioulas, G.R. Jones, Extraction of information from acoustic vibration signals using Gabor transform type devices, Measurement Science and Technology 9 (1998) 1282–1290.
- [24] I.S. Koo, W.W. Kim, Development of reactor coolant pump vibration monitoring and a diagnostic system in the nuclear power plant, ISA Transactions 39 (2000) 309–316.
- [25] A. Francois, F. Patrick, Improving the readability of time–frequency and time–scale representations by the reassignment method, IEEE Transactions on Signal Processing 43 (1995) 1068–1089.
- [26] D. Leducq, Hydraulic noise diagnostics using wavelet analysis, Proceedings of the International Conference on Noise Control Engineering, 1990, pp. 997–1000.
- [27] W.J. Wang, P.D. McFadden, Application of the wavelet transform to gearbox vibration analysis, American Society of Mechanical Engineers, Petroleum Division (Publication) PD 52 (1993) 13–20.
- [28] D.E. Newland, Wavelet analysis of vibration, Part I: theory, Journal of Vibration and Acoustics, Transactions of the ASME 116 (1994) 409–416.
- [29] D.E. Newland, Wavelet analysis of vibration, Part 2: wavelet maps, Journal of Vibration and Acoustics, Transactions of the ASME 116 (1994) 417–425.
- [30] D.E. Newland, Some properties of discrete wavelet maps, Probabilistic Engineering Mechanics 9 (1994) 59–69.
- [31] D.E. Newland, Progress in the application of wavelet theory to vibration analysis, American Society of Mechanical Engineers, Design Engineering Division (Publication) 84 (1995) 1313–1322.
- [32] D.E. Newland, Ridge and phase identification in the frequency analysis of transient signals by harmonic wavelets, Journal of Vibration and Acoustics, Transactions of the ASME 121 (1999) 149–155.
- [33] D. Boulahbal, G.M. Farid, F. Ismail, Amplitude and phase wavelet maps for the detection of cracks in geared systems, Mechanical Systems and Signal Processing 13 (1999) 423–436.
- [34] S.A. Adewusi, B.O. Al-Bedoor, Wavelet analysis of vibration signals of an overhang rotor with a propagating transverse crack, Journal of Sound and Vibration 246 (2001) 777–793.
- [35] Z. Peng, F. Chu, Y. He, Vibration signal analysis and feature extraction based on reassigned wavelet scalogram, Journal of Sound and Vibration 253 (2002) 1087–1100.
- [36] Z. Peng, Y. He, Q. Lu, F. Chu, Feature extraction of the rub-impact rotor system by means of wavelet, Journal of Sound and Vibration 259 (2003) 1000–1010.
- [37] Vyas N.S., Jain N., Pandey S., “Fault identification in rotating machinery using neural networks”, accepted for publication in the Journal of Vibration Institute of India, 2000.
- [38] Sohre, J.S., “*Turbo machinery Problems and Their Correction*”, Standardization and Condition Monitoring Workshop, Chapter 7, Houston, 1991.

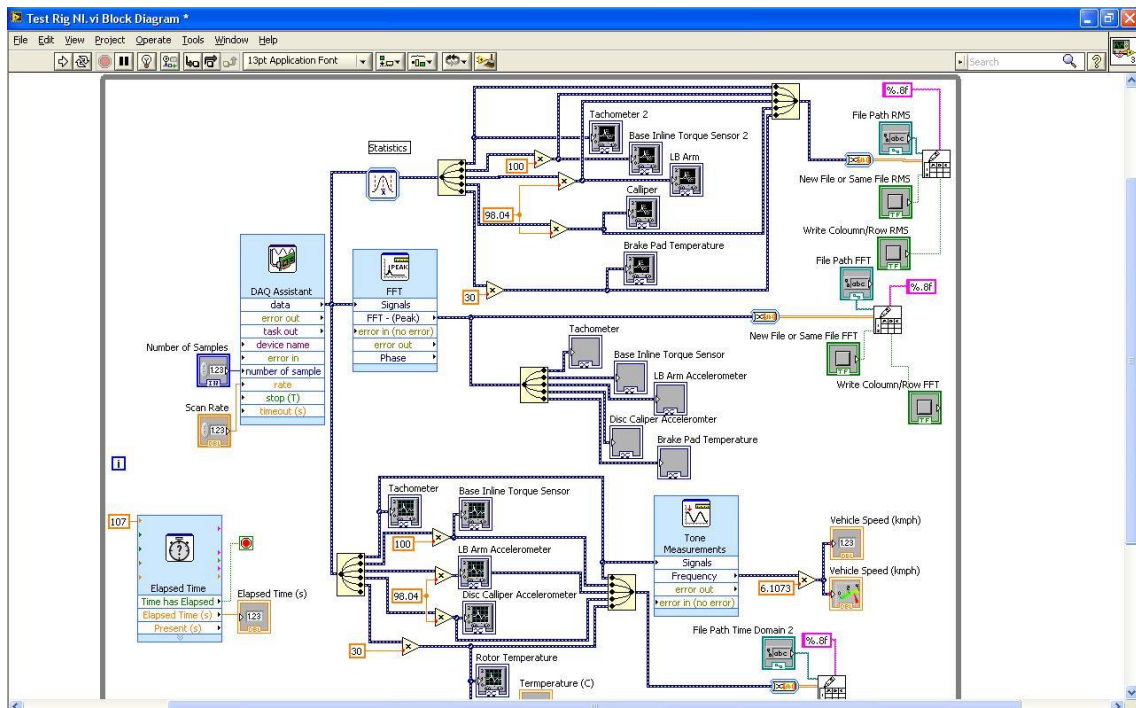
- [39] McCormick A.C., Nandi A.K., "Real time classification of rotating shaft loading conditions using artificial neural networks", IEEE Transactions on Neural Networks, Vol. 8, No. 3, pp 748-757, May 1997.
- [40] Abu-Mahfouz, I., A Comparative Study of Three Artificial Neural Networks for the Detection and Classification of Gear Faults. International Journal of General Systems, Vol. 34, No. 3 (June, 2005), pp. 261-277.
- [41] Singh Jasdeep, 'Condition monitoring of geared rotor systems using neural networks', M.Tech. Thesis, Indian Institute of Technology, Kanpur, (2006).
- [42] Michel, M., Yves, M., Oppenheim, G. and Poggi, M., "Wavelet Toolbox 4 User'sGuide," The MathWorks, Inc., Natick, MA, 1(11), 2009.

## APPENDIX

A simple VI developed in LabVIEW 2010, for data display, possessing and acquisition:



Front Panel



Block Diagram